Impacts of climate change on the coastal margins of the Bay of Plenty

NIWA Client Report: HAM2006-031
May 2006

NIWA Project: BOP05234

Impacts of climate change on the coastal margins of the Bay of Plenty

Rob Bell
Derek Goring, Mulgor Consulting Ltd
Richard Gorman
Murray Hicks
Helen Hurran
Doug Ramsay

Prepared for

Environment Bay of Plenty

NIWA Client Report: HAM2006-031
May 2006

NIWA Project: BOP05234

National Institute of Water & Atmospheric Research Ltd
Gate 10, Silverdale Road, Hamilton
P O Box 11115, Hamilton, New Zealand
Phone +64-7-856 7026, Fax +64-7-856 0151
www.niwa.co.nz

Contents

Executive Summary iv

1. Introduction 1
   - 1.1 Background 1
   - 1.2 An overview of climate change. 2

2. Tides, sea levels and storm surges 5
   - 2.1 Introduction 5
   - 2.2 Previous studies on extreme sea level 6
   - 2.3 Data 8
   - 2.3.1 Sea levels 8
   - 2.3.2 Atmospheric pressure 9
   - 2.3.3 River flow 10
   - 2.3.4 Weather systems 10
   - 2.4 Analysis methods 10
   - 2.5 Tide, storm surge and water level characteristics in the Bay of Plenty 11
   - 2.5.1 Comparison of tide and storm-surge oscillations in the sea level records 11
   - 2.5.2 Tides 14
   - 2.5.3 Storm-surge distributions 15
   - 2.5.4 Relationship between atmospheric pressure and storm surge at Moturiki Island 17
   - 2.5.5 Relationship between storm surge at Moturiki Island and storm surge at other sites 19
   - 2.5.6 Storm surge characteristics in the eastern Bay of Plenty 21
   - 2.6 Analysis of storm surge events and trends 22
   - 2.6.1 Weather bomb of 21 June 2002 24
   - 2.6.2 Other events 28
   - 2.6.3 Comparison with de Lange and Gibb (2000) 28
   - 2.7 Extreme sea levels and their composition 30
   - 2.7.1 Analysis of the mean level of the sea (MLOS) 30
   - 2.7.2 Storm tide levels 32
   - 2.8 Accelerated sea level rise in the Bay of Plenty region 33
   - 2.8.1 Historic rate of sea-level rise 33
   - 2.8.2 Projected sea-level rise for the Bay of Plenty 37
   - 2.8.3 Changes in storm tide elevations 40

3. Nearshore waves and longshore transport 41
   - 3.1 Introduction 41

3.2 Wave and wind data 42
3.2.1 NIWA New Zealand Regional Hindcast 42
3.2.2 NOAA/NCEP Wavewatch III hindcast 45
3.3 Nearshore wave data 47
3.4 Nearshore wave modelling methods 49
3.5 Surf zone and sediment transport properties 50
3.6 Climate change scenarios 51
3.7 Simulated climatology of nearshore wave conditions and sediment transport, including the influence of potential climate change impacts 56
3.7.1 Nearshore wave variability and longshore flux 56
3.7.2 Longshore sediment transport 64
3.7.3 Wave induced longshore currents 69
3.7.4 Wave induce runup and setup 73
3.7.5 Seasonal and interannual variability 76

4. Fluvial sediment supply 79
4.1 Introduction 79
4.2 Methodology for assessing current sediment supplies to coast 79
4.2.1 General approach 79
4.2.2 Annual average suspended sediment yields from sediment ratings 80
4.2.3 Empirical sediment yield prediction model 83
4.2.4 Sand fractions of suspended load 83
4.2.5 Bedload 84
4.2.6 Estuary entrapment 87
4.3 Current annual average sediment supplies to coast 87
4.3.1 Suspended sediment yields by catchment 87
4.3.2 Stationarity of sediment ratings 87
4.3.3 Sand and gravel supplies to coast 91
4.4 Methodology for assessing annual variability 93
4.4.1 Annual sediment yields 93
4.4.2 Climate variability indices 93
4.5 Annual variability in sediment yields 94
4.6 Correlation analysis 95
4.7 Impacts of climate change 99
4.7.1 Future Bay of Plenty rainfall scenarios 99
4.7.2 Sensitivity of coastal sediment yield to changes in rainfall 100
4.8 Impacts of climate change on sediment yields 101
4.9 Recommendations for planning 101

5. Overview of climate change impacts on present day coastal hazard drivers 103

5.1 Tides, storm surges and sea levels 103
5.2 Nearshore waves and longshore transport patterns 105
5.3 Fluvial sediment supply 107

6. Acknowledgements 110

7. References 111

8. Appendix 1: Summary of tide gauge data analysis methodologies 116
8.1 Fourier spectra 116
8.2 Tidal analysis 117
8.3 Extracting storm surge 118
8.4 Extracting MLOS 119
8.5 Statistical Moments 120
8.6 Regression analysis 121
8.7 Event analysis 121
8.8 Storm tide analysis 122
8.9 References 123

9. Appendix 2: Description of the nearshore wave model, verification and application 124
9.1 The SWAN wave model 124
9.2 Wave climate applications 124
9.3 SWAN model application to the Bay of Plenty coast 126
9.3.1 Scenario simulations 126
9.3.2 Comparison with measurements 127
9.4 References 132

10. Appendix 3: Surf zone wave and sediment transport properties 133
10.1 References 137

Reviewed by: *Approved for release by:*

Dr T Hume *Mr A Swales*

Formatting checked

Executive Summary

The Intergovernmental Panel on Climate Change (IPCC) in its Third Assessment Report in 2001 concluded that there was new and stronger evidence that most of the global warming observed over the last 50 years could be attributed to increased greenhouse gas concentrations in the atmosphere due to human activities. Whilst there are still many uncertainties associated with predicting future climatic changes, the general broad pattern of change over New Zealand is expected to consist of:

- Increased air temperatures (with greater increases in the winter season, and in the north of New Zealand);
- Decreased frost occurrence but increased occurrence of very high temperatures;
- Stronger west-east rainfall gradient (wetter in the west and drier in the east);
- Increased frequency of extreme (heavy) daily rainfalls;
- Increased sea level;
- Increased proportion of westerly winds.

The focus of this particular study is to assess how potential climate changes may affect the "drivers" of coastal erosion and inundation hazards at a regional scale in the Bay of Plenty, to ensure any such changes are identified and accounted for within the Council's long-term development planning over the next 50 to 100 years. Specifically the study summarises our present knowledge of the impacts of potential climate change on:

- Tides, storm surges and sea levels within the Bay of Plenty;
- Wave conditions along the Bay of Plenty coastline;
- Sediment supply from rivers in the Bay of Plenty to the coastline;
- The potential movements of beach sediment and hence impact on the patterns of coastal erosion or accretion along the Bay of Plenty coastline.

Tides, storm surges and sea-levels.

Sea levels are important along the Bay of Plenty coastline for two primary reasons: a) the tide height governs the likelihood of coastal inundation, especially when combined with storm surge; and b) sea-levels also determine the degree to which waves may

become depth limited at the coastline and hence is important in determining factors such as the magnitude of wave run-up, or storm induced beach and dune erosion.

The main component of sea level is the astronomical tide but sea level at any location can be elevated (or lowered) due to:

- Climatic fluctuations operating over annual to decadal timescales (for example the 2 – 4 year El Niño Southern Oscillation and the 20 – 30 year Interdecadal Pacific Oscillation);
- Storm surge due to atmospheric pressure and wind effects;
- Wave breaking and ensuing set-up and run-up at the shoreline.

Storm surge in the eastern Bay of Plenty tends to be higher than that in the western Bay of Plenty. However, storm surge heights measured at sea-level gauges within the Whakatane River and Ohiwa Harbour do not always provide a true indication of storm surge conditions on the open coast in the eastern Bay of Plenty. In Tauranga Harbour, extreme storm-tide levels are generally lower than those recorded at Moturiki. This confirms the conclusions from the Tonkin and Taylor (1999) study. Until a sufficient period of sea level data is recorded at the recently installed open coast tide gauge at Kohi Point by EBOP, or a detailed hydrodynamic model study of the Bay of Plenty nearshore and harbour areas is conducted, quantifying the differences in storm surge over the region relative to Moturiki will continue to be subjective.

Previous studies of storm surge in the Tauranga area have noted a correlation between the occurrence of storm surge events and the 20 to 30 year phase of the Interdecadal Pacific Oscillation (IPO), with a general reduction in storm surge events over the period from about 1976 to 1998 compared to the prior period of 1960 to 1976. This would suggest that the 20 to 30 year IPO period starting around 1998 should see increased occurrence of storm surge events, relative to the previous period. However, despite there being a slight increase in the frequency of small storm surge events (< 0.1 m in size) over the last seven years, there has been no recent resurgence in the occurrence of storm surge events observed yet in the sea-level records.

Sea levels have been rising around New Zealand since the early to mid part of the 1800s. The Port of Auckland sea-level gauge operating since 1899 (the closest long-term tide gauge record to the Bay of Plenty) provides a reasonable indication of how sea levels have risen in the Bay of Plenty. This rise in the mean level of the sea has been around 0.14 m over the last 100 years, which is slightly less than the average for New Zealand of 0.16 m, but within the global range of 0.1 to 0.2 m. It is expected that this rate of sea-level rise will accelerate in the future due largely to thermal expansion

of the world's oceans and the melting of many of worlds glaciers due to a warmer climate.

Future sea-level rise in the Bay of Plenty region also needs to account for any potential vertical movements in the landmass. For example if the land is subsiding, the relative rate of sea-level rise could be greater, or if tectonic uplift occurs, relative sea-level rise will reduce. Vertical land movements are an important consideration in the Bay of Plenty which has a history of tectonic movements. Over geological timscales, the area between Waihi and Papamoa has been relatively stable. Between Whakatane and East Cape land has been uplifted (hence potentially reducing the relative impact of long-term sea-level rise). The Whakatane Graben region between Maketu and the Whakatane River entrance, (within the Taupo Volcanic Zone), has been subsiding over geological time. However, this tends to occur episodically during seismic events rather than necessarily at a continuous rate. A GPS system to accurately monitor land movements has only been in place since 2003 (by GeoNet and LINZ) and does not provide a long enough record to provide meaningful rates of vertical land movement at this stage.

Until a longer record of continuous vertical land movements is available it is recommended that future rates of sea level rise within the Bay of Plenty be considered similar to the current absolute global estimates. Whilst there is still uncertainty as to the likely magnitude of these estimates, it is recommended for planning purposes that allowance be made for a rise of 0.2 m by 2050 (relative to 1990) and of 0.5 m for 2100 which is in keeping with present guidance from the Ministry of the Environment. This corresponds to a mean level of the sea of 0.26 m relative to Moturiki Vertical Datum-53 by 2050 and 0.56 m Moturiki Vertical Datum-53 by 2100.

Wave conditions

Wave action is the dominant forcing process causing changes in erosion and accretion patterns along the Bay of Plenty coastline. It also contributes to coastal inundation through locally raising water levels (set-up) at the shoreline and wave run-up on to the land. The potential effects of climate change on wave conditions experienced at the coastline of the Bay of Plenty is complex, depending on the interaction between both changes in regional conditions around New Zealand and in the wider South Pacific (e.g. changes in local and regional winds, storm and cyclone tracks and intensity).

Wave conditions in the Bay of Plenty are moderately influenced by the El Niño Southern Oscillation. More stormy conditions than average tend to occur during La Niña periods, which are associated with an increase in northeasterlies in the New Zealand region. During El Niño years, where a higher occurrence of southwesterlies

occurs, wave conditions in the Bay of Plenty are somewhat reduced although episodic extra-tropical cyclones still occur. Given that since 1998 we have entered a negative phase of the Interdecadal Pacific Oscillation where neutral or La Niña conditions may be more likely to occur, it is possible that the Bay of Plenty region may experience increased rates of erosion over the next 20 to 30 years, similar to that experienced in the late 1960s and early to mid 1970s.

Average breaking wave heights are generally between 1 m to 1.3 m along the majority of the Bay of Plenty coast and tend to decrease from west to east along the coast from Whangamata to Opotiki before increasing again towards East Cape, largely reflecting variation in exposure to ocean swell. Under likely climate change scenarios, increases in average breaking wave height are estimated to be less than 0.05 m between Waihi and Whakatane and up to 0.1 m further east towards East Cape over the next 50 years.

Potential changes to swell wave conditions reaching the Bay of Plenty have a considerable influence on wave induced set-up and run-up which, although highly variable along the coastline, could result in increases in annual maximum set-up and run-up of up to around 1 m due to climate change effects.

Sediment supply and beach erosion and accretion

Remotely generated swell waves are also the dominant factor moving sediment along the Bay of Plenty coast, particularly between Waihi and Opape. The climate change scenarios suggest in general that changes in longshore movements of beach and nearshore sediments will be relatively uniform within the region and relatively small compared to typical present day inter-annual variability.

A further factor influencing coastal-erosion patterns within the Bay of Plenty region are changes to the input of sand and gravel from river sources to the coast. Rainfall is the main climatic diver that affects the amount of sediment transported down rivers, since it affects both the rates of erosion on hillslopes and the transport capacity of runoff down river channels. Bay of Plenty rivers show large inter-annual variability in sediment yields, with annual yields ranging over at least a factor-of-ten. However, in general, there does not appear to be a significant correlation between annual sediment yield and El Niño Southern Oscillation or the Interdecadal Pacific Oscillation index. The exception is the Tarawera River, which tends to have higher yields during La Niña phases.

Projections of future annual average rainfall in the region vary widely, ranging from a 15% decrease to a 2% increase by the 2080s. This translates to anywhere from a 25% reduction in average annual sediment yields to a 3% increase which is small compared

to the existing inter-annual variability. Taking this, and the likelihood that changes to the general longshore movement of beach material is also likely to a have relatively small effect at a regionwide scale, suggests that the patterns of erosion experienced along the open coast of the Bay of Plenty region are unlikely to change substantially relative to that occurring at present and over the last few decades. The most susceptible areas to coastal changes will still occur at locations such as estuary and river mouths, adjacent to promontories and along spit features. However, areas that have traditionally been relatively stable, such as to the south of Papamoa, in the lee of Motiti Island, may begin to show a greater tendency to erode.

1. Introduction

1.1 Background

Environment Bay of Plenty have commissioned NIWA to assess potential climate change impacts on the drivers of coastal hazards that may affect the coastal margin of the Bay of Plenty region over the coming 50 to 100 years. This is the second phase of a climate change impact study and builds on the first phase study report: *The Climate of the Bay of Plenty: Past and Future?* (Griffiths et al., 2003) prepared for Environment Bay of Plenty.

The primary focus of the study is to assess changes and trends in the "drivers" of coastal physical processes and hazards, and assess the potential impacts these changes or trends may have on the coastal margin of the Bay of Plenty region. In particular it looks to summarise our present knowledge, in the context of the Bay of Plenty region, of the impacts of potential climate change on:

- Tides, sea levels and storm surges
- Nearshore waves, and potential longshore drift
- Fluvial sediment supply

Coastal hazards, such as inundation and coastal erosion, tend to be caused by a range of inter-relating factors or "drivers" which can be both natural and caused or exacerbated by human actions. These coastal hazard "drivers" also have behind them one or more fundamental causes. A breakdown of the main natural causes and hazard drivers that govern coastal erosion and inundation is shown schematically in Figure 1.1.

Besides earthquakes and underwater landslides (which can cause a tsunami or coastal subsidence) and ocean tides, the main natural causes of coastal hazards arise from extremes in weather such as storms and cycles in ocean-atmosphere response (sea level and currents). It is these weather and climate-related causes that will be altered most by climate change arising from global warming, mostly exacerbating the potential problems for the coast e.g., heightened storm tides, stronger winds and waves, sea-level rise.

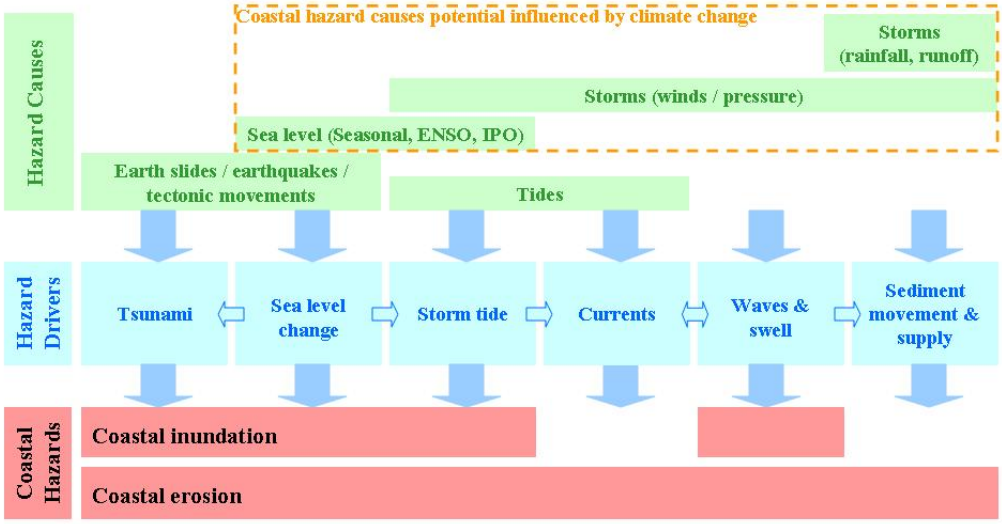

Figure 1.1: Natural causes and hazard "drivers" for coastal inundation and coastal erosion, together with those causes and "drivers" affected by climate change. Note: ENSO = El Niño–Southern Oscillation cycle; IPO = Interdecadal Pacific Oscillation.

Further descriptions of these hazard drivers and the implications for coastal planning are contained in a guidance manual, *Coastal Hazards & Climate Change: A Guidance Manual for Local Government in New Zealand*, published by the Ministry for the Environment (MfE, 2004b)[1].

1.2 An overview of climate change.

The Intergovernmental Panel on Climate Change in its Third Assessment Report (IPCC, 2001) concluded that there was new and stronger evidence that most of the warming observed over the last 50 years could be attributed to increased greenhouse gas concentrations in the atmosphere due to human activities. As an introduction to the assessments summarised within this report, this section provides a very brief summary of potential climate change and where available details of 'downscaled' global predictions at the national and region level. More detailed information is available from the IPCC series of reports (with the Fourth Assessment Reports currently being drafted and due for completion by 2007) and in the New Zealand context, from the Ministry of Environment funded *Climate Change effects and impacts assessment. A guidance manual for local Government in New Zealand.* (MfE, 2004a) (defined as the *guidance manual* in the remainder of this document).

[1] Available at web site: http://www.climatechange.govt.nz/resources/local-govt/coastal-hazards-may04/index.html

Whilst there are still many uncertainties associated with predicting future climatic changes, the IPCC Third Assessment Report summarised current climate projections as:

- An increase in globally averaged surface temperatures of between 1.4ºC and 5.5ºC by 2100 (this rate of warming is thought to be unprecedented during at least the last 10,000 years);

- Both increased and decreased rainfall (depending on location) of between 5-20% at regional scales during the 21st century;

- Continued widespread retreat of glaciers throughout the 21st century;

- A rise of global mean sea-level of between 0.09 to 0.88 m between 1990 and 2100.

These global averages do not necessarily reflect what may occur at the national or regional level in New Zealand with such global projections requiring 'downscaling'. Full details of available national and regional 'downscaled' predictions, in the context of Local Government, is summarised in the guidance manual with broad patterns of change over New Zealand expected to consist of:

- Increased temperatures (with greater increases in the winter season, and in the north of New Zealand;

- Decreased frost risk but increased risk of very high temperatures;

- Stronger west-east rainfall gradient (wetter in the west and drier in the east);

- Increased frequency of extreme (heavy) daily rainfalls;

- Increased sea levels;

- Increased westerly winds.

More detailed information is provided in the guidance manual for New Zealand as a whole, and, for the Bay of Plenty region, in the report *The Climate of the Bay of Plenty: Past and Future?* (Griffiths et al., 2003). Within this report, climatic changes

of relevance to coastal hazard causes and drivers are summarised in the relevant sections following this introduction, along with other potential changes.

2. Tides, sea levels and storm surges

2.1 Introduction

Episodic extreme sea levels are typically caused by a range of inter-relating factors or "drivers". Other than oceanic tides (or geological events such as seabed ruptures or landslides causing tsunamis), the main factors causing inundation or erosion events arise from extremes in weather such as storms and cycles in ocean-atmospheric response. It is these weather and climate-related causes that will be altered most by climate change arising from global warming.

Sea level, as measured by a sea-level recorder or tide gauge, has a number of components as follows:

- *Tides:* Most tides have periods between 3 and 29 hours. They are the response of Earth's oceans to the gravitational attraction of the Moon and Sun. In most places around New Zealand, the tidal height is strongly linked to the likelihood of coastal inundation from storm surge, river flooding or backed up stormwater networks during flash floods.

- *Long Period Oscillations:* Long-period (≥6 month) oscillations in sea-level arise from the effects of:

    - Annual seasonal heating and cooling cycle by the sun on the ocean surface waters;

    - Interannual (2 to 4 year El Niño-Southern Oscillation[2] cycles); and

    - Interdecadal (20 to 30 year Interdecadal Pacific Oscillation[3] or IPO cycles).

  We refer to the combination of these components as the "mean level of the sea" (MLOS). It is different from mean sea level (MSL), which is mostly used as a fixed survey datum. MSL has historically been determined as the regional vertical datum based on measurements at various stations around New

[2] Cycle of alternate El Niño and La Niña episodes that govern climate and sea-level variations around the Pacific and Indian Oceans—commonly called the El Niño–Southern Oscillation or ENSO system.
[3] Longer "El-Niño–like" 20–30 year cycles of alternate positive and negative phases that effect the wider Pacific Ocean region, abbreviated as IPO. Since 1998 the IPO has been negative.

Zealand defined as the MLOS for a particular set of years. Moturiki MSL or Vertical Datum is one such regional datum set in 1953.

- *Storm Surge:* Storm surge has timescales between 24 and 360 hours. It is the response of the ocean to changing atmospheric pressure and wind and can propagate into the region from remote storm locations.

- *Storm Tide:* Storm tide is the combined sea level height from storm surge and the tide. This is the water level that causes inundation, particularly in association with high wave activity. The tide is independent from storm surge (they are caused by completely different phenomena), though the highest storm-tide levels usually occur at high tide. This is because in New Zealand, high tide heights are generally much larger than storm surge heights, even in periods when the tidal range is low (e.g., neap tides).

This section reviews existing information on tides, storm surges and sea levels within the Bay of Plenty region and how climate variability and change may impact on them. Part of this section has been adapted from a report produced by Mulgor Consultants Ltd commissioned as part of this study to investigate storm surge in the Bay of Plenty (Goring, 2006). A substantial amount of information was also made available to NIWA by Peter Blackwood (EBOP, pers. comm.) which has been woven into this section to maintain compatibility with existing EBOP storm-tide and wave run-up design levels.

Consequently, the focus of this report is on comparisons between the Moturiki gauge (operated by NIWA) and the newer sea-level gauge records from Ohope and Whakatane Wharves (operated by EBOP), and three sites within Tauranga Harbour (operated by Tauranga City Council). This is followed by an assessment of how climate variability and climate change will affect extreme sea levels across the BOP region.

2.2 Previous studies on extreme sea level

Goring (1995) analysed sea level data from 15 tide gauges around New Zealand, including Moturiki Island in the Bay of Plenty. He showed that storm surge at Moturiki Island generally leads changes in atmospheric pressure at Rotorua Airport[4] by around 3 hours and the magnitude of the inverted-barometer factor is less than

[4] Barometric pressure data from Rotorua are available for the entire Moturiki sea-level gauge record back to 1973, whereas Tauranga Airport digital record does not extend that far back.

unity[5]. The correlation between pressure and storm surge is low, with only 53% of the variance of sea level being explained by atmospheric pressure. These factors indicate that sea levels in the Bay of Plenty are not responding directly to local pressure changes, but are influenced by waves propagating into the region. Local wind was found to have little effect on storm surge at Moturiki (but will do inside harbours).

Goring et al. (1997) undertook a joint-probability analysis of extreme storm-tide levels based on 23 years of digital record from the Moturiki sea-level gauge. They estimated the 2% AEP and 1% AEP storm-tide levels were respectively 1.85 m and 2.06 m above Moturiki Vertical Datum–1953 (MVD-53).[6]

Blackwood (1997) examined sea-level data and wave run-up observations for Cyclones *Fergus* (Dec. 1996) and *Drena* (Jan. 1997) around the Bay of Plenty. Observations during *Fergus* revealed that storm-surge heights reached around 1 m above the expected tide at Whakatane, Ohiwa inlet and Opotiki Wharf, with a peak storm-tide level reaching 1.84 m above MVD-53 at Opotiki Wharf. By comparison, the storm surge at Tauranga was only about 0.5 m. and 0.6 m (estimated) at Moturiki. This storm in the Bay of Plenty was deemed to be only a 10% AEP event, which implies the observed storm-tide levels at the eastern sites also involved a component of wave set-up induced inside the respective entrances. More recent analysis (P. Blackwood, pers. com.) indicates that the 2% AEP storm-tide level in the Whakatane-Ohope area is about 2.15 m above MVD-53. This is 0.3 m higher than the equivalent 2% AEP level for Mt. Maunganui (1.85 m from Goring et al., 1997). These results indicate that storm-tide levels in the eastern section of the region are somewhat higher than that recorded by the open-coast Moturiki gauge and even higher compared with Tauranga Harbour.

Tonkin & Taylor (1999) analysed extreme storm-tide levels within Tauranga Harbour, based on GEV analyses of annual maximum sea-level data from three gauges: i) Moturiki (outside harbour); ii) Tug Berth, otherwise known as Salisbury Wharf; and iii) Tauranga (variously moved from the Slipway to Sulphur Pt Wharf). The latter two datasets covered a relatively long period from 1962 to 1997, and included the TC *Giselle* (Wahine) event in 1968 (which isn't in the Moturiki record). Their conclusions were: a) Moturiki wasn't a good indicator of storm-tide levels inside Tauranga Harbour due to damping of open-coast storm surge through the entrance; b) the 1% AEP storm-tide level at the Port of Tauranga was 1.56 m above MVD-53.

[5] In the deep ocean, the theoretical response to changes in barometric pressure is 1 cm rise for every 1 hPa fall in pressure, which gives an inverted-barometer factor of -1cm/hPa.
[6] The RJPM removes the mean, so these values have had 0.07 m added to get back relativity to MVD-53.

de Lange and Gibb (2000) analysed storm surge events from 1960 to 1998 in the context of climate variability — El Niño/Southern Oscillation (ENSO) and Inter-Decadal Pacific Oscillation (IPO). They showed that there were substantially more storm surge events in the La Niña-dominated phase of the IPO that occurred from 1960 to the mid-1970s than in the El Niño-dominated phase of the IPO that occurred from the mid-1970s to the late 1990s.

2.3 Data

Updated sea-level data from existing gauges plus data from more recent gauges in Tauranga and Ohiwa Harbours is described and analysed in this section, with the primary focii on: a) updating long-period climate variability signals in the records; and b) using sea-level and barometric pressure data from recent storms to spatially compare the storm-surge response at different localities where the gauges are located.

2.3.1 Sea levels

The sea levels from 8 recorders (Figure 2.1) were used in this study, as indicated in Table 2.1. The quality of the data varied considerably, with some sites having many data dropouts, gaps and spikes, and others (such as Moturiki Island and Ohiwa) having very few.[7] Unfortunately, there are few overlapping periods except for the period from 2001 to 2004, and only Moturiki Island has more than 20 years of digital time-series record. Digital records are not available for the earlier periods for the other two long term gauges within Tauranga Harbour (Tug Berth–Salisbury Wharf at Mt. Maunganui and Slipway–Sulphur Pt Wharf at Tauranga) although high and low tides and annual maxima have been previously analysed by Tonkin & Taylor (1999) and de Lange and Gibb (2000).

Figure 2.1 shows that the sites fall in three categories:

- Open Coast: Moturiki Island;
- Inside Tauranga Harbour: Sulphur Point, Salisbury Wharf (Tug Berth), Kotuku Reserve, Hairini Bridge, and Oruamatua;
- Eastern BOP: Whakatane and Ohiwa.

[7] However, because of the high wave exposure of the Moturiki gauge, some severe storms have damaged the facility causing the instrument to fail before the peak of the storm e.g. Cyclone *Fergus* in December 1996.

The Whakatane site is different to all the others in that it is situated on a river. Therefore, we would expect it to have some response during river floods, which may or may not be correlated with storm surge.

2.3.2 Atmospheric pressure

The atmospheric pressure from Rotorua Airport was used in the study as an indication of inverted barometer – the theoretical isostatic response of sea level to changing pressure:

- A 1hPa *drop* in pressure results in a 1 cm *rise* in sea level, and
- A 1hPa *rise* in pressure results in a 1 cm *fall* in sea level.

The Rotorua record was used in preference to a site on the coast (such as Tauranga Airport) because the Rotorua record extends back to the start of digital pressure recordings at airports in 1964.

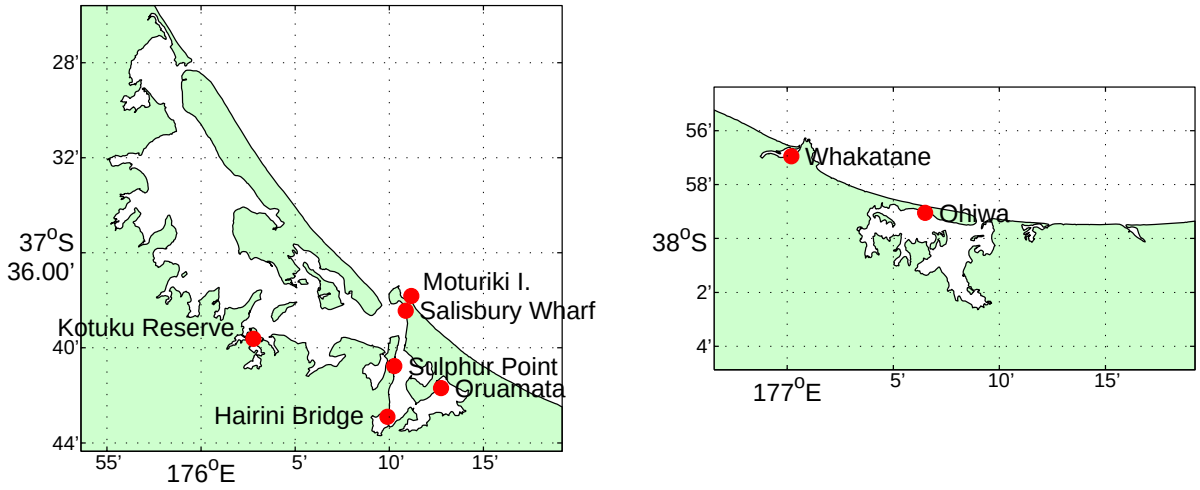

Figure 2.1: Location of the eight sea-level recorders used in the present assessment.

Table 2.1: Data used in this study. Length is the number of hours of data available (excluding gaps and bad data). Tidal analysis lists the start and finish dates of the data used to identify the tides.

			Length	Tidal Analysis	
Station	**Start**	**Finish**	**hrs**	**Start**	**Finish**
Sulphur Point	2-Jun-89	3-Aug-99	82,154	14-Oct-98	3-Aug-99
Salisbury Wharf	1-Jun-90	18-Mar-05	125,133	1-Jan-99	1-Jan-00
Kotuku Reserve	25-Nov-00	16-Sep-04	32,722	1-Jan-02	1-Jan-03
Hairini Bridge	21-Sep-01	8-Oct-04	26,585	1-Dec-02	1-Dec-03
Oruamatua	20-Jan-01	12-Oct-04	25,170	17-Jul-03	15-Jul-04
Whakatane	25-Aug-93	30-Nov-04	90,401	1-Jan-02	1-Jan-03
Ohiwa	23-Sep-98	13-Jan-05	55,200	1-Jan-02	1-Jan-03
Moturiki	5-Jun-74	25-Nov-05	275,903	1-Jan-00	1-Jan-01
Rotorua BP	*1-Apr-64*	*17-Dec-05*	*365,641*	*1-Jan-00*	*1-Jan-01*

2.3.3 River flow

Water levels in the Whakatane River from the recorder at Whakatane (Site 15514) were obtained from the National Hydrometric Database and a rating was applied to convert them into flow.

2.3.4 Weather systems

Atmospheric pressure at 6-hourly intervals of time and 1° intervals of longitude and latitude were obtained from "analyses" from NOAA's GFS global atmospheric model. Analyses are the initial conditions used in the model and thus are a best estimate of the actual conditions.

2.4 Analysis methods

Standard time-series data analysis methodologies commonly used in analysis of sea level data were used. Details of the methodologies are provided in Appendix 1 with the process involving:

- A Fourier analysis to identify the various frequencies and measure of the relative energy in the various components causing sea level variation at each tide gauge site;

- Identification of the main tidal constituents and generation of the non-tidal residual at each tide gauge site;

- Extraction of Mean Level of the Sea from the records;
- Identification of storm-surge height distribution at each site based on statistical moments;
- Updated analysis of the correlations between atmospheric pressure and storm surge at Moturiki Island;
- Analysis of the correlations between storm surge at Moturiki Island and storm surge at the other tide gauge sites.

2.5 Tide, storm surge and water level characteristics in the Bay of Plenty

2.5.1 Comparison of tide and storm-surge oscillations in the sea level records

The Fourier spectra (see Appendix 1 for more information) of the periods of record used for sea-level analysis are presented for each gauge site in Figure 2.2.[8] The largest peak is the twice-daily semi-diurnal tide at 29 º/h (or period of 12.4 hours).

The most notable difference between the various spectra is in the shallow-water tide region from 45 º/h and above (i.e., periods below 8 hours). For Moturiki Island, there are few spikes in this region, but for Salisbury Wharf and Sulphur Point there are spikes at 45, 60 and 90 º/h (or periods of 8, 6 and 4hours), and for the other sites there are numerous spikes. The reason for this is that as the primary tides propagate into a harbour or up a river, the shape of the tidal wave changes, with the front face becoming steeper (i.e. flooding tide is shorter and faster) and the back face becoming flatter (ebbing tide longer and slower) and low tide extending for a longer time than high tide. These frictional effects become more pronounced the further the station is from the mouth of the harbour or river.

[8] The frequency along the x-axis is presented in terms of degrees around a cycle per hour. To derive the cycle period, simply divide 360° by the frequency in º/h.

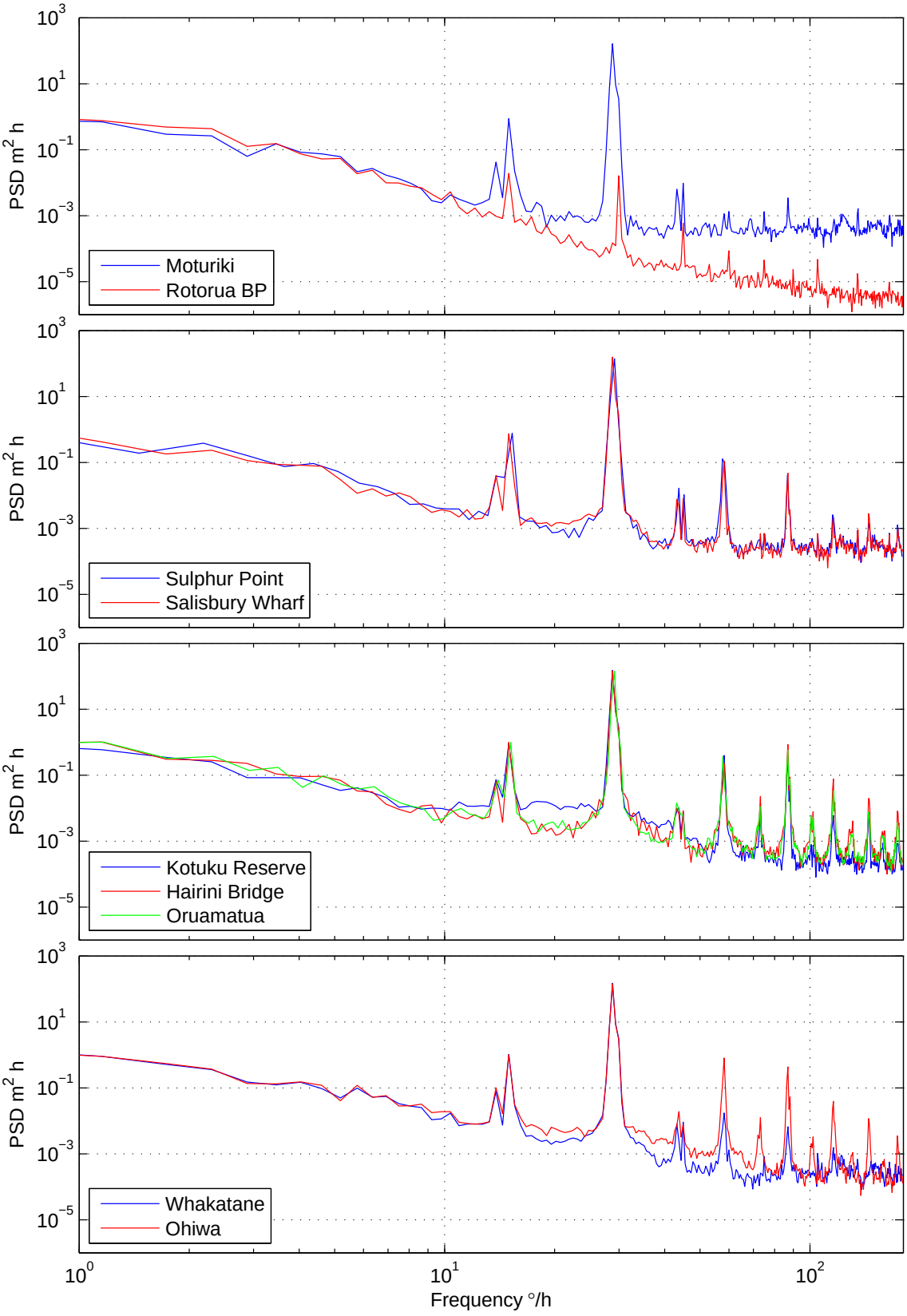

Figure 2.2: Fourier spectra of each of the gauge sites used in sea-level analysis (see Table 2.1).

The shape of the atmospheric pressure spectrum from Rotorua barometric data is somewhat different (Figure 2.2), though there are some small spikes that appear to coincide with the tidal spikes in the Moturiki Island spectrum. These spikes are in fact atmospheric tides generated by absorption of water vapour in the stratosphere. They are at periods of 24, 12, 8, 6, 4 h, being generated by solar effects. There is also a tiny peak at 12.42 h corresponding to the effect of the Moon on atmospheric pressure. The peak is relatively insignificant compared to the Sun's effects and this repudiates the notion that the Moon affects weather.

The slopes of the storm surge portions of the spectra (left-hand side of plots) and the corresponding Hurst parameters[9] are presented in Table 2.2. Atmospheric pressure is highly persistent and storm surge at Moturiki Island, Sulphur Point, Salisbury Wharf and Hairini Bridge is only slightly less persistent. However, storm surge at Kotuku Reserve, Whakatane and Ohiwa are all essentially non-persistent indicating there is a degree of randomness in the storm-surge signal. Thus, in-harbour effects appear to be influencing the storm surge propagation, leading to a reduction in harbour persistence of storm-surge events.

Table 2.2: Spectral slopes and corresponding Hurst parameters derived from the storm surge portion of the spectra ($1 < f < 10$ °/h) in Figure 2.2.

Station	β	H
Sulphur Point	2.500	0.750
Salisbury Wharf	2.643	0.822
Kotuku Reserve	2.170	0.585
Hairini Bridge	2.512	0.756
Oruamatua	2.521	0.761
Whakatane	2.017	0.508
Ohiwa	1.874	0.437
Moturiki	2.689	0.845
Rotorua BP	*2.949*	*0.974*

[9] The Hurst parameter takes values between zero and unity and is an indication of "persistence". If a signal is persistent (close to unity), then the data up to the present can be used to forecast future values, but if the signal is non-persistent (less than 0.5), then there is insufficient pattern to the data and forecasting is not possible.

2.5.2 Tides

The four major tidal constituents derived from the tidal analysis are presented in Table 2.3, where the symbols denote:

- K_1: the lunisolar diurnal[10] tide, which arises from Sun and Moon's paths over the Equator being at various inclines or declines (angles) to the Equator line;
- N_2: the elliptical semi-diurnal[11] tide, which arises from Moon's elliptical (non-circular) orbit about Earth;
- M_2: the lunar semi-diurnal tide, which arises from the direct gravitational attraction of Moon on Earth's waters;
- S_2: the solar semi-diurnal tide, which arises from the direct gravitational attraction of Sun on Earth's waters.

The time shift for a particular station is the number of hours that high tide occurs there after it has occurred at Moturiki Island. Thus, a negative number indicates that high tide occurs there **before** it occurs at Moturiki Island.

Amplitude is the **half-range** (metres) of the relevant tide component.

Table 2.3: Amplitudes and time shifts, Δt , from Moturiki Island of the 4 major tidal constituents.

Station	K_1		N_2		M_2		S_2	
	Amp (m)	Δt (hrs)	Amp (m)	Δt (hrs)	Amp (m)	Δt (hrs)	Amp (m)	Δt (hrs)
Sulphur Point	0.053	0.70	0.155	0.35	0.740	0.35	0.091	0.46
Salisbury Wharf	0.053	0.44	0.150	0.32	0.704	0.30	0.088	0.36
Kotuku Reserve	0.053	1.49	0.132	1.52	0.719	1.17	0.083	1.62
Hairini Bridge	0.052	1.13	0.126	1.07	0.709	0.97	0.081	1.20
Oruamatua	0.051	1.17	0.129	1.33	0.705	1.08	0.086	1.40
Whakatane	0.056	-0.42	0.142	0.18	0.714	0.09	0.093	0.22
Ohiwa	0.055	0.05	0.139	0.84	0.702	0.62	0.087	0.90
Moturiki	0.055	0.00	0.161	0.00	0.731	0.00	0.100	0.00

[10] Diurnal means once-daily.
[11] Semi-diurnal means twice-daily.

M_2 is by far the largest tide, followed by N_2, S_2 and K_1. That N_2 is greater than S_2 is relatively unusual. It means that monthly perigean/apogean tides predominate over fortnightly spring/neap tides and that large tidal ranges can occur when lunar perigee[12] coincides with Full Moon and New Moon. The reasons for this relate to the way S_2 propagates around New Zealand, as explained by Walters et al. (2001). M_2 penetrates into the harbours and river with little attenuation, as does K_1, but N_2 and S_2 attenuate the further the station is from the open sea. Time shifts in excess of 1 hour occur for stations far from the open sea. The tides occur at Whakatane at about the same time as Moturiki Island (in fact, K_1 arrives earlier) because the tides are propagating around the coastline in a counter-clockwise direction with the land on their left, so the tides take about the same time to propagate towards the Whakatane Wharf site as they do to reach Moturiki Island.

Such tidal comparisons (amplitude and high-water time delays) between sites are important as they are inter-connected with the occurrence of peak storm-tides at each gauge (usually at high tide) compared with the open sea.

2.5.3 Storm-surge distributions

Statistical moments (see Appendix 1 for more information) provide information on how data (storm surge in this case) are distributed. These are presented in Table 2.4 for the eight tide gauge locations. The storm surge signal was extracted according to the method outlined in Appendix 1, and is relative to the mean level of the sea at the time the sea-level data was recorded. The variation of the mean level of the sea is discussed in Section 2.7.

[12] Perigee is when Moon is closest to Earth in its elliptical orbit and apogee is when Moon is furthest from Earth.

Table 2.4: Statistical moments of storm surge where *N* is the number of hourly data that were used in the analysis, SD is the standard deviation (square root of the variance), and the percentages represent storm-surge heights from the cumulative distribution function (CDF).

Station	N	SD (m)	Skewness	Kurtosis	5% (m)	50% (m)	95% (m)
Sulphur Point	82,154	0.069	0.649	1.214	-0.103	-0.007	0.122
Salisbury Wharf	125,133	0.066	0.615	1.075	-0.098	-0.007	0.118
Kotuku Reserve	32,722	0.067	0.721	1.402	-0.094	-0.007	0.120
Hairini Bridge	26,585	0.078	0.675	1.949	-0.118	-0.006	0.137
Oruamatua	25,170	0.070	0.507	0.886	-0.101	-0.006	0.127
Whakatane	90,401	0.114	2.836	21.671	-0.133	-0.014	0.179
Ohiwa	55,200	0.083	0.831	1.424	-0.114	-0.011	0.154
Moturiki	275,903	0.064	0.716	2.033	-0.094	-0.006	0.113
Rotorua BP	*365,641*	*0.072*	*-0.348*	*0.285*	*-0.128*	*0.005*	*0.110*

The standard deviations are all greater than the standard deviation at Moturiki Island indicating a slight overall amplification of storm surge as it propagates into Tauranga Harbour, and this is enhanced the further up the harbour the station is. For the eastern sites (Whakatane and Ohiwa) the amplification is substantial, but it is not clear if this is because the storm surge on the coast is larger (digital records not available) or if it is also a river or harbour effect. The observations and analysis of Blackwood (1997) would echo the former, with larger storm surges occurring in the eastern localities. Certainly, for Whakatane there is a river effect overall on the record that is reflected in the much higher skewness and kurtosis than other sites, corresponding to flood peaks (which are always positive). Neglecting Whakatane, the pattern is for slightly positive skewness and kurtosis indicating peaks (positive storm surges) outnumber the troughs (negative storm surges)[13] and are higher.

This is also indicated in the cumulative distribution function where the 5% level has smaller magnitude than the 95% level. Notice that for atmospheric pressure the opposite is true, with negative skewness and the 5% magnitude being higher than the 95% magnitude. This indicates the troughs are deeper than the peaks, but the small kurtosis indicates they are not very much deeper. That atmospheric pressure exhibits the opposite effect to storm surge is entirely consistent with the inverted barometer relationship (see Section 2.1).

[13] Negative storm-surges usually occur during high pressure weather systems (anti-cyclones) when the barometric pressure is high and/or when winds are persistently directed offshore (e.g. south-westerlies).

2.5.4 Relationship between atmospheric pressure and storm surge at Moturiki Island

A regression analysis was performed on the data in two sets:

- Atmospheric pressure versus storm surge at Moturiki Island; and
- Storm surge at Moturiki Island versus storm surge at other sites (see next section).

The analysis between atmospheric pressure and storm surge was limited to the Moturiki Island sea-level gauge data as data for the other sites are somewhat patchy, whereas the atmospheric pressure and Moturiki Island data overlap for the extended period from June 1974 to November 2005.

The first step was to carry out a cross-correlation analysis to determine the optimum lag. The result of this is shown in Figure 2.3 in which the atmospheric pressure data have been inverted. The figure indicates that maximum cross correlation occurs when atmospheric pressure lags storm surge at Moturiki Island by 3 hours (which is consistent with the earlier findings of Goring, 1995).

In the subsequent regression analysis the atmospheric pressure record was lagged by 3 hours. The results of the regression for each of the 4 wavelet decomposition levels are presented in Figure 2.4, and listed along with the regression on the total storm surge in Table 2.5. There is an almost direct inverse relationship between atmospheric pressure and storm surge at timescales of 48 h (i.e., almost the theoretical inverted barometer factor of –1 cm/hPa), but for longer timescales, the barometric factor is c. –0.6 cm/hPa indicating attenuation of the effect of changes in atmospheric pressure. The coefficient of determination, r^2, is a measure of the proportion of the variance of Moturiki storm surge that is explained by atmospheric pressure, so only between 50 and 60% of the storm surge can be explained by changes in atmospheric pressure. The possible reasons for this will be addressed later.

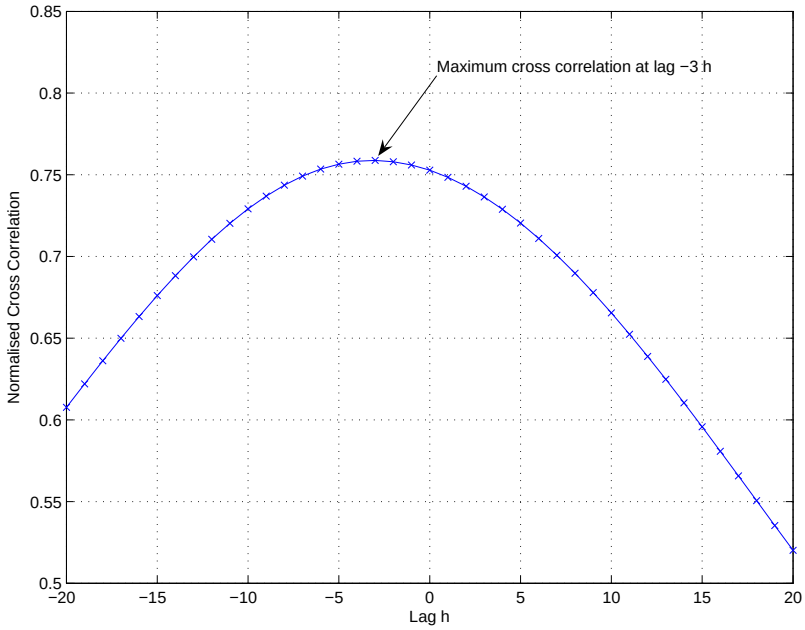

Figure 2.3: Cross correlation of Rotorua Airport inverted barometer with Moturiki Island storm surge.

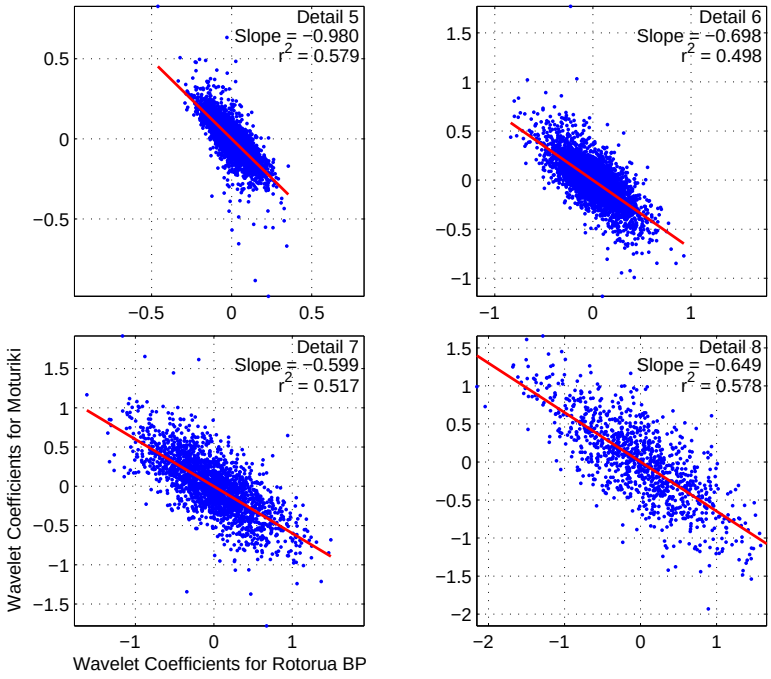

Figure 2.4: Regression of wavelet detail coefficients of Rotorua Airport atmospheric pressure against Moturiki Island storm surge. See Table 2.5 for list of results and the timescales that relate to each wavelet detail.

Table 2.5: Results of regression of Rotorua Airport atmospheric pressure against storm surge at Moturiki Island, showing the slope of the regression line (i.e., inverted-barometer factor) and the coefficient of determination, r^2.

Regression parameter	Storm surge timescale (centre of band) (wavelet detail)				All 4 timescales
	48 hr (detail #5)	96 hr (detail #6)	192 hr (detail #7)	384 hr (detail #8)	
Slope (cm/hPa)	-0.980	-0.698	-0.599	-0.649	-0.673
r^2	0.579	0.498	0.517	0.578	0.566

2.5.5 Relationship between storm surge at Moturiki Island and storm surge at other sites

The overall lag between storm surges at Moturiki and storm surges at the other sites is presented in Table 2.6, remembering this only applies to fairly short records when concurrent data were available (Table 2.1). The results show the overall lag to nearest hour varies from zero for Salisbury Wharf, Kotuku Reserve and Hairini Bridge, to 4 h for Whakatane. The exact lag is not well-defined because the peak of the cross-correlation function (Figure 2.3) is rather broad and this explains why adjacent sites like Sulphur Point and Salisbury Wharf have different lags.

Table 2.6: Results of cross correlation between storm surge at Moturiki Island and storm surge at other sites.

Station	Lag (hrs)	R_{max}
Sulphur Point	1	0.934
Salisbury Wharf	0	0.767
Kotuku Reserve	0	0.886
Hairini Bridge	0	0.833
Oruamatua	2	0.780
Whakatane	4	0.657
Ohiwa	1	0.857

The lags from Table 2.6 were applied to the storm surge time series for the relevant sites and regression was carried out against storm surge at Moturiki Island. The resulting regression parameters are presented in Tables 2.7 and 2.8, with typical results shown in Figure 2.5. Table 2.7, lists the amplitude of the relationship between storm surge at Moturiki and storm surge at the other sites. This indicates that for the

sites in Tauranga Harbour there was little difference from Moturiki Island (for different periods in the records between 1998 and 2004) , but for the eastern sites there is a 10 to 20% amplification. For Whakatane, this result is not conclusive because the record includes storm surge-like events that are actually river floods, and this explains the low coefficient of determination (Table 2.8).

Table 2.7: Slope of the regression line between storm surge at Moturiki Island and at other sites with the 95% confidence intervals.

Station	Storm surge timescale				All 4
	48 hrs (detail #5)	96 hrs (detail #6)	192 hrs (detail #7)	384 hrs (detail #8)	timescales
Sulphur Point	1.08±0.02	1.10±0.02	1.08±0.02	0.99±0. 04	1.01±0.00
Salisbury Wharf	1.02±0.01	1.05±0.01	1.04±0.02	1.00± 0.03	0.96±0.00
Kotuku Reserve	1.06±0.04	1.05±0.03	1.03±0.05	1.05±0.09	0.9 5±0.01
Hairini Bridge	1.03±0.05	1.02±0.04	0.99±0.06	0.97±0 .17	1.04±0.01
Oruamatua	1.00±0.05	1.00±0.04	0.95±0.07	0.91±0.12	0 .88±0.01
Whakatane	1.21±0.07	1.27±0.08	1.34±0.13	1.38±0.16	1 .21±0.01
Ohiwa	1.21±0.05	1.25±0.05	1.20±0.06	1.16±0.10	1.13± 0.01

Table 2.8: Coefficient of determination, r^2, between storm surge at Moturiki Island and at other sites.

Station	Storm surge timescale				All 4
	48 hrs (detail #5)	96 hrs (detail #6)	192 hrs (detail #7)	384 hrs (detail #8)	timescales
Sulphur Point	0.866	0.936	0.955	0.925	0.890
Salisbury Wharf	0.854	0.928	0.919	0.935	0.843
Kotuku Reserve	0.738	0.908	0.898	0.872	0.786
Hairini Bridge	0.716	0.890	0.837	0.578	0.693
Oruamatua	0.727	0.865	0.852	0.803	0.609
Whakatane	0.303	0.479	0.480	0.618	0.431
Ohiwa	0.574	0.778	0.806	0.773	0.735

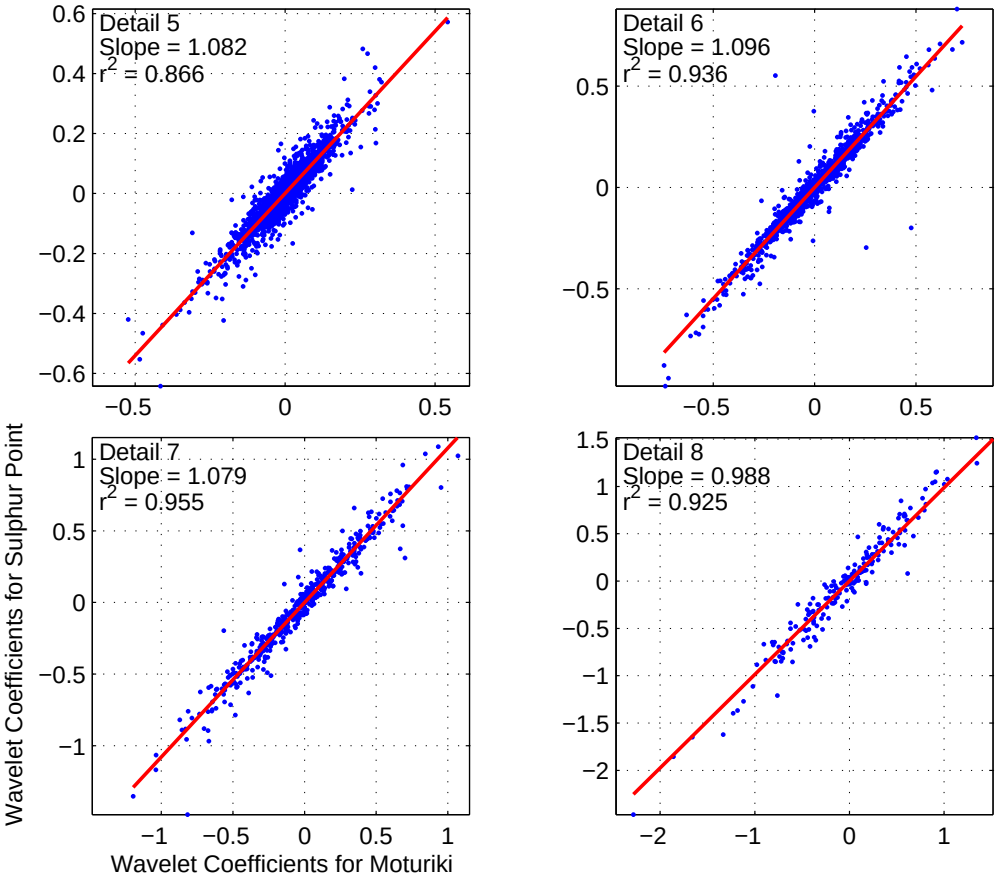

Figure 2.5: Typical regression of Moturiki Island storm surge wavelet-detail coefficients for 48, 96, 192, 384 hour timescales against storm surge at another site (in this case, Sulphur Point).

2.5.6 Storm surge characteristics in the eastern Bay of Plenty

The storm surges at Ohiwa and Whakatane appears to be different from the storm surge at the other sites. Firstly, the Hurst parameter is low (Table 2.2) indicating low persistence and therefore less internal structure. Secondly, the storm surge heights are generally greater, especially during events. For Whakatane, these differences can sometimes be explained by higher river flow at the time of storm surge (but not always the case). However, the differences at Ohiwa cannot be so simply explained. To examine this further, the tidal part of the Ohiwa record was examined in more detail, especially during large storm surge events. This revealed that during storm surge events, the shape of the tidal wave at Ohiwa changes slightly, with low tide being up to 0.2 m higher than expected and the front face of the wave steepening. These effects indicate there is a nonlinear interaction occurring between the tide and storm surge. A similar interaction occurs in a river when a flood propagating down the river interacts with the tide propagating up the river, but the rivers flowing into the

Ohiwa Harbour seem too small for this to be a factor. Therefore, it is suggested that during storm surge events, the flow through the harbour entrance is modified in some way that affects how the tide propagates into the harbour. Detailed analysis of this process is beyond the scope of this study and would require a hydrodynamic model to resolve. However, it indicates that some caution may be required in applying Ohiwa Harbour storm-surge heights to the open coast of the eastern region. This situation has already been recognised by EBOP, who installed a sea-level gauge in 2005 off Kohi Point between Ohope and Whakatane.

2.6 Analysis of storm surge events and trends

The Moturiki Island storm surge record from 1974 was analysed for events above a series of thresholds of maximum storm surge level. Each event was assumed to be separated from the next event by at least 36 hrs.

It should be noted that this Moturiki storm-surge record doesn't include the severe Cyclone *Giselle* storm surge (occurred earlier in 1968) and the gauge was damaged before the peak storm surge from Cyclone *Fergus* in December 1996. Also there is a degree of smoothing of storm surge peaks from the wavelet filtering process. Also steeper, shorter storm surges of less than 36 hours in duration are damped considerably in the analysis. However this analysis is common across all gauge records, so provides a consistent basis for comparison between sites.

The main focii with the analysis discussed below is: a) are there any trends in the number and intensity of small to moderate storm surges (given the period since 1974 has been relatively benign in terms of severe storm surge apart from Cyclone Fergus); and b) comparing the response at each gauge location with Moturiki for some particular storm events that have occurred more recently since 2000.

The results for the annual composition of storm-surge events are shown in Figure 2.6 in the form of histograms for the various thresholds. A number of points arise from this figure:

- The number of events greater than 0.1 m maximum storm surge height occurring each year was between 12 and 23, with a mean of 19 per year (593 events in 30 years).

- Increasing the threshold to 0.2 m has the effect of reducing the mean number of events to 3 per year (89 in the 30 years).

- Events greater than 0.3 m occur occasionally (14 in 30 years) and events greater than 0.4 m are infrequent (7 events in 30 years).

- There appears to be a slight trend of increasing numbers of events per year exceeding 0.1 m over the 30 years of record (1974–2005), but the number of events per year exceeding 0.2 m shows a slight downwards trend.

- The shift of the 20-30 year Interdecadal Pacific Oscillation (IPO) to it's negative phase around 1998 doesn't, at this stage anyway, seem to have provided the background Pacific-wide climate state to engender any increase in numbers or intensity of storm surges at Moturiki than the previous positive phase of the IPO (1976–1998).

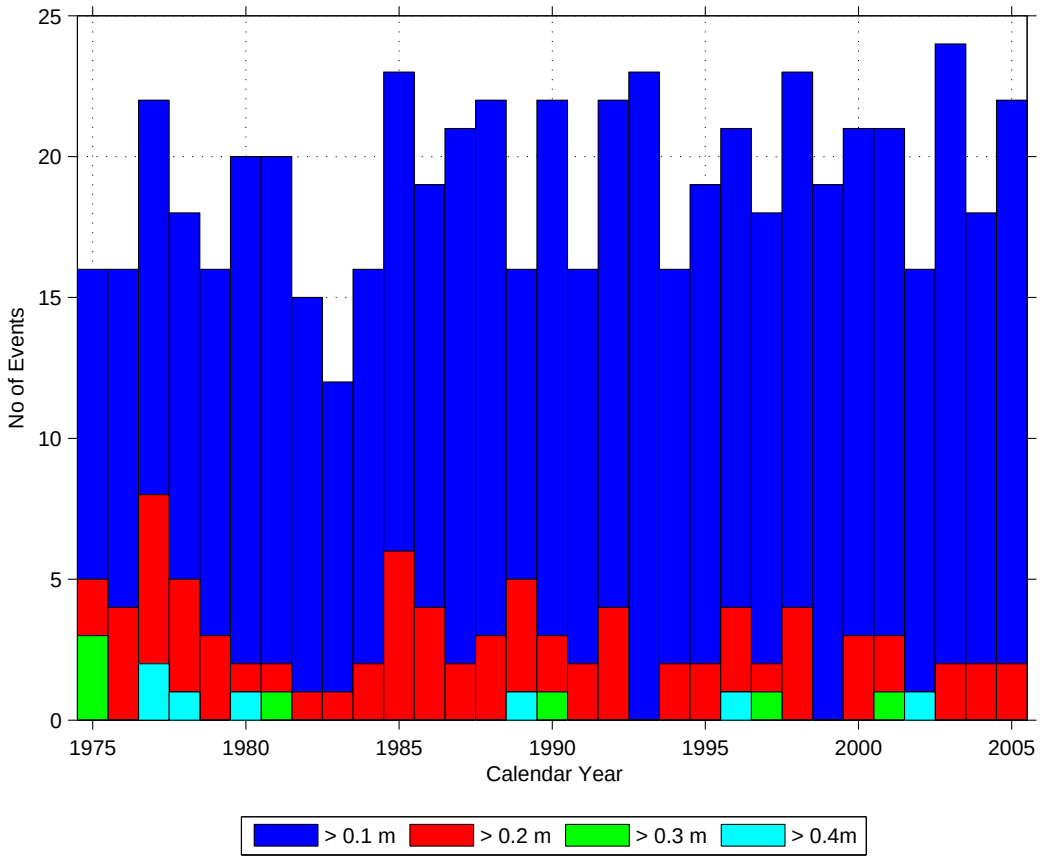

Figure 2.6: Histograms of the number of storm surge events at Moturiki Island exceeding various thresholds in each calendar year.

2.6.1 Weather bomb of 21 June 2002

The so-called weather bomb that occurred on 21-Jun-2002 resulted from a low-pressure system that had propagated rapidly down from the tropics (see Figure 2.7) being squeezed by a large anticyclone to the east of New Zealand, thus generating sustained northerly winds in the Bay of Plenty. The eye of the depression (minimum pressures of 980 hPa) passed well to the southwest of the Bay of Plenty, so local pressures were not particularly low (minimum local pressure was 992 hPa).

The resulting storm surges at each of the gauges that were operating (using the same analysis technique for all records) are shown in Figure 2.8. A number of points arise from this figure:

- Moturiki Island storm surge height peaked at 0.4 m, the 6th highest event to occur in the 30 years of record;
- There were no data for Sulphur Point, and the Salisbury Wharf (Tug Berth) gauge failed the day before the event;
- Kotuku Reserve and Hairini Bridge gave similar results, with peaks of 0.35 m occurring a few hours before Moturiki (i.e., lower than Moturiki, confirming the relationship in the analysis by Tonkin & Taylor (1999);
- Oruamatua showed much lower storm surge than other sites;
- The peak at Ohiwa was slightly higher than that at Moturiki Island and occurred a few hours later.

Apparently the storm surge at Whakatane was much larger than elsewhere (Figure 2.8) and occurred later, but this is likely to have been caused by the flood that occurred in the Whakatane River, as shown in Figure 2.9.

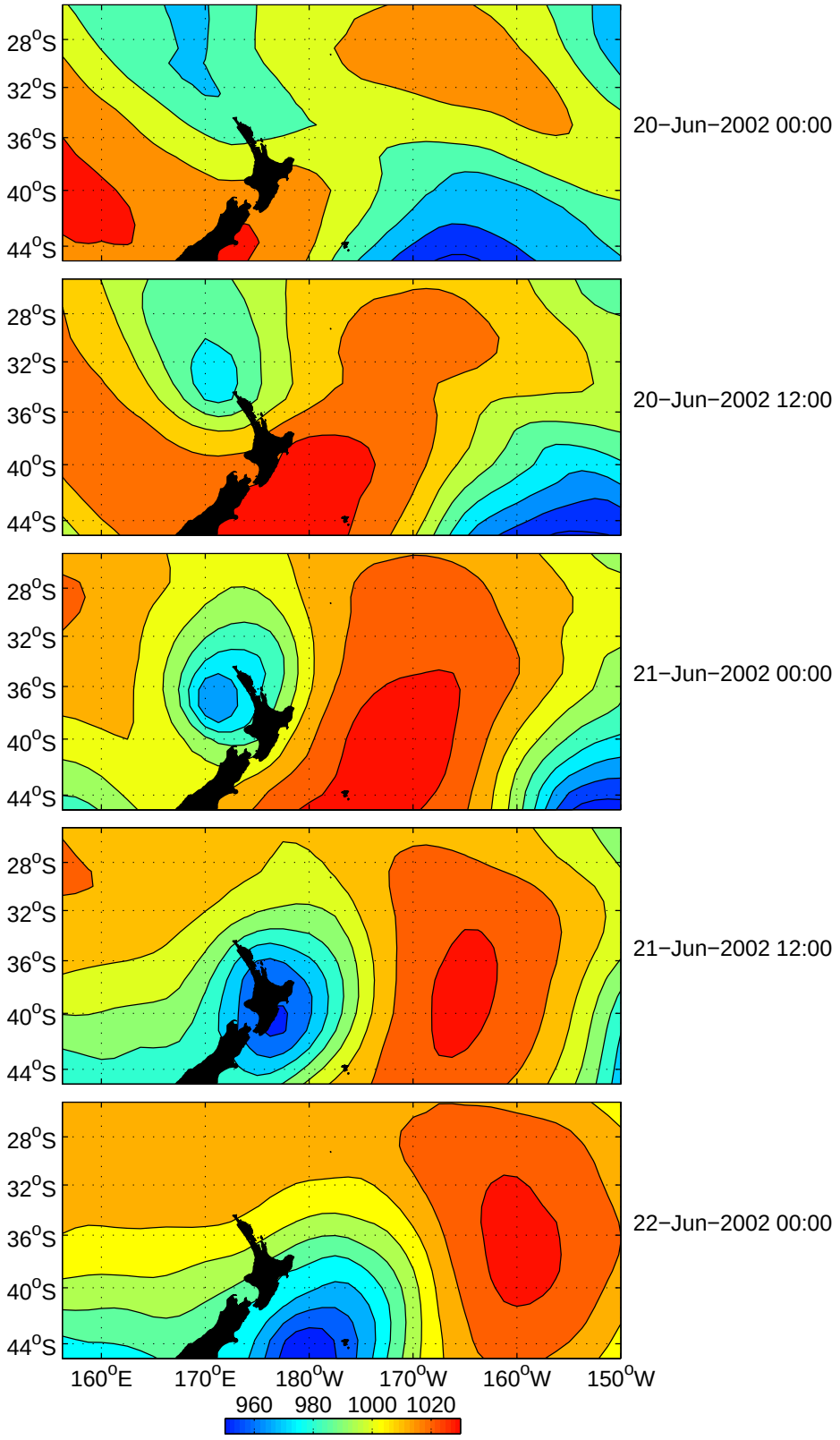

Figure 2.7: Maps of MSL pressure (in hPa) for the New Zealand region during the weather bomb of 21-Jun-2002.

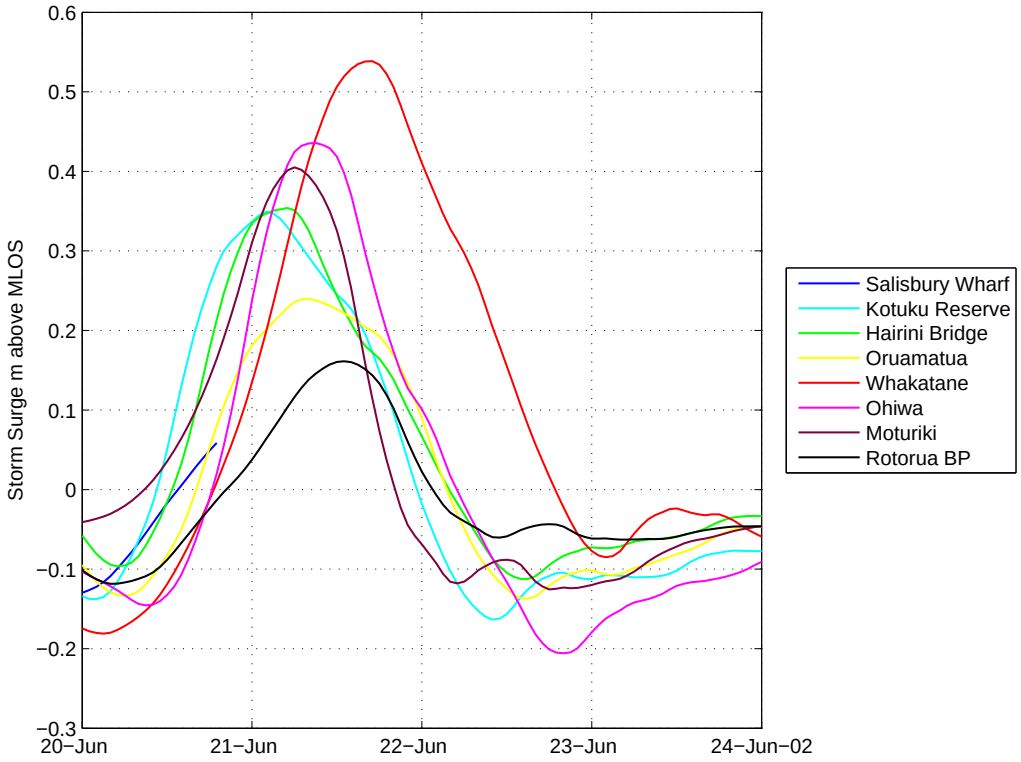

Figure 2.8: Storm surge above the prevailing mean level of the sea at the time for various gauge locations in the Bay of Plenty for the weather bomb of 21-Jun-2002.

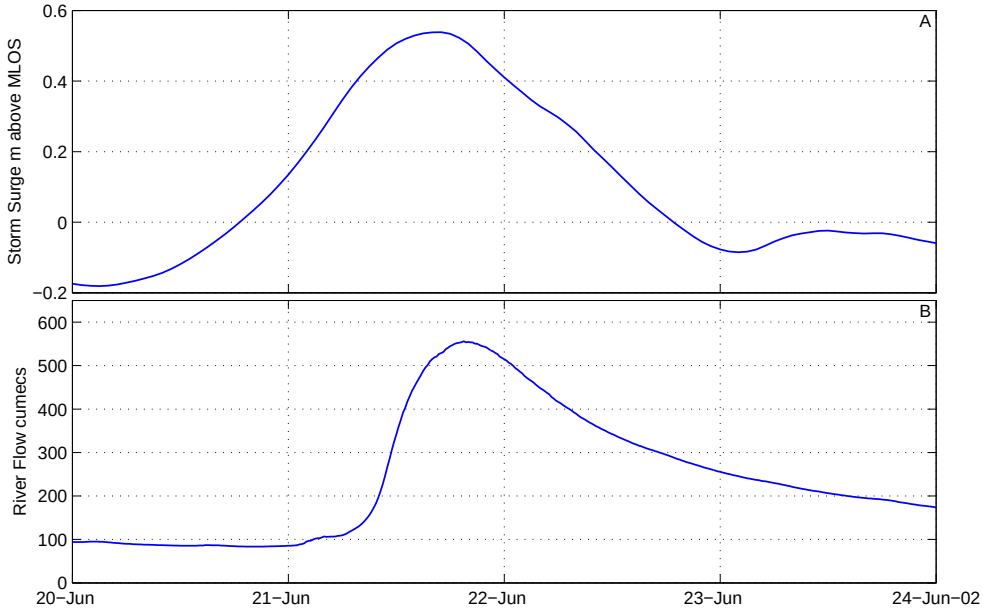

Figure 2.9: Comparison of apparent storm surge at Whakatane (A) and flow in the river at an upstream site (B) for the weather bomb.

It is interesting to compare the wavelet details for storm surge at Moturiki Island with inverted barometer and their difference (the anomaly) for the weather bomb, as shown in Figure 2.10. First of all, there is essentially no difference between storm surge and inverted barometer at 384 hr timescales; while at 192 hr timescales the inverted barometer is essentially zero, though storm surge exhibits an oscillation of 0.1 m amplitude which peaked on 20 June. It is likely that this oscillation is a wave that has propagated into the region, having been generated by a previous pressure change perhaps a week or more before this event. Notice that if this wave had peaked a day later, the storm surge would have been even greater. At 96 hr timescales, the storm surge appears to be in phase with inverted barometer but amplified; whereas at 48 hr timescales, storm surge and inverted barometer appear to be in phase before and after the event, but during the event storm surge has a single oscillation that appears not to be related to inverted barometer. This may be a wind effect, or it could be a wave generated elsewhere that has propagated into the area.

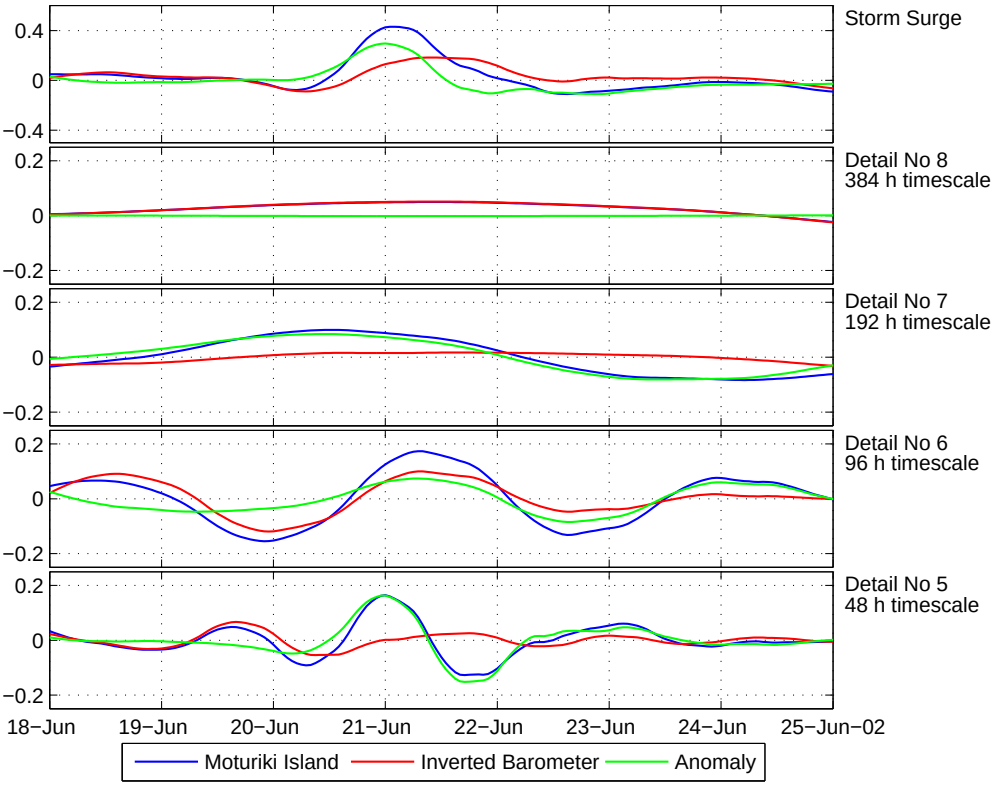

Figure 2.10: Comparison of wavelet details and their sum (top panel) at Moturiki for the weather bomb of 21 June 2002.

2.6.2 Other events

The weather bomb of June 2002 was by far the largest storm surge event that has occurred since 2000. A comparison of storm surge at the various locations for the next three largest events since 2000 (April 2001, August 2003, and July 2004) is presented in Figures 2.11, where Whakatane has been excluded because in each case it was somewhat affected by high river flow. For the first two events, Ohiwa exhibited much larger storm surge than any other site, but for the third (and smallest) event, the storm surge was much less. For the Tauranga sites, there appears to be little pattern, with storm surge being higher than Moturiki Island sometimes and being smaller at other times. In all three cases, the inverted barometer contribution is substantially less than Moturiki Island storm surge.

2.6.3 Comparison with de Lange and Gibb (2000)

Some of the results found in this study seem to conflict with those found in de Lange and Gibb (2000). In particular, the number of events per year (Figure 2.6) appears to be quite different, with there being little discernible variation over the 30 years, even for the 6 or 7 years since 1998 when the IPO changed sign to a negative phase (maybe too early to discern yet). de Lange and Gibb (2000) found that the magnitude and frequency of storm surges was considerably higher during the previous negative phase of the IPO (1960–1976 part of the Salisbury Wharf record) than during the positive IPO period (1976 to 1997).

One of the reasons for this difference is that in this study, we isolated storm surge from MLOS at the time of the event, whereas in previous studies, including that of de Lange and Gibb (2000), storm surge included the long-period effects and rising sea level. Furthermore, de Lange & Gibb used tidal peaks less forecast high tide height to estimate storm surge, whereas in this study we calculated storm surge by band-pass filtering the non-tidal residual. Unfortunately, it is not possible to repeat our analysis on the data prior to 1974 which de Lange & Gibb found gave the largest storm surges. Whether de Lange & Gibb's prediction that storm surges that they calculated for 1960–76 will recur in the next few decades is correct must await further data, but so far there is no evidence of a change in association with the change to the negative phase of the IPO that occurred in 1998 (see Figure 2.6).

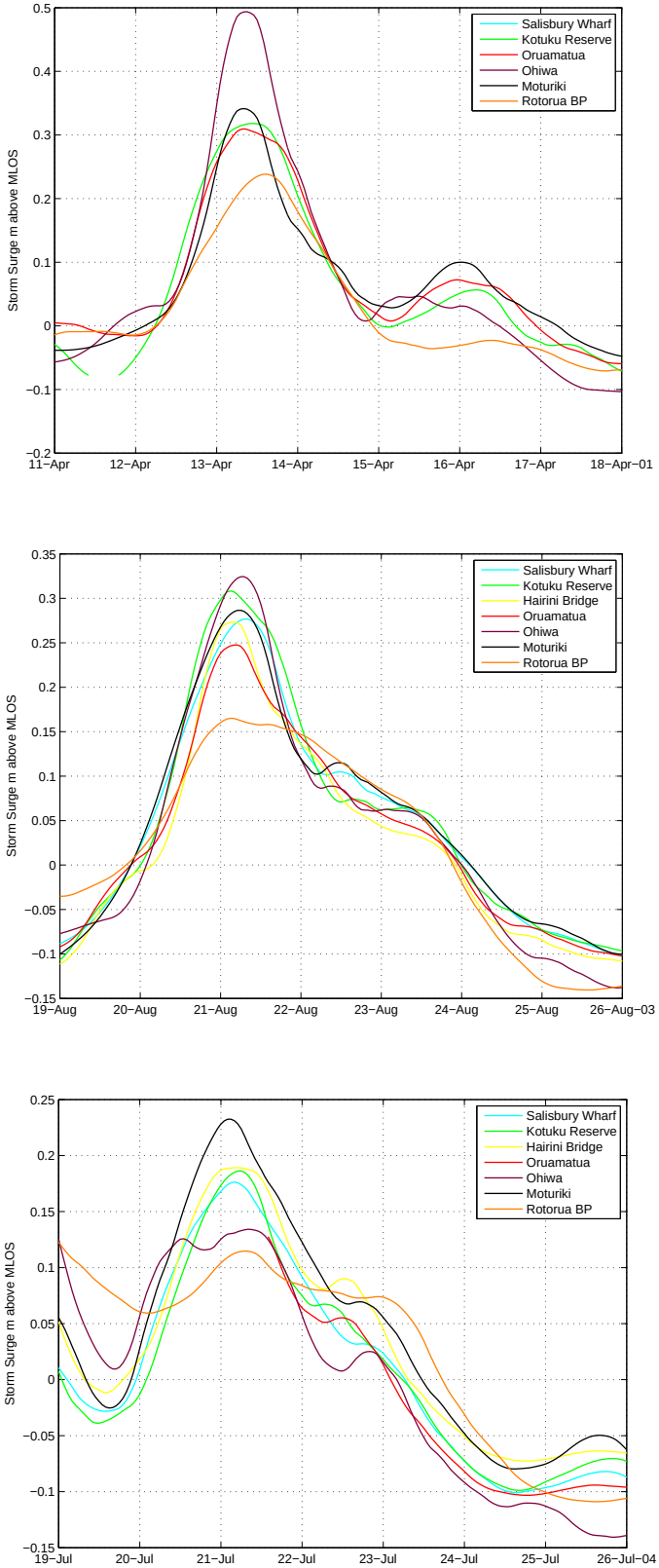

Figure 2.11: The next three largest storm surge events since 2000 after the weather bomb.

2.7 Extreme sea levels and their composition

2.7.1 Analysis of the mean level of the sea (MLOS)

The results of analysis of MLOS for Moturiki Island are presented in Figure 2.12 and Figure 2.13.

The month-to-month variation in MLOS averaged over the 33-year Moturiki record (Figure 2.12) shows an oscillatory pattern, though the seasonal average peak of 0.093 m above MVD-53 (in May) is much flatter than the average seasonal trough of 0.015 m above MVD-53 (in October). The average annual (seasonal) range is 0.078 m. While small, this can make a difference to extreme event inundation on gently-sloping beaches.

The annual means for Moturiki (Figure 2.13) show a rising trend over the 33 years of record, though the variation in MLOS each year about this trend is considerable. This pattern is consistent with other tide gauge data around New Zealand, notably an analysis of over 100 years of mean annual sea levels from the Port of Auckland tide gauge, which shows:

- During El Niño episodes (negative SOI), the mean level of the sea is depressed below normal levels by up to 0.12 m. The converse is true for strong La Niña episodes, where sea levels are higher than normal by a similar amount;

- The IPO signal at 20–30 year cycles facilitates sea-level fluctuations of up to ±0.05 m, with the higher sea levels being recorded during the negative phase of the IPO.

The effect of this has resulted in the average rate of mean sea level rise over the period between 1977 to 1998 (–ve IPO with more frequent and intense El Niño conditions) being relatively flat compared to the 20 to 30 year period prior to that where the rate was much greater. Such a trend would suggest that the rate of mean sea level rise over the next 20 or so years (excluding any influence of global climate change) will be greater than that experienced over the latter two decades of the last century. A hint of this is displayed in Figure 2.13 with the rise since 1998.

A frequency analysis was carried out on the monthly MLOS using the Fred facility in Tideda. It was found that of Gumbel, GEV, and normal distributions, MLOS fitted the normal distribution most closely at extreme values, so this was used. The results are

presented in Table 2.9. As an example, the 1% AEP height of the monthly mean sea level due to climate variability (e.g., ENSO, IPO) is estimated to be 0.21 m above MVD-53 (excluding any climate-change effects or sea-level rise).

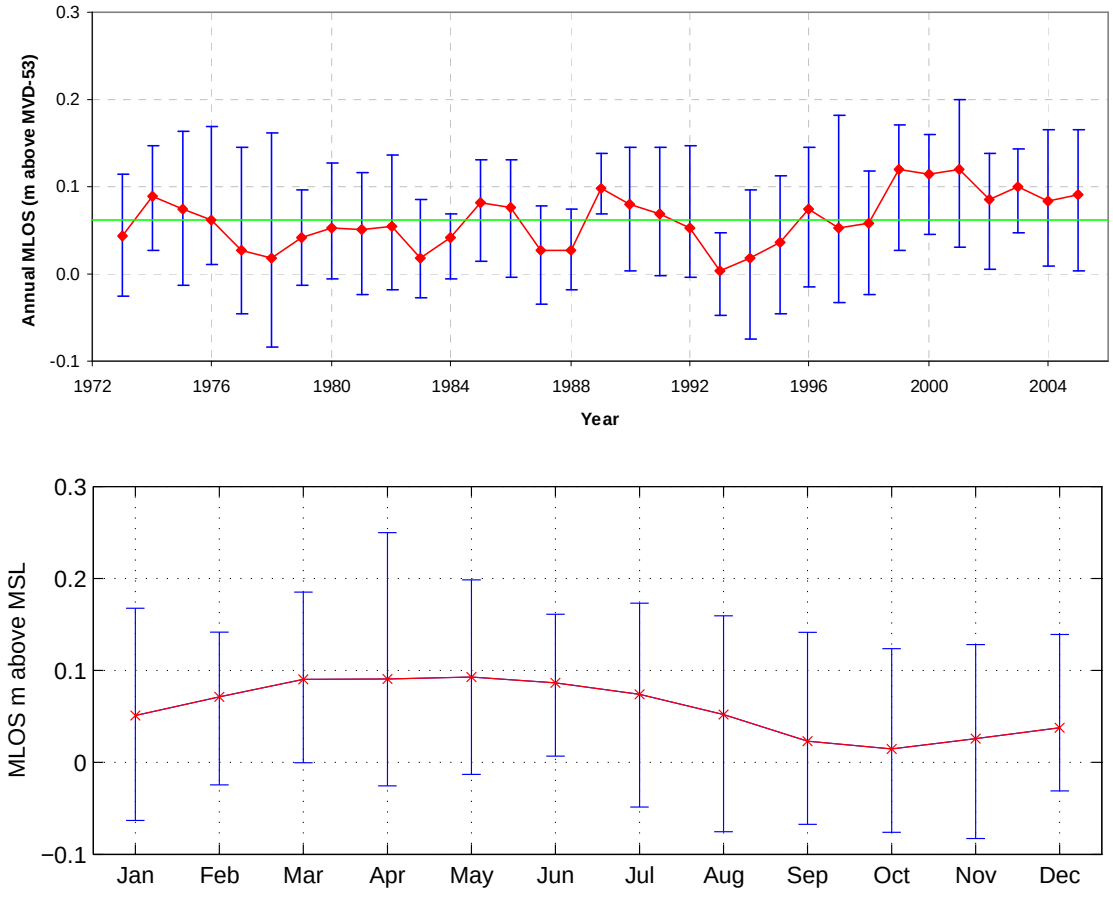

Figure 2.12: MLOS at Moturiki Island for annual means (top) and 33-year means for each calendar month above MVD-53 (Bottom). The bars represent the minimum and maximum value in each year and month respectively.

Table 2.9: Annual exceedance probability for MLOS in m above MVD-53 at Moturiki Island using a normal distribution.

Annual Exceedence Probability	Level (m)
0.2	0.15
0.1	0.17
0.05	0.18
0.02	0.20
0.01	0.21

2.7.2 Storm tide levels

One of the reasons for analysing storm tides in detail is to generate statistics of extreme sea levels that can be used for design. The actual height of the storm tide depends on exactly when the waves of the two phenomena occur. To ascertain the correlation between tide and storm surge at Moturiki Island, and hence extreme sea levels, NIWA's EXTLEV software package has been utilised (see Appendix 1 for more details) using the "revised joint probability method"(RJPM) (Tawn & Vassie, 1991). The present analysis was carried out after correcting for errors in the storm surge record, including an erroneously high event in July 1977 that was included in the earlier RJPM analysis of Goring et al. (1997).

The Annual Exceedence Probability (AEP) estimates for storm tide at Moturiki from the present analysis provided levels that are too low compared with those analysed and used by EBOP (e.g., Blackwood, 1997; Tonkin & Taylor, 1999). The main reason for this is that while Moturiki provides a virtually continuous digital dataset over 33 years for using the RJPM, it only covers a reasonably benign period for storm surge. During that period, the largest storm surge occurred during Cyclone *Fergus*, which damaged the Moturiki gauge before the peak was recorded (estimated to be around a 10% AEP storm-surge event – P. Blackwood, pers. comm.).

In the light of this lack of larger storm surge events, it is suggested that the extreme AEP heights for storm surge that have been based on historic annual maximum observations (e.g., Cyclone *Giselle* in April 1968 estimated to have been about a 2% AEP event) as detailed by Blackwood (1997) and Tonkin & Taylor (1999) be continued to be used for design and planning purposes for the present-day situation depending on the locality. However, these AEP estimates already implicitly include the inter-annual and inter-decadal MLOS variability, through the use of an annual maxima, so the estimates in Table 2.9 should not be added onto the present EBOP extreme AEP values for storm surge.

Previous sections and the observations of Blackwood (1997) and EBOP staff have shown there are spatial differences in the storm surge response for the present-day climate. Table 2.3 indicates that the tides at the other sites in the western and central Bay of Plenty are within a cm or two of Moturiki Island, so there is unlikely to be a significant effect from the tide. However, the storm surge relationship in Table 2.7 and the analysis of small storms in Section 2.6 (e.g., weather bomb of June 2002) confirms that the storm surge in Tauranga Harbour is generally less than at Moturiki Island, whereas in the central-eastern Bay of Plenty it is generally greater than at Moturiki Island. These differences appear to be reinforced during large events, as indicated in Figures 2.8 and 2.11 and confirmed by the analysis of larger extra-tropical cyclone events like *Fergus* by Blackwood (1997).

2.8 Accelerated sea level rise in the Bay of Plenty region

Since the early to mid 1800s, relative sea level around New Zealand has been rising at an average linear rate of 0.16 m per century. However, as global warming becomes established and the oceans begin to warm, the rise in sea level is projected to accelerate in the near future and continue to rise over several centuries.

2.8.1 Historic rate of sea-level rise

The Moturiki record, which commenced in 1973, is relatively short even at 33 years long to adequately gauge the rate of long-term sea-level rise in the Bay of Plenty region. Therefore, annual means of sea level at Moturiki were compared with the Port of Auckland annual means during the corresponding period 1973 to 2005. By undertaking this comparison, it will become clear if the much longer Port of Auckland gauge record (since 1899) can be used as a surrogate for sea-level rise in the Bay of Plenty, given they are on the oceanographically-similar north-east coast. Figure 2.13 shows the comparison between the annual MLOS at Moturiki and the Port of Auckland from 1973 to 2005 inclusive.[14] The annual means at both gauge sites track reasonably closely, given a consistent offset. Little change in the trend of relative sea level occurred from 1973 to 1998 (apart from inter-annual ENSO-driven cycles), but sea level has been generally higher since 1999 (probably due to change to negative phase of the IPO).

[14] Auckland data supplied courtesy of Ports of Auckland Ltd. and LINZ.

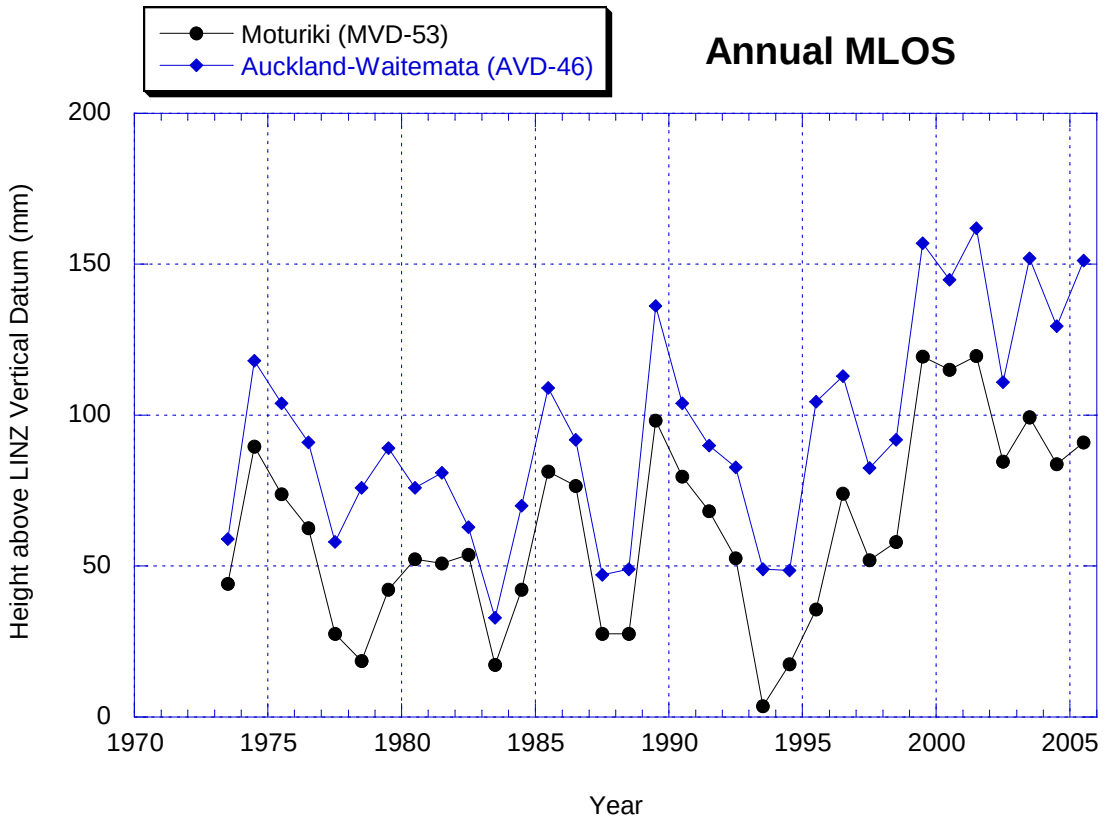

Figure 2.13: Comparison of the last 33 years of annual mean level of sea (MLOS) for Moturiki relative to Moturiki Vertical Datum-1953 (MVD-53) and the Port of Auckland-Waitemata record for the same period relative to Auckland Vertical Datum-1946 (AVD-46).

The close relationship is confirmed by the high correlation between the annual means at the two gauges shown in Figure 2.14. The average offset between the annual means at Auckland is about 3 cm higher than at Moturiki, generally reflecting the difference between the two respective LINZ vertical datums. The standard deviation in the annual MLOS for the Moturiki gauge record of 31 mm is slightly lower than the 35 mm for the Auckland record. This is probably explained by the longer gaps in the Auckland record before a new port gauge commenced in 2001, but also would include variability in response to climate signals between the two sites. Note: the 2005 annual MLOS for Moturiki is probably higher than plotted in Figure 2.13 due to no data for half of December 2005 when other gauges recorded a monthly increase.

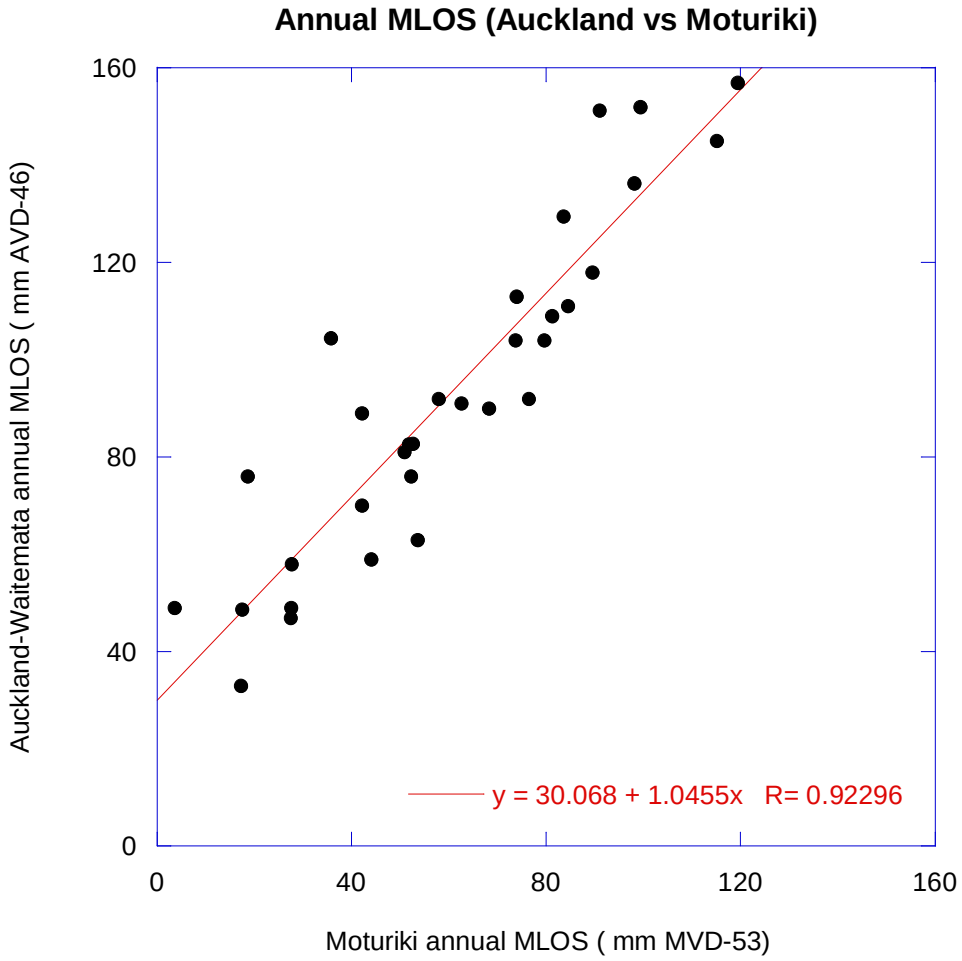

Figure 2.14: Regression between annual mean level of sea (MLOS) for Moturiki and Auckland-Waitemata, resulting in a Pearson's *R* value of 0.92, indicating a strong correlation between the two sites.

The annual values for mean level of the sea from the Moturiki (Figure 2.13) are plotted in Figure 2.15 within context of the linear trend in relative sea-level rise from the much longer Port of Auckland gauge (since 1899) and the IPCC (2001) projections for the average global sea-level rise over this century. Sea level data and projections in Figure 2.15 are all reduced to Moturiki Vertical Datum-1953 (MVD-53) to facilitate a direct link to engineering and planning design levels.

The above analysis and comparison between Auckland (Waitemata Harbour) and Moturiki indicate that the longer Port of Auckland record can be used as a surrogate for the historic sea-level rise at Mt. Maunganui.

Hannah (2004) concluded from his thorough analysis of the Auckland record from 1899 to 1999 (incl.) that the relative rate of rise between sea and land was 1.30 mm/yr.

This value was confirmed by NIWA performing a simple linear regression analysis of the annual MLOS for Auckland (without invoking any atmospheric pressure, temperature or long-period tide corrections) which resulted in a similar rate of rise of 1.34 mm/yr for the same period. Any departure from a linear trend (i.e., acceleration in sea level rise) was found by Hannah (2004) to be not statistically significant.

Updating the analysis over the recent period for years 2000 to 2005 inclusive, not covered in Hannah's analysis, results in a slightly higher rate of rise of 1.40 mm/yr (due to the increased level of the annual MLOS in the last few years—see Figure 2.13). The vertical land movement at Auckland was deemed to be insignificant by Hannah (2004). This rate of rise is also within the commonly accepted 1–2 mm/yr range (with a mean around 1.7–1.8 mm/yr) for the global average rate of rise over last century [IPCC(2001)]. This comparison suggests that the measured relative rate of rise at Auckland is similar to the global average rate of rise and by inference, the IPCC projections for global average sea-level rise should also apply.

In lieu of long-term, accurate sea-level records for either Mt. Maunganui or Tauranga, we have assumed the same rate of rise (1.40 mm/yr) has applied to the Bay of Plenty in the period 1899 to 2005. This same trend has been plotted in Figure 2.15, but transformed to MVD–53 levels such that the average MLOS around 1980 was anchored to 0.05 m above MVD-53 (see Figure 2.13). Calculations based on the 1.4 mm/yr trend anchored at 1980, result in a 2005 value of the average MLOS of 0.085 m above MVD–53 (confirmed by Figure 2.13) and a 1950 value of 0.008 m (i.e., close to zero), which straddles the 1949–1952 period of sea-level measurements used to originally set the zero level of the Moturiki Vertical Datum in 1953.

The only remaining question on historic rates of rise for the Bay of Plenty is the vertical land stability that may regionally or locally modify this assumed relative sea-level rise trend of 1.40 mm/yr. Coastal subsidence results in a higher relative sea-level rise than the global average rate, and vice versa for coastal uplift. From the literature, vertical land movements appear to vary considerably along the coastline from Waihi Beach to Lottin Point (near Cape Runaway) that defines the Bay of Plenty region. Pillans (1986, 1990) reported that the western section (Waihi Beach to Papamoa) has been relatively stable. In contrast, the central portion of the region where the Taupo Volcanic Zone intersects with the coast (broadly between Maketu and Whakatane River) is an area of long-term subsidence, especially the Whakatane Graben between Matata and Whakatane River, where average subsidence rates have been of the order of 0.4–0.8 mm/yr at Otakiri (15 km back from the coast) and possibly up to 1–2 mm/yr at the coast over geological timescales (Nairn and Beanland, 1989, Berryman and Hull, 2003). Along the coastal margin of the Whakatane Graben during the March

1987 Edgecumbe earthquake, the maximum co-sesimic subsidence of about 0.4 m occurred immediately west of Thornton (Blick and Flaherty, 1989). Then from Whakatane to East Cape, situated in the North Island Shear Belt, the costal margin has been uplifting at average rates of 0.1 to 2.5 mm/yr in geological timeframes (Pillans, 1986, 1990; Berryman and Hull, 2003).

Vertical rates of movement over geological timeframes in seismically-active areas are often not smooth with time, but usually occur in incremental steps due to co-seismic and post-seismic deformation (e.g., Edgecumbe earthquake). To obtain reliable estimates of present-day smooth and incremental vertical land movements requires: a) regularly-updated 1st-order geodetic levelling surveys of benchmark circuits, and b) continuous global position system (CGPS) stations, both of which are expensive undertakings (J. Beavan, GNS Science and G. Blick, LINZ, pers. comm.). A CGPS station south-west of Tauranga City has been operating within the GeoNet CGPS Network (http://www.geonet.org.nz/) since 2003. However, meaningful rates of vertical land movement are only possible after about 10 years of CGPS monitoring (J. Beavan, GNS Science, pers. comm.). Until definitive values of present-day vertical land movements are known with some certainty, the historic relative sea-level rise of 1.4 mm/yr (transferred to Mt. Maunganui from Auckland) should be used as the basis for the historic and projected sea-level rise in the Bay of Plenty region. This assumption doesn't include possible future incremental co-seismic deformations, which can't be forecast. To cover this, a marginal safety factor could be built in for the Whakatane Graben area after further research and monitoring to arrive at an appropriate increase in the projected rise in sea level (discussed in the next section) to cover long-term smooth and incremental subsidence. In the eastern area (Whakatane to Cape Runaway), the projected sea level rise values will be somewhat conservative due to tectonic uplift.

2.8.2 Projected sea-level rise for the Bay of Plenty

At this stage, we have little definitive data on: a) present-day vertical land movements in the Bay of Plenty and, b) any differences in sea-level response in the SW Pacific compared to the global average response. Consequently, we assume the global-average rate of rise projections promulgated by IPCC (2001) provide values that are reasonable at this stage for planning and design purposes, given the historic 1.4 mm/yr rate is well within the range of the global average rate of 1–2 mm/yr.

The full spread of projections of sea-level rise for the next 100 years [IPCC(2001)] are joined with the historic information for the previous 100 years in Figure 2.15. The

height datum in Figure 2.15 is relative to MVD-53 with the sea-level projections anchored to the 1990 value of 0.064 m above MVD-53.

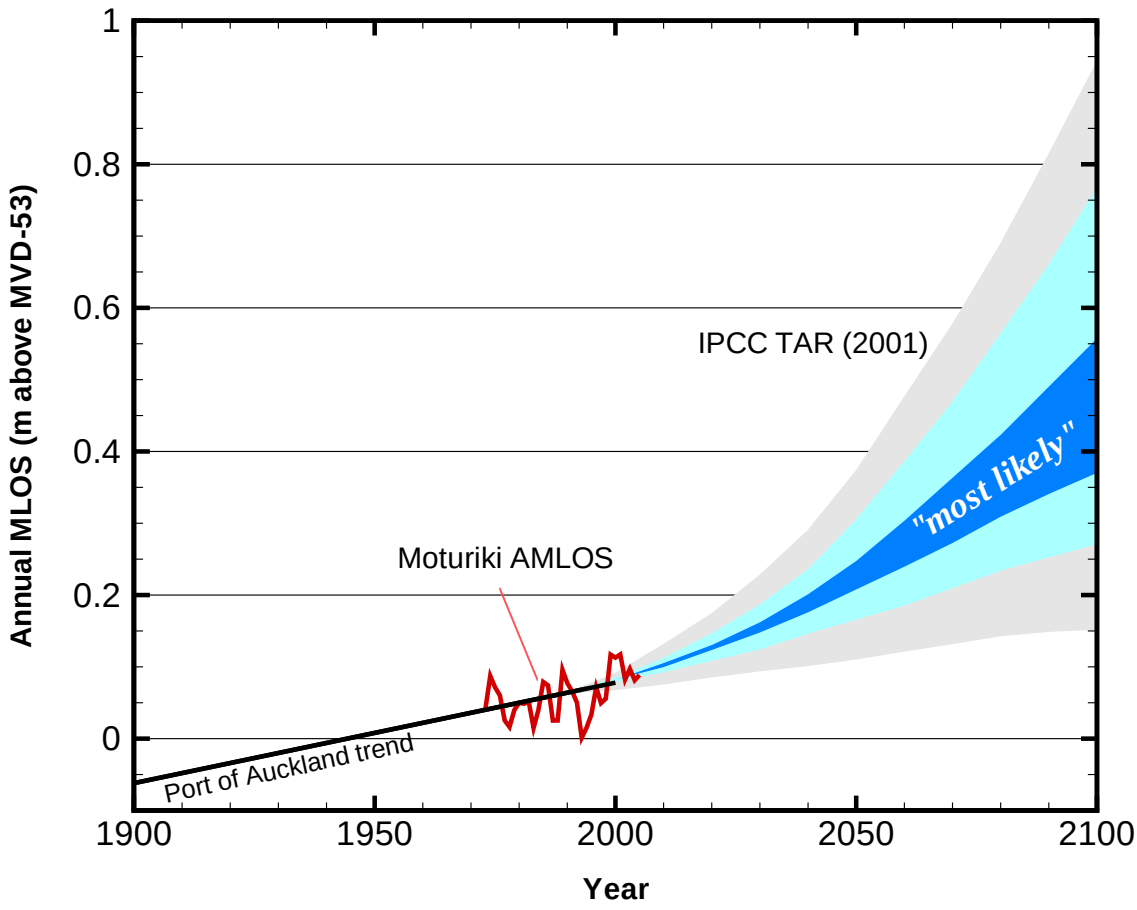

Figure 2.15: Comparison of the last 100 years of annual mean level of sea (AMLOS), represented by the relatively short Moturiki record since 1973 and the linear trend from the longer Port of Auckland record [0.14 m/century], with the IPCC (2001) projections for absolute global sea level rise over the next 100 years. The height datum is relative to Moturiki Vertical Datum-1953.

The "most likely" band for projected sea-level rise covers the range of average computer model predictions (using several different models) and a range of possible socio-economic scenarios of how we might live and use energy throughout this century [IPCC(2001)]. It is the latter difficulty of estimating the changing socio-economic structures of society across the world in response to climate change that these sea-level rise values/ranges are referred to as "projections" rather than "predictions".

A comparison of the sea-level rise projections from IPCC(2001) are given in Table 2.10 in terms of relativity to 1990 MLOS and also relative to MVD-53. Guidance in

the recent Ministry for the Environment document 'Coastal Hazards and Climate Change" (MfE, 2004b) recommended that rounded values of sea-level rise of 0.2 m and 0.5 m (relative to 1990 sea level) be used respectively for 2050 and 2100 planning horizons. These values are also listed in Table 2.10

Table 2.10: Projections of future mean sea-level height (SLH) for the Bay of Plenty, relative to Moturiki Vertical Datum-1953 (MVD-53) in top section, and in the bottom section the same projections expressed as sea-level rise (SLR) relative to the 1990 mean level of the sea (=0.064 m MVD-53 in the case of Bay of Plenty). Values in the respective shaded rows are the recommended values arising from MfE (2004b) for use in coastal planning.

Scenario	Climate factors	SLH by 2050 (m MVD-53)	SLH by 2100 (m MVD-53)
Recommended sea-level heights for Bay of Plenty		0.26	0.56
IPCC–2001 'Most-likely' mid-range [Figure 2.15]	Averages of climate models & socio-economic scenarios	0.20–0.24	0.37–0.55
IPCC–2001 Outer ranges [Figure 2.15]	Intermediate zones	0.16–0.30	0.27–0.76
	Upper & lower extreme zones	0.11–0.37	0.15–0.94
Average historic trend continues (1.4 mm/yr)	If NO acceleration in sea-level this century	0.15	0.22

Scenario	Climate factors	SLR by 2050 (m)	SLR by 2100 (m)
Recommended NZ sea-level rise magnitudes		0.2	0.5
IPCC–2001 'Most-likely' mid-range [Figure 2.15]	Averages of climate models & socio-economic scenarios	0.14–0.18	0.31–0.49
IPCC–2001 Outer ranges [Figure 2.15]	Intermediate zones	0.10–0.24	0.21–0.70
	Upper & lower extreme zones	0.05–0.31	0.09–0.88
Average historic trend continues (1.4 mm/yr)	If NO acceleration in sea-level this century	0.08	0.15

As an example, by 2100, the "most likely" range for sea level rise is projected to lie between 0.37 m and 0.55 m above MVD-53, the extreme range lies between 0.15 and 0.94 m above MVD-53, and the recommended MfE (2004b) value for coastal planning purposes translates to 0.56 m above MVD-53. This compares with sea level reaching 0.22 m above MVD-53 in 2100 if the same linear trend continued with no acceleration.

As discussed in the previous section, any additional component to these projections for potential subsidence areas of the Bay of Plenty (e.g., Whakatane Graben) would

need to be determined after further research and CGPS monitoring (e.g., another 7 years data may be needed).

It is important to note that IPCC expect sea level will continue to rise for several centuries, even if greenhouse gas emissions are stabilised. This is due to the long lag times needed for the deep oceans to respond to ocean surface heating and the expected substantial contributions from polar ice sheets, particularly from the Greenland and Antractica ice sheets after 2100. The expected continued melting of ice sheets or increase in iceberg calving from these land-based ice sheets is expected to lead to a sea-level rise in the order of several metres over the next several centuries, even for the lower range of projected future climate-change scenarios.

2.8.3 Changes in storm tide elevations

Of perhaps greater concern than mean sea-level rise, from the viewpoint of flooding, overtopping, the design and assessment of coast protection works and stormwater networks is any increase in the magnitude and/or frequency of storm-tide water levels. As discusses in Section 2.7.2 storm-tide levels depend mainly on the magnitude and frequency of storm surges as well as the timing of high tides. If deeper atmospheric low pressure systems and stronger winds occur, then surge levels may increase in magnitude. Potential changes to future storm systems are discussed in the next section. Whilst there is some evidence to suggest that strong cyclone systems will increase in intensity (see Section 3.6 for more information), and weak to medium strength storms will decrease slightly, there is still much uncertainty as to likely future changes. Due to the complex way that such low pressure systems interact with the continental shelf and coastline to produce storm surge, there is no clear evidence as yet to indicate whether there will be either an increase or decrease in storm surge magnitudes in the next 50 to 100 years, and hence how storm tide levels will change. The release of the next IPCC Fourth Assessment Report in 2007 is unlikely to change this present uncertainty.

Due to the lack of such information, it is normally assumed that storm tide elevations will rise at the same rate as mean sea level rise. Taking the present-day storm-tide annual exceedence probabilities accepted by EBOP, an additional contribution from sea-level rise should be added in accordance with Table 2.10. The recommended values to use are the magnitudes provided in the fifth row of the table, i.e., 0.2 m and 0.5 m for the appropriate planning time-frame (2050 or 2100).

3. Nearshore waves and longshore transport

3.1 Introduction

Wave action is the dominant forcing process causing changes in erosion and accretion patterns along the Bay of Plenty coastline. Any changes in wave and swell conditions may alter the current pattern and rate of such coastal changes. There are three major types of wave climate change that are important:

- Changes in storm frequency or intensity
- Changes in mean and extreme wave heights
- Changes in mean wave direction

This component of the report looks to assess the potential variability and change in the nearshore wave climate and hence affect on regional scale longshore transport patterns within the region. The main objectives are to:

- Assess the sensitivity of long-term nearshore wave climate to the effects of potential climate variability and change on offshore wave climate.
- Assess extreme wave height variability along the BOP coast.
- Calculate the relative average net and gross magnitude (and direction), and annual variation of longshore sediment transport along the beach sections of the BOP coast.
- Assess the sensitivity of the longshore transport rate (and direction) to changes in mean wave height and direction, ENSO and IPO fluctuations.
- Identify the sections of coast that are most sensitive to climatic changes in terms of variation in longshore transport rate.
- Assess extreme wave run-up potential at locations corresponding to beach profile surveys.

To provide this information, numerical modelling of wave propagation is used to deduce nearshore wave conditions from deep-water wave data, as provided by long term ocean wave hindcasting.

3.2 Wave and wind data

The modelling procedures described here rely on the availability of long-term records of deep water wave conditions outside the region of interest. In this section we describe the numerical hindcasts used to provide these data.

We have made use of two numerical hindcasts. The NIWA simulation covering the years 1979 through 1998 provides a sufficiently long record to provide satisfactory climate statistics, averaging over seasonal and interannual variability. Use was also made of outputs from the NOAA Wavewatch global simulation from 1997 to 2005, which includes the 2004 period for which nearshore wave data were available from instruments in the Bay of Plenty, as well as having an overlap period with the NIWA hindcast. This allows simulations based on the NIWA hindcast to be validated indirectly through comparisons with simulations based on the Wavewatch hindcast which are in turn compared with measurements.

3.2.1 NIWA New Zealand Regional Hindcast

The WAM wave model (WAMDIG, 1988) has in recent years become widely used for describing the generation, propagation and dissipation of surface waves in the world's oceans. It is a spectral model in that it describes the sea state in terms of the amount of energy in each band of wave frequency and propagation direction. The model computes the evolution of this wave spectrum by accounting for the input, transfer and loss of energy through the various physical processes. In its present form (Cycle 4), the model accommodates the processes of generation by wind stress, propagation with refraction by the seabed and/or currents, transfer of energy between interacting waves of different frequencies and directions (a nonlinear effect), and dissipation by white-capping and bottom friction.

For hindcasting wave conditions in the New Zealand region, a rectangular grid was established covering latitudes 78.75°S to 9°S and longitudes 99°E to 220.5°E (139.5°W) at 1.125° resolution. This region centres on New Zealand, extending westward beyond Australia's Indian Ocean coast, southward to the Antarctic, and into the Pacific Ocean as far as the Marquesas Islands in the northeast corner of the grid. Spectra were computed at 16 equally spaced propagation directions and 25 logarithmically spaced frequencies, between f_1 = 0.0418 Hz and f_{25} = 0.4518 Hz. It

has been found (Komen et al., 1994) that these choices adequately cover the range of wave conditions commonly found in the world's oceans, and that finer resolution provides minimal improvement in model accuracy at considerable cost to model running times. Refraction due to currents or bathymetry was not included. Wind data were sourced from the European Centre for Medium-Range Weather Forecasts (ECMWF) "Reanalysis" dataset. This provides winds on a 1.125° latitude/longitude grid at 10 m elevation evaluated in a consistent way over all the years of the record. The data are provided at the analysis times of 00, 06, 12 and 18 hours (Universal Time) on each day.

The model was then run for a 20-year hindcast of the years 1979-1998 inclusive. Wave statistics over the entire grid were output at 3 hourly intervals. Full directional spectra were also archived at 3-hour intervals from a set of 53 selected model cells, including all those adjacent to the New Zealand coast. The model has been validated against available nearshore data (Gorman and Laing, 2001) and, after correcting for the effects of limited fetch to the actual coastline, has been found to provide an accurate description of the wave climate incident on the New Zealand coast from deep water.

In the present work we have wave statistics (significant wave height, mean wave direction and peak wave period), extracted from the model cell centred on latitude 37.125°S, longitude 177.5°E, in deep water off the Bay of Plenty (Figure 3.1). The wind fields used in the wave model are also included in this data set. Occurrence distributions for the wind and wave parameters from this time series are shown in Figures 3.2 and 3.3.

Wind speeds most commonly occurred in the range 5-10 ms^{-1} (Figure 3.2a), having a mean value of 6.6 ms^{-1}, and a standard deviation of 3.2 ms^{-1}. There was a predominance of winds from the western quadrant (Figure 3.2b).

The significant wave height (Figure 3.3a) most commonly lay in the 1 – 2 m range, having a mean value of 1.50 m, and a standard deviation of 0.69 m. Wave directions (Figure 3.3c) showed a bimodal distribution, with the prevailing westerlies producing a strong presence of waves from that quadrant, for which there is a moderate fetch of approximately 150 km to the Coromandel coast. A strong presence of waves from the eastern quadrant results largely from more distant weather systems. Peak wave period had a mean value of 8.1 seconds, and a standard deviation of 2.43 seconds.

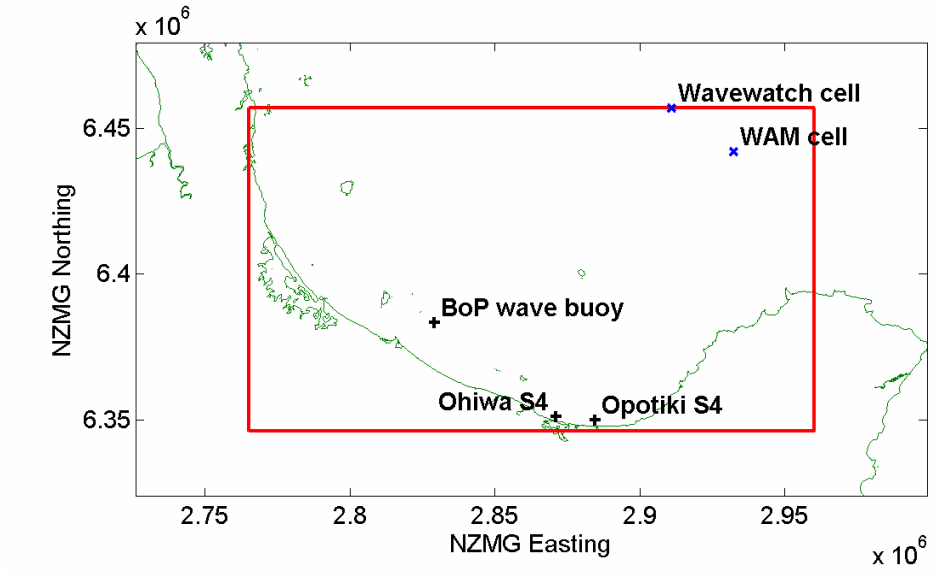

Figure 3.1: Map showing the locations of the Bay of Plenty wave buoy, the two nearshore S4 current meter deployments, along with the centres of the model cells from which statistics from the WAM and Wavewatch III wave hindcasts were extracted to provide boundary conditions for wave modelling. The model domain for SWAN simulations is shown by the red box (see Section 8.3)

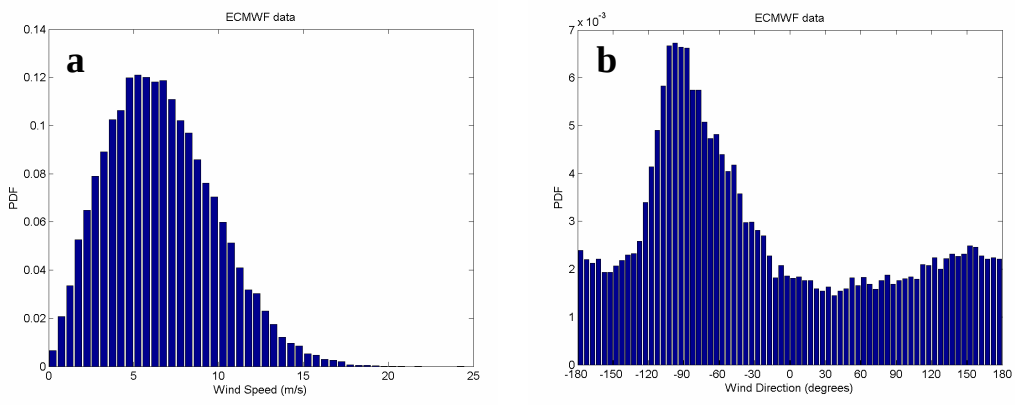

Figure 3.2: Occurrence plots for wind speed (a) and wind direction (b) from the ECMWF Reanalysis used in the WAM hindcast, at the grid cell adjacent to the northern grid boundary. The direction FROM which the wind is blowing is shown in degrees clockwise from North.

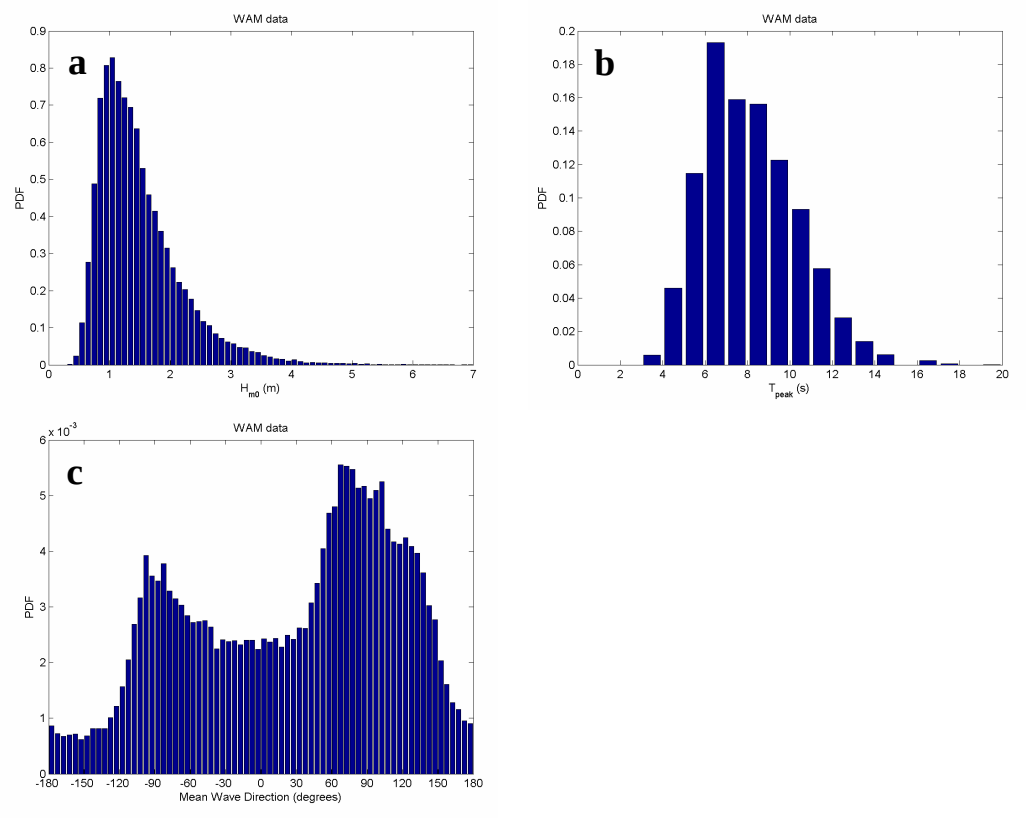

Figure 3.3: Occurrence plots for significant wave height (a), peak wave period (b), and mean wave direction (c) from the WAMhindcast data at the grid cell adjacent to the northern grid boundary. The direction FROM which the waves propagate is shown in degrees clockwise from North.

3.2.2 NOAA/NCEP Wavewatch III hindcast

A simulation of wave conditions is carried out by the National Centers for Environmental Prediction (NCEP), part of the National Ocean and Atmospheric Administration (NOAA) in the United States. This uses the Wavewatch III code (Tolman, 1999; Tolman et al., 2002) to provide hindcasts and forecasts on a global domain at a resolution of 1.25° in longitude and 1.0° in latitude. Input winds are taken from NCEP's operational Numerical Weather Prediction models. Forecasts up to 126 hours ahead are run starting every 6 hours (00, 06,12 and 18 hours UT), initialised from an "analysis" run which incorporates assimilated atmospheric data.

In the present work we have used results from these analysis runs, in the form of significant wave height, peak wave direction and peak wave period data for the global domain collated over the period 1/2/1997 - 1/6/2005. The wind fields used in the wave model are also included in this data set. The model cell centred on latitude 37°S, longitude 177.5°E, in deep water off the Bay of Plenty was selected (Figure 3.1).

Occurrence distributions for the wind and wave parameters from this time series are shown in Figures 3.4 and 3.5.

Wind speeds most commonly occurred in the range 5-10 ms^{-1} (Figure 3.2a), having a mean value of 7.84 ms^{-1}, and a standard deviation of 3.49 ms^{-1}. There was a predominance of winds from the western quadrant (Figure 3.4b).

The significant wave height (Figure 3.5a) shows a similar distribution to that seen from the WAM hindcast (Figure 3.3a), in this case having a mean value of 1.68 m, and a standard deviation of 0.78 m, while peak wave directions (Figure 3.5c) also showed a bimodal distribution. Peak wave period had a mean value of 7.20 seconds, and a standard deviation of 2.43 seconds. However the distribution of wave periods is clearly bimodal (Figure 3.5b), with distinct peaks around the 4-6 second and 9-10 second ranges. By plotting peak period against peak wave direction (Figure 3.5d), it can be seen that the bimodality in the two variables arises from distinct populations of short period waves predominantly from the west, and longer period swell predominantly from the east and north-east.

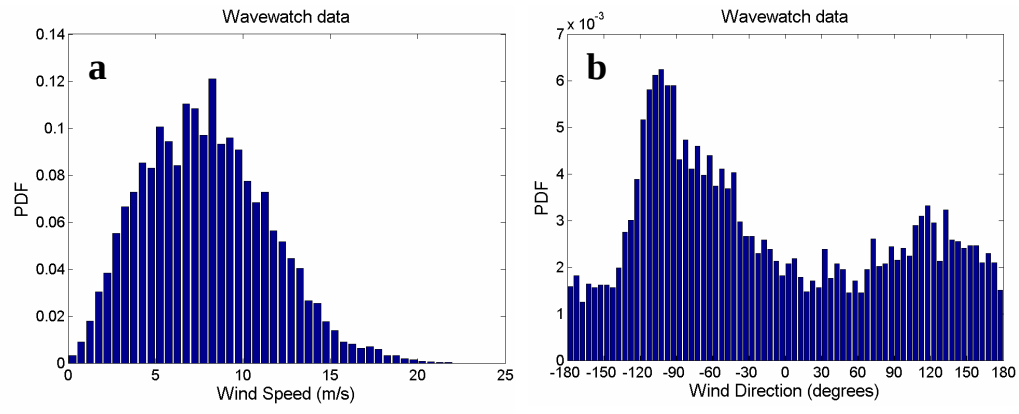

Figure 3.4: Occurrence plots for wind speed (a) and wind direction (b) from the NOAA/NCEP Wavewatch III hindcast data at the grid cell adjacent to the northern grid boundary. The direction FROM which the wind is blowing is shown in degrees clockwise from North.

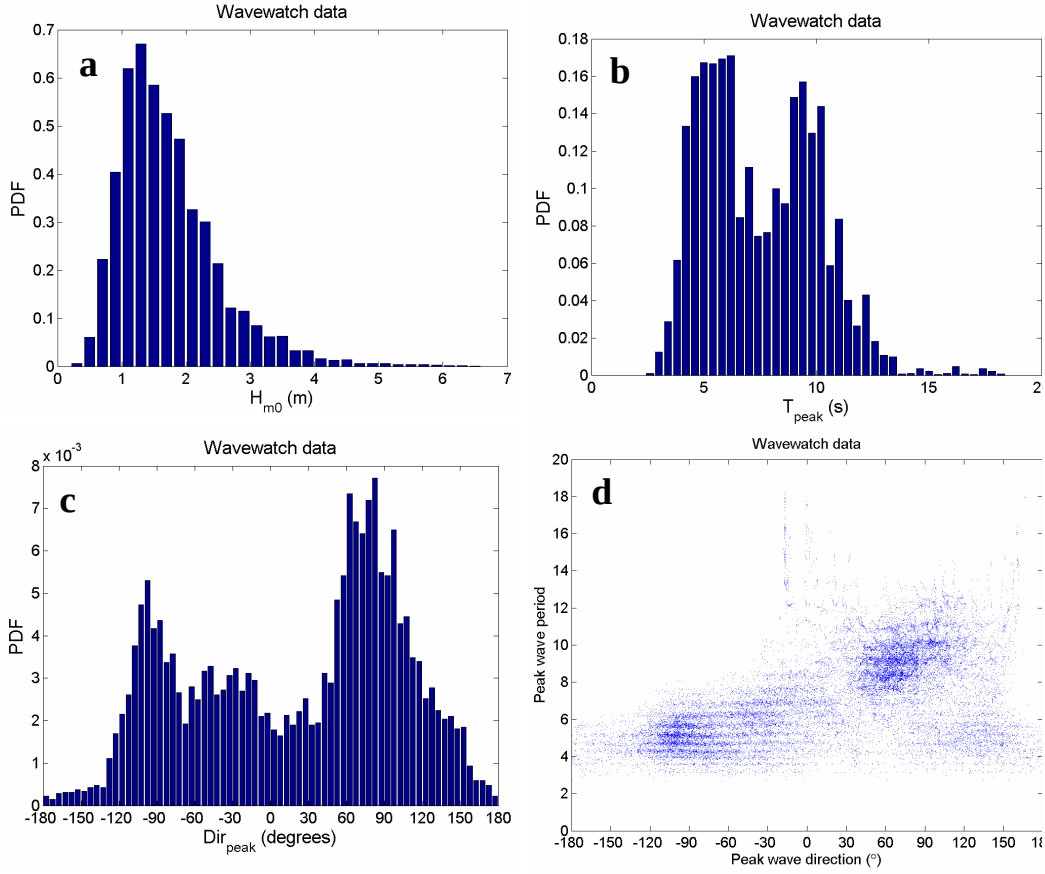

Figure 3.5: Occurrence plots for significant wave height (a), peak wave period (b), and peak wave direction (c) from the NOAA/NCEP Wavewatch III hindcast data at the grid cell adjacent to the northern grid boundary. The direction FROM which the waves propagate is shown in degrees clockwise from North. Also shown is a scatter plot for peak wave direction and peak wave period (d).

3.3 Nearshore wave data

A Directional Triaxys wave buoy, operated by Environment Bay of Plenty, has been deployed since 22/9/2003 at latitude 37° 41.770′S, longitude 176° 36.972′E, some 13 km off Pukehina Beach, in approximately 50 m water depth (Figure 3.1). Nearshore wave data during the study period were also available from two InterOcean S4 current meters deployed off Opotiki (37° 58.483′S, 177° 15.750′E) and off Ohiwa (37° 58.100′S, 177° 06.400′E).

Occurrence distributions for data from the wave buoy are presented in Figure 3.6. Significant wave heights are lower than at the offshore site, with the peak of the occurrence distribution lying below 1 m. Wave directions are largely limited to the north and northeast sectors, as a result of the limited fetch in other directions. In particular, the predominant westerly winds have only some 30 km of fetch to generate

waves at the buoy site, so in such conditions any level of swell from other directions is more likely to dominate the sea state than is the case further offshore. Hence the maximum around 5 seconds seen in the distribution of peak periods offshore does not occur at the wave buoy, but there is still a strong contribution of 9-10 second peak period waves from northeast swell.

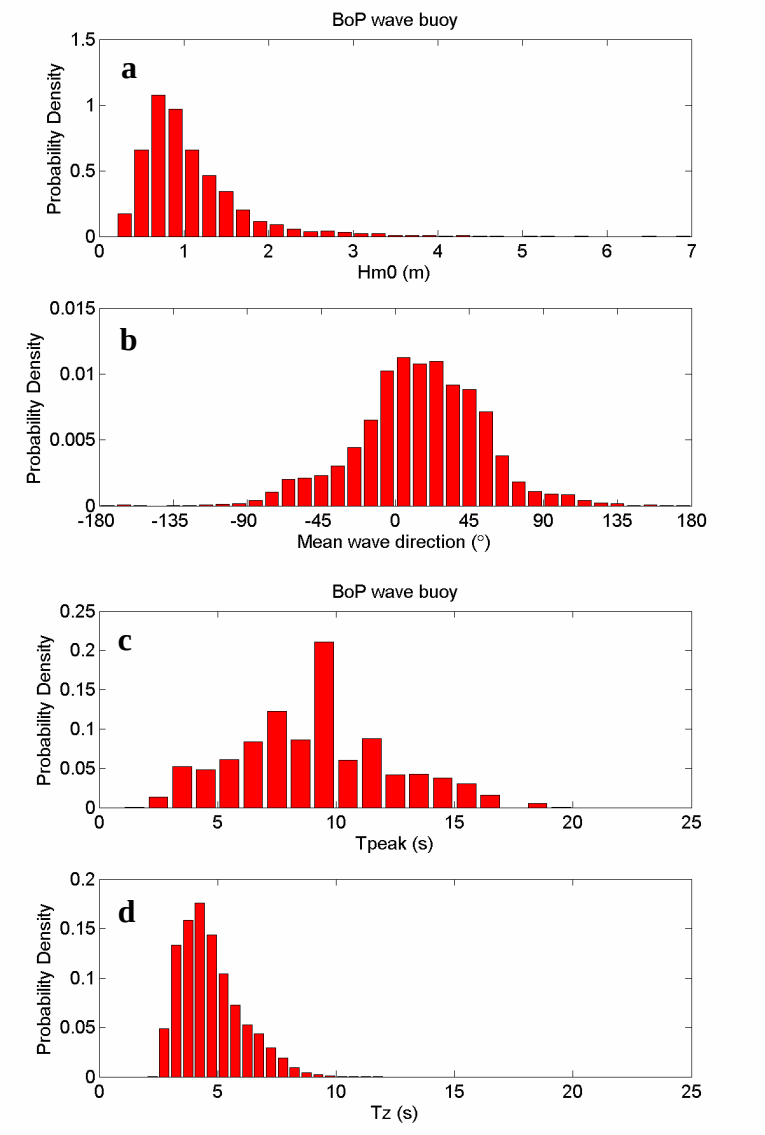

Figure 3.6: Occurrence plot for significant wave height (a), mean wave direction relative to true North (b), peak wave period (c), and zero-crossing wave period (d) from Bay of Plenty wavebuoy data. The direction FROM which waves propagate is shown, in degrees clockwise from true North.

3.4 Nearshore wave modelling methods

While both the wave hindcasts described above provide a valuable measure of deepwater wave conditions, neither suffices to give a complete description of nearshore wave processes on the Bay of Plenty coast. The effects of wave generation by local winds, and refraction over the seabed still need to be taken more fully into account. This is most adequately addressed by using a numerical model covering the coastal region at sufficiently fine resolution that incorporates these effects.

The SWAN nearshore wave model, described in more detail in Appendix 2, was used to simulate the effects of shallow water processes on the wave climate as waves propagate towards the shoreline within the Bay of Plenty. A model grid was established covering the Bay of Plenty (Figure 3.1). The wave model was run at 1000 m resolution on a grid of 196 cells in the east-west direction by 112 cells in the north-south direction. The grid origin (cell (1,1)) was at NZMG (2765000.0E, 6346000.0N). An example of the model output is shown in Figure 3.7.

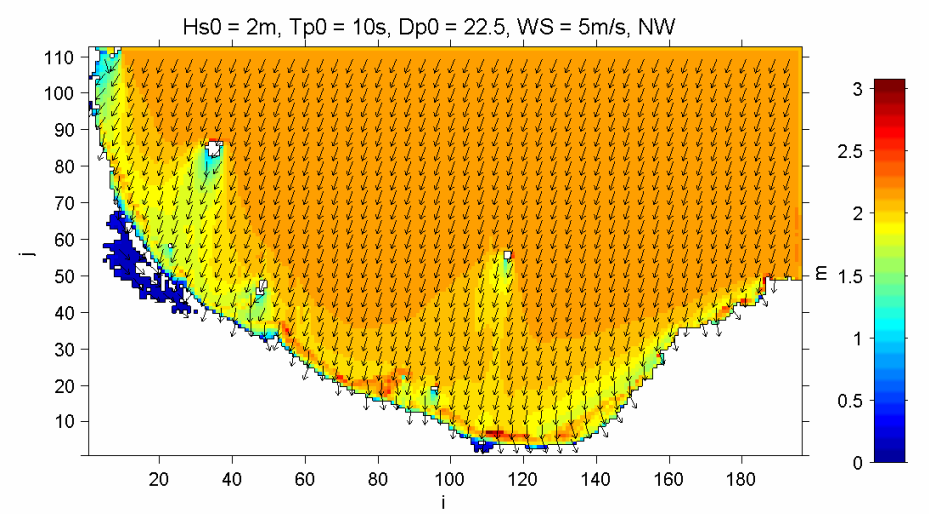

Figure 3.7: Example output from SWAN simulations. In this case, incoming waves from the NNW with H_{s0} = 2 m, T_{p0} = 10 s are applied at the boundary, while the wind is 5 ms^{-1} from the Northwest. The significant height is represented by colour-scaling, while arrows (in every fourth cell) are aligned in the peak wave direction.

The SWAN model was first applied to directly simulate wave conditions for a short period (26/2/2004 – 8/3/2004), during which data from the Bay of Plenty wave buoy and the nearshore S4 deployments were available. For this simulation, time-varying wave parameters from the Wavewatch III hindcast taken from the model cell centred on latitude 37°S, longitude 177.5°E were applied as model inputs along the northern and eastern grid boundaries. The corresponding time-varying model wind speed and

direction from the same model cell were applied uniformly over the full spatial domain.

Predicted wave conditions at the Bay of Plenty wave buoy, were taken from model outputs, and compared with the data to verify model performance, as described in Appendix 2.

Computing limitations mean that such a fine-resolution simulation covering a large area is only feasible for relatively short time periods, typically up to several weeks. Less direct methods are required to simulate the multi-year time scales needed to provide information on seasonal and interannual variations in wave climate, and also allow the sensitivity of the wave climate to changes in wind climate to be readily investigated.

An alternative method was therefore used for long-term simulations, based on first running the model under a full range of nominal forcings, then applying the resulting transfer functions to long term records of observed or hindcast forcing parameters, to derive nearshore wave conditions. This scenario-based method is described further in Appendix 2.

For the present study, long-term simulations were carried out using either of the two deep-water hindcasts as inputs, allowing multi-year time series of nearshore wave statistics to be derived along the 10 m isobath, as well as at instrument locations for validation purposes. Results from the 1997-2005 simulation (based on the Wavewatch III deep-water hindcast) were compared to wave buoy data, as well as to results from the direct simulation. Comparisons were also made between results from the two long-term simulations during the 1997-1998 overlap period. These comparisons are presented in Appendix 2. This provided a two-step validation of the 20-year nearshore wave climate simulation based on the WAM deep-water hindcast, which could then be applied to investigate surf zone and sediment transport properties under the existing climate, as well as under possible modified climate scenarios.

3.5 Surf zone and sediment transport properties

From the nearshore wave modelling results at the 10 m isobath, wave conditions further inshore were derived by refraction and shoaling relationships using uniform straight coast approximations, and sediment transport parameters were then derived using a set of relationships from the Shore Protection Manual (CERC, 1984) as described in Appendix 3.

For the present study we have not attempted to incorporate information on varying beach sediment properties across the Bay of Plenty region, rather the assessment aims to identify potential variability and change in the nearshore wave climate and associated potential sediment transport patterns at a regional scale. Parameters assessed include:

- Root mean square breaking wave height along the Bay of Plenty coastline
- Mean onshore energy transport
- Mean net longshore flux
- Mean north-westward longshore flux
- Mean south-eastward long shore flux
- Divergence of mean net longshore flux
- Mean net longshore sediment transport
- Mean net north-westward longshore transport
- Mean net south-eastward longshore transport
- Divergence of the mean net longshore transport
- Net to gross drift ration
- Drift to swash ratio
- Mean longshore current at the breakpoint produced by oblique wave incidence
- Mean longshore current at the breakpoint produced by longshore wave height gradient
- Mean longshore current at the breakpoint produced by combining oblique wave incidence and longshore wave height gradient
- Mean values of expected annual maxima of wave runup (including and excluding wave setup).

3.6 Climate change scenarios

In the simulation technique used here, changes in wind climate have an influence both directly, through the local wind forcing parameters (wind speed and direction), and indirectly, through the parameters (Significant wave height, peak period and peak direction) representing arriving swell that had been generated by wind action over wide expanses of the Pacific Ocean. This means that we must consider climate change at a range of geographic scales. At a New Zealand regional scale, the mean westerly wind component is predicted to increase by approximately 10% over the next 50 years (Mullan et al., 2001). At a wider scale, the incidence and intensity of storms is expected to change. This is possibly more significant for wave climate, particularly the incidence of the more extreme events that can have strong effects on coastal morphology. We first consider the possible variations in storm activity.

A recent modelling study (Geng and Sugi, 2003) compared the occurrence of mid-latitude cyclonic storm events in simulations of the present-day climate and a scenario of 50-year climate change associated with greenhouse warming. It found that, for the Southern Hemisphere, the occurrence of weak- to medium-strength storms was expected to decrease by approximately 7% in both summer and winter, but the occurrence of strong cyclones was expected to increase by more than 20% for both seasons. Other climate simulations show somewhat varying results: Sinclair and Watterson (1999) found a general decrease in Southern Hemisphere storm activity, while the results of Brandefelt and Källén (2004) showed a spatial pattern of changes in storm activity for the South Pacific/Southern Ocean east of New Zealand varying between increases in more southern waters to decreases further north, along with a seasonal variation showing more increases in winter and more decreases in summer.

We have taken the approach of accepting the Geng and Sugi (2003) results as a plausible scenario for changes in storm wind statistics in the southern Pacific, and considered what corresponding changes could be expected in the statistics of swells that reach the Bay of Plenty region, having originally been generated by these storms. For simplicity, we average the summer and winter statistics from Geng and Sugi (2003), and note the occurrence of storms of various categories (based on central pressure gradient) as given in Table 3.1.

We start from a time series of wave heights produced from a period in the recent past, for which the storm occurrence statistics are appropriate to the present day climate. If we imagine "replaying" that time period in a revised climate, with the magnitude of all weather events rescaled by an intensity-dependent factor, to have occurrence statistics appropriate to a climate change scenario, but with the same intensity ordering. For example, a storm which was exactly at the borderline between Categories 2 and 3 would be at the 84.6^{th} percentile of the record. In the "replayed" record, the corresponding event will still be at the 84.6^{th} percentile, which in the new statistics places it into the lower end of Category 3, i.e., its intensity has been scaled up slightly, while the storm which was at the 83.6^{th} percentile will be scaled up to now be at the border between categories 2 and 3. We then make the assumption that wave heights occurring during this event will also be rescaled in a similar way, so that the significant wave height which is at the 83.6^{th} percentile in the original record will be rescaled to match the significant height which was originally at the 84.6^{th} percentile. This procedure gives a scaling factor to apply at each of the percentile values given for storm category boundaries given in Table 3.1. Scaling factors at intermediate wave heights are then obtained by linear interpolation.

Table 3.1: Occurrence statistics for southern hemisphere cyclonic storms derived from the global climate model study of Geng and Sugi (2003), using averages of summer and winter simulations.

Storm intensity category	Present climate simulation	Climate change scenario
C1 (<1 Pa/km)	36.2%	36.7%
C1-2 (<2 Pa/km)	84.6%	83.6%
C1-3 (<3 Pa/km)	97.5%	96.6%
C1-4 (<4 Pa/km)	99.7%	99.0%

In reality, the significant wave height at one location is not directly proportional to the intensity of a single Pacific storm event. The above procedure only makes the assumption that, in a statistical sense, the magnitude of the p^{th} percentile wave height is related to the average intensity of the p^{th} percentile storm. The same approach can be applied to other statistics which should have a similar correspondence. This means we can apply this procedure to the significant wave height $H_{s0}(t)$ and peak wave period $T_{p0}(t)$ used in the boundary forcing, but not to the peak wave direction $\theta_{p0}(t)$, which is left unchanged. The changes in distribution of these forcing parameters are shown in Figure 3.8. In all cases, the tail of the distributions is shifted to more energetic values for the more extreme events, but there are minimal changes to the main body of the distributions.

The original wind record from the Wavewatch III simulation had a mean westerly component of 1.81 ms^{-1}. When the time series was adjusted by the method described above, the mean westerly component increased to 1.83 ms^{-1}, an increase of 1.1%. This is considerably less than the 10% increase suggested by Mullan et al (2001). Therefore it is necessary to consider an alternative adjustment of local winds in a way that reflects this change in the mean wind. There is no single unique way to implement this. Perhaps the most natural possibility is to add 0.18 ms^{-1} to the eastward component of all local winds, superimposing a constant mean flow increased by 10%. This has the effect of strengthening westerlies and weakening easterlies. The effect will be relatively large in mild conditions. For example, a calm period will become a light westerly wind, while light easterly winds will be considerably reduced. The relative impact on strong winds will be small.

An alternative possibility is that all wind speeds will be scaled up by 10%, regardless of wind direction. This is a more dramatic scenario than can be considered likely , but is included as a form of “upper bound”

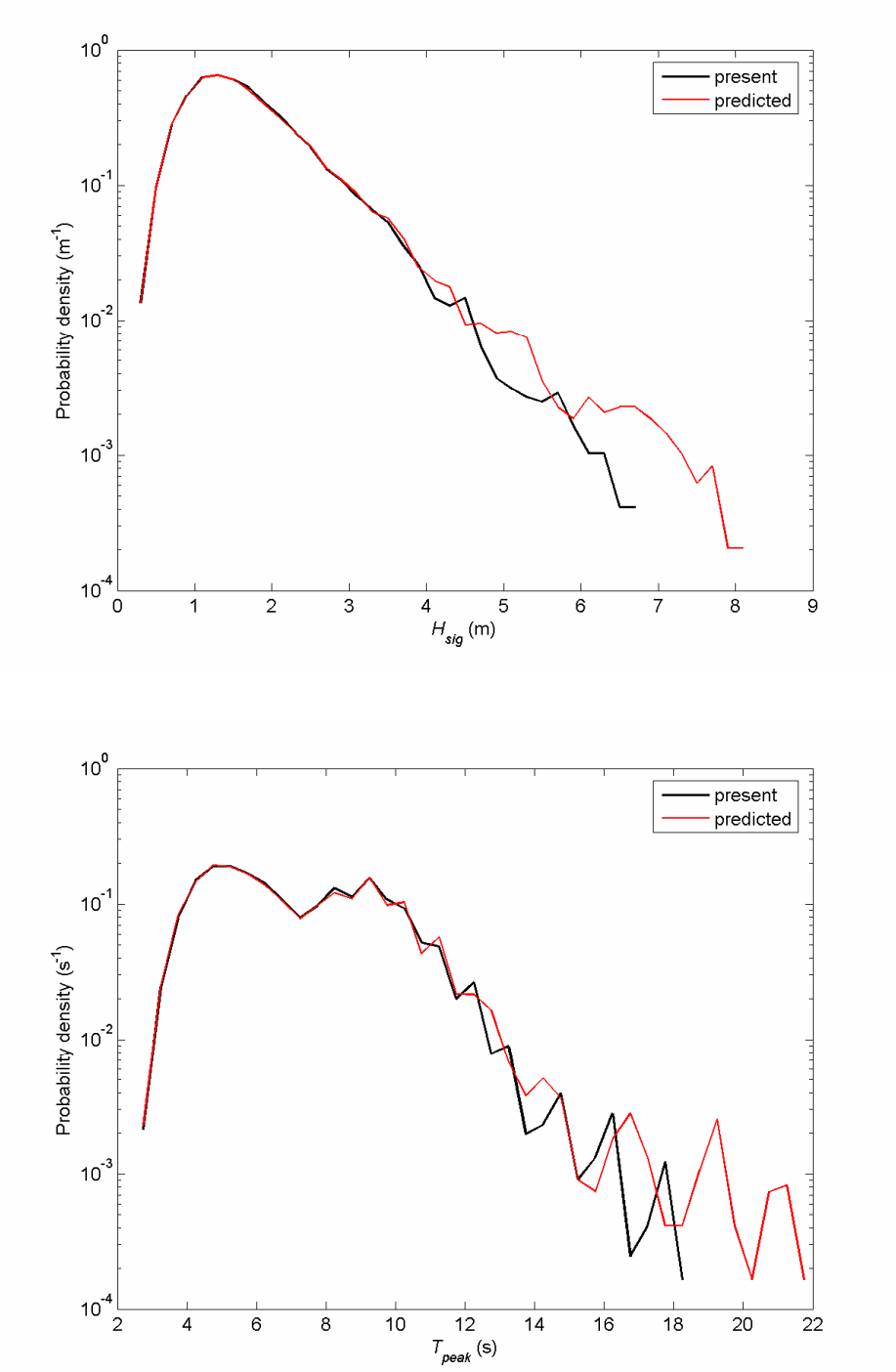

Figure 3.8: Probability distribution functions for significant wave height (top) and peak wave period (bottom) derived from the Wavewatch hindcast unmodified (black) and adjusted to reflect changes predicted by the global climate model study of Geng and Sugi (2003) (red).

Hence four simulations were carried out:

1. A baseline simulation with unadjusted environmental forcing, to represent the present day climate.

2. A climate change scenario with offshore significant wave height and peak period, adjusted according to reflect the expected change in cyclonic storm occurrences from the Geng and Sugi (2003) study, as described above.

3. A climate change scenario with offshore significant wave height and peak period adjusted according to reflect the expected change in cyclonic storm occurrences from the Geng and Sugi (2003) study, as described above, and local wind velocities adjusted by adding 0.18 ms^{-1} to the eastward components.

4. A climate change scenario with offshore significant wave height and peak period adjusted according to reflect the expected change in cyclonic storm occurrences from the Geng and Sugi (2003) study, as described above, and local wind velocities adjusted by increasing all wind speeds by 10%.

It should at this point be stressed that global climate modelling is still a rather coarse tool for predicting climate change effects relevant to coastal wave conditions. These models are most suitable for considering changes in large scale dynamics of the ocean-atmosphere system. Hence a prediction of a 10% increase in mean westerly flows in the New Zealand region can be made with a reasonable level of confidence. The climate models are less suited to accurately describing variability in more transient phenomena, such as the occurrence of intense storms responsible for major changes to beaches. So how these large scale climate changes will influence more extreme winds is more speculative. Even our assumption that the occurrence of the most intense storms in the Southern Pacific will increase is not supported by all of the limited number of relevant studies carried out to date. Hence we have taken the approach of presenting possible scenarios that are consistent with some of the results of global climate change modelling, in order to get some estimates of possible magnitude of the effects nearshore, but note that these scenarios are by no means definitive.

3.7 Simulated climatology of nearshore wave conditions and sediment transport, including the influence of potential climate change impacts

Time-averaged values of wave and sediment parameters obtained along the coast from the climate simulation are plotted in Figures 3.9 to 3.23. Results are plotted both by colour-scaled points plotted on the 10 m isobath, representing the existing wave climate, and as a set of line plots against distance along the 10 m isobath. The middle panel of each Figure repeats the information in the colour-scaled plots by showing values from the simulation of the present climate, while the top panel shows changes in values (relative to the present climate), predicted for each of the climate scenarios. Note that different scales are generally used in the top and middle panels.

3.7.1 Nearshore wave variability and longshore flux

The RMS breaker height (Figure 3.9) shows a generally decreasing trend from west to east along the coast from Whangamata to Opotiki, then increases again towards East Cape, largely corresponding to variation in exposure. Shifting the climate by an additive adjustment in the eastward wind component (red line) produces a slight increase (< 1%) in wave heights towards the eastern end of the coast, and a slight decrease towards the western end. Also including an adjustment to the swell (blue line) produces height increases of order 0-5% for the majority of the coast, while applying a multiplicative scaling give larger height increases (>5% for the eastern Bay). The onshore component of wave energy flux (Figure 3.10) shows a similar pattern, but with some additional fine-scale variation associated with local changes in coastline orientation.

The longshore flux factor (Figure 3.11) has positive (i.e. eastward) values over most of the western Bay of Plenty, with some negative (i.e. westward) values, mostly in the east. This is a result of the sweeping curve of the Bay of Plenty coastline bringing large scale variation of the coast's alignment to predominent wave directions. There are smaller-scale variations associated with local topographic features, for example Okurei Point at Maketu produces a locally high negative value on its western side (at the 100 km mark on the distance scale), but positive on its eastern side where the coastline resumes an alignment close to equilibrium with the wave climate. The flux factor is relatively sensitive to changes in local wind climate, particularly the longshore wind component, compared to changes in the occurrence of swell, which becomes nearly shore-normal in the nearshore zone. Hence all climate change scenarios, having an increase in westerly winds, lead to an increase in eastward flux factor over most of the coast.

Because of the variation in alignment, accumulated westward longshore flux factors (Figure 3.12) are minimal north-west Matakana Island (50 km mark), while negative values (Figure 3.13) have low occurrence south-east Papamoa (80 km mark) until Cape Runaway near the end of the model domain, except in isolated locations such as the eastern side of Okurei Point. Only in a relatively small region around Tauranga is there a fine balance between fluxes in both longshore directions. We find that scaling up the wind speed has a large effect on both positive and negative flux factors, but that these tend to balance out and only have a moderate affect on the net flux factor.

The divergence of the longshore flux factor (Figure 3.14) is sensitive to (possibly spurious) local variations in the isobath alignment, so we have applied some smoothing, in the form of a 15-point running mean, to the divergence data. This quantity gives an indication of where either net accretion or net depletion of coastal sediment might result from imbalances in wave-driven longshore transport. For example, there is a predominance of positive values around the entrance to Ohiwa Harbour, indicating that a given sediment type, if universally available for transport, would have higher flux leaving this area than entering, suggesting that there would be a tendency for erosion to occur in this area. On the other hand, along the beaches either side of Ohiwa Harbour there is a region of negative divergence (i.e. convergence), which would tend to have sediment deposited by the wave-driven longshore transport process. Positive divergence also tends to occur at prominent headlands, with convergnce either side. The immediate vicinity of both the Tauranga and Katikati entrances to Tauranga Harbour are zones of positive divergence which would tend to lose sediment by longshore transport to adjacent negative divergence areas. Of course, this analysis only identifies the potential for sediment erosion and deposition by the one process of longshore sediment transport. Indeed positive divergence in P_{ls} is often associated with bulges in the isobath near river mouths, that are themselves the result of *deposition* of material discharged by the rivers.

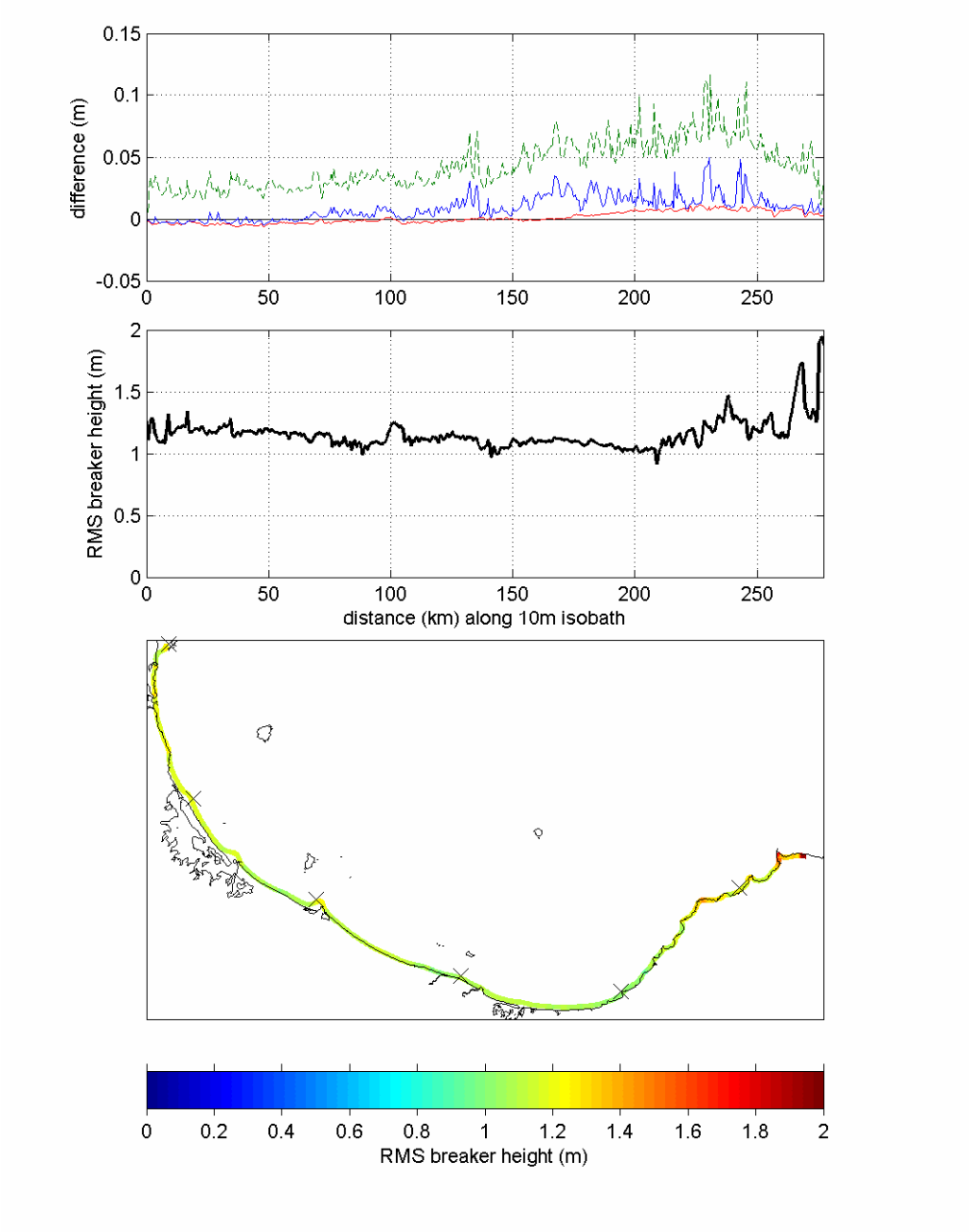

Figure 3.9: Root-mean-square breaking wave height for wave climate derived from hindcast data. Values for the existing climate are plotted in the lower panels in colour-scaled form, and as a function of distance along the 10 m isobath from an origin at its northwest limit. Longshore distance tick marks are marked × in the colour-scaled plot. The top panel shows changes in values relative to the present climate as predicted under the climate change scenarios: unchanged swell and 0.18 m/s added to eastward winds (red line), adjusted swell and 0.18 m/s added to eastward winds (blue line), adjusted swell and wind speed scaled up by 10% (dashed green line).

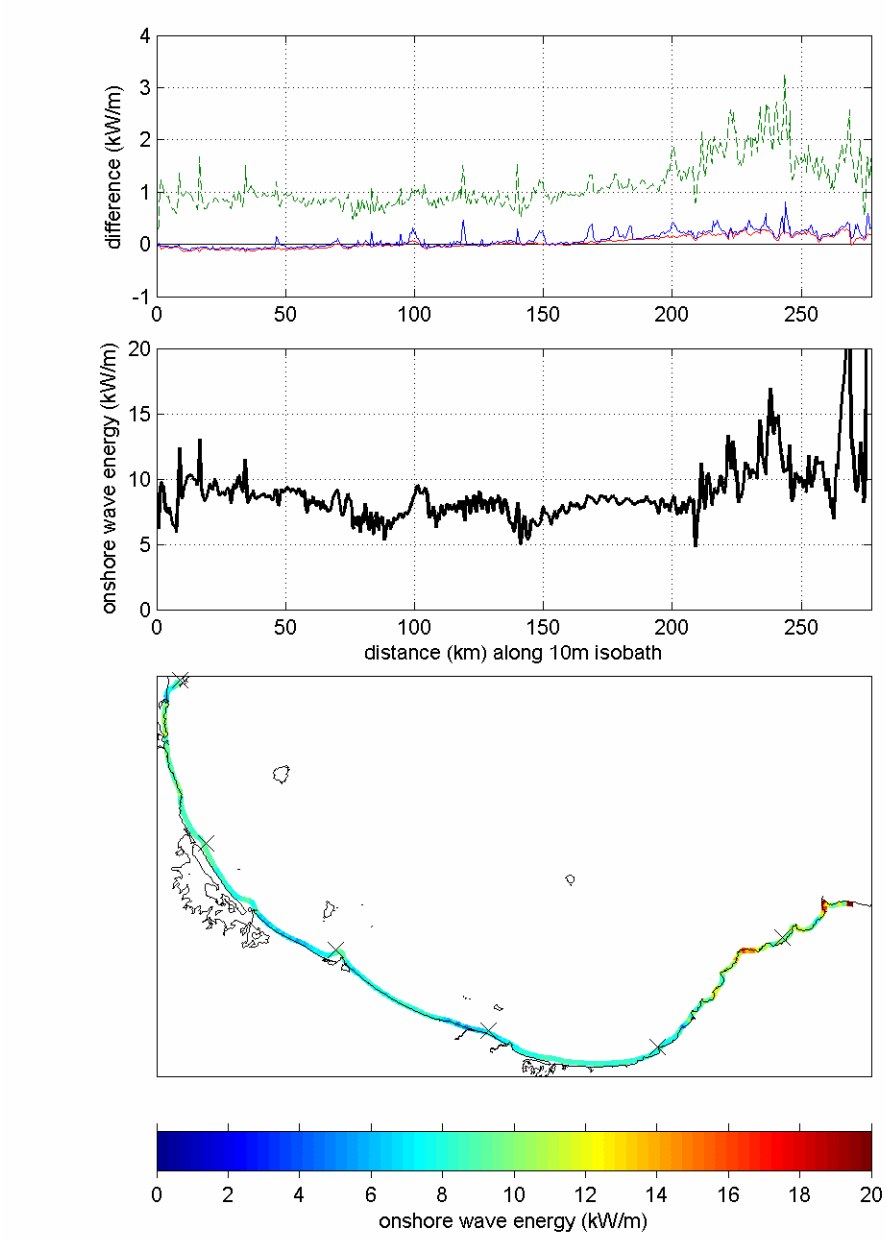

Figure 3.10: Mean onshore energy transport F_{os} for wave climate derived from hindcast data. Values for the existing climate are plotted in the lower panels in colour-scaled form, and as a function of distance along the 10 m isobath from an origin at its northwest limit. Longshore distance tick marks are marked × in the colour-scaled plot. The top panel shows changes in values relative to the present climate as predicted under the climate change scenarios: unchanged swell and 0.18 m/s added to eastward winds (red line), adjusted swell and 0.18 m/s added to eastward winds (blue line), adjusted swell and wind speed scaled up by 10% (dashed green line).

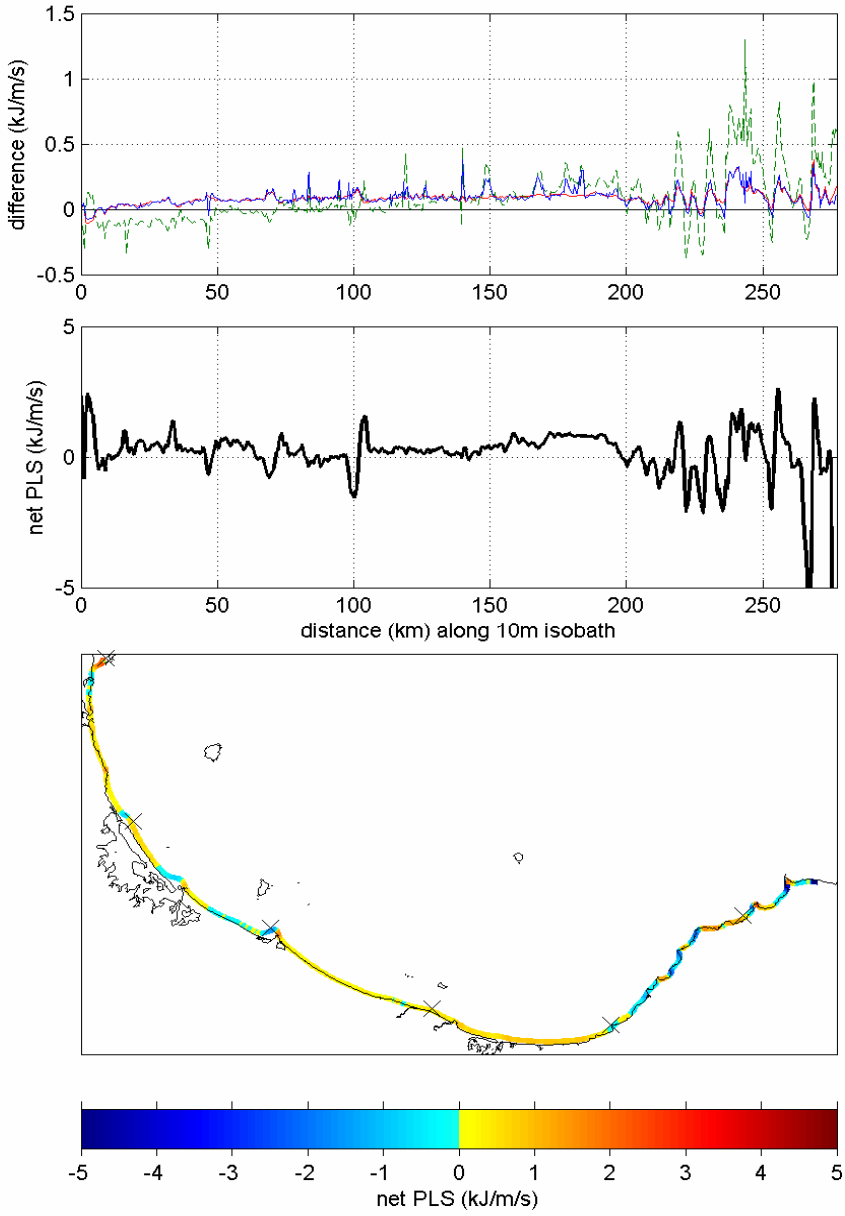

Figure 3.11: Mean net longshore flux factor P_{ls} for wave climate derived from hindcast data. Values for the existing climate are plotted in the lower panels in colour-scaled form, and as a function of distance along the 10 m isobath from an origin at its northwest limit. Longshore distance tick marks are marked × in the colour-scaled plot. Positive (red) values denote eastward longshore energy flux. The top panel shows changes in values relative to the present climate as predicted under the climate change scenarios: unchanged swell and 0.18 m/s added to eastward winds (red line), adjusted swell and 0.18 m/s added to eastward winds (blue line), adjusted swell and wind speed scaled up by 10% (dashed green line).

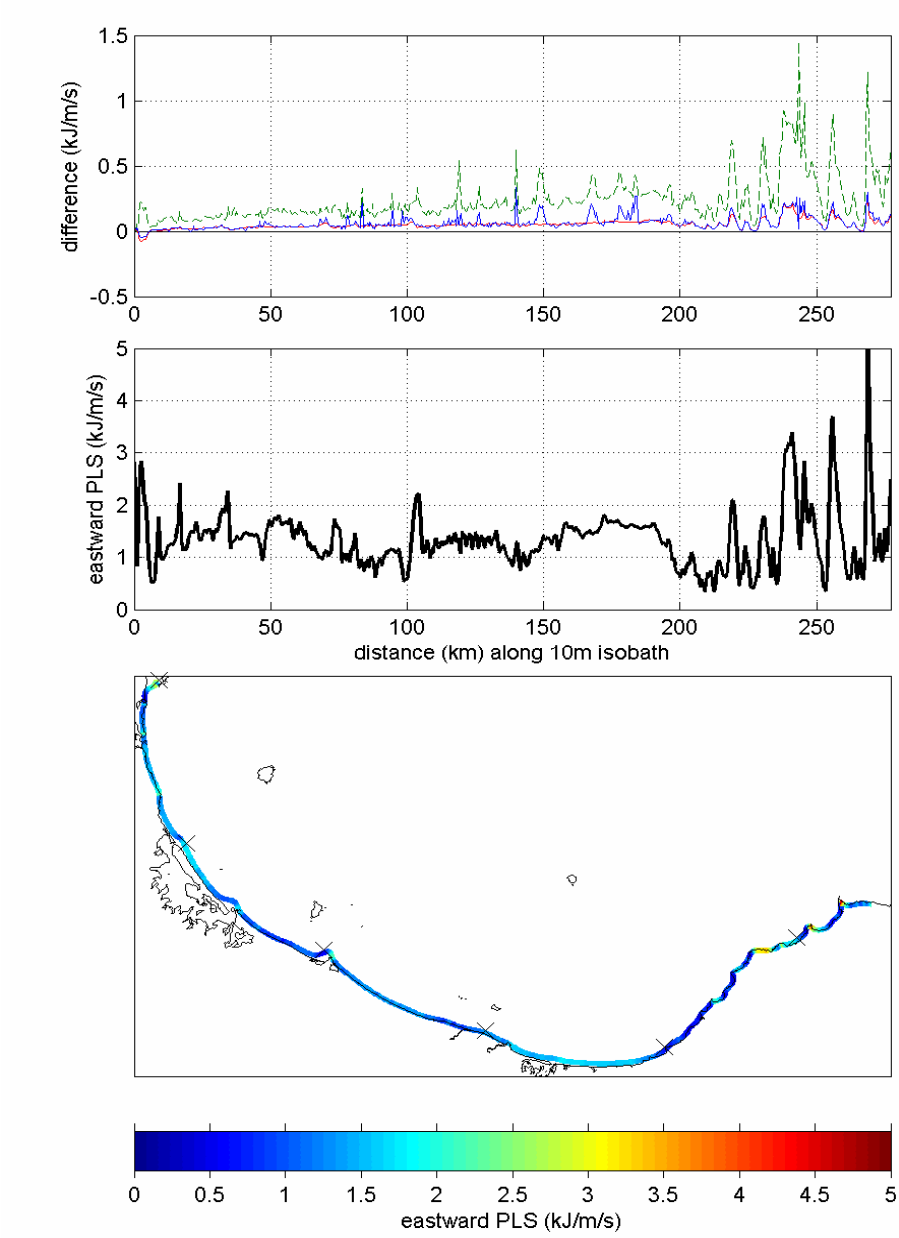

Figure 3.12: Mean eastward longshore flux factor P_{ls+} for wave climate derived from hindcast data. Values for the existing climate are plotted in the lower panels in colour-scaled form, and as a function of distance along the 10 m isobath from an origin at its northwest limit. Longshore distance tick marks are marked × in the colour-scaled plot. The top panel shows changes in values relative to the present climate as predicted under the climate change scenarios: unchanged swell and 0.18 m/s added to eastward winds (red line), adjusted swell and 0.18 m/s added to eastward winds (blue line), adjusted swell and wind speed scaled up by 10% (dashed green line).

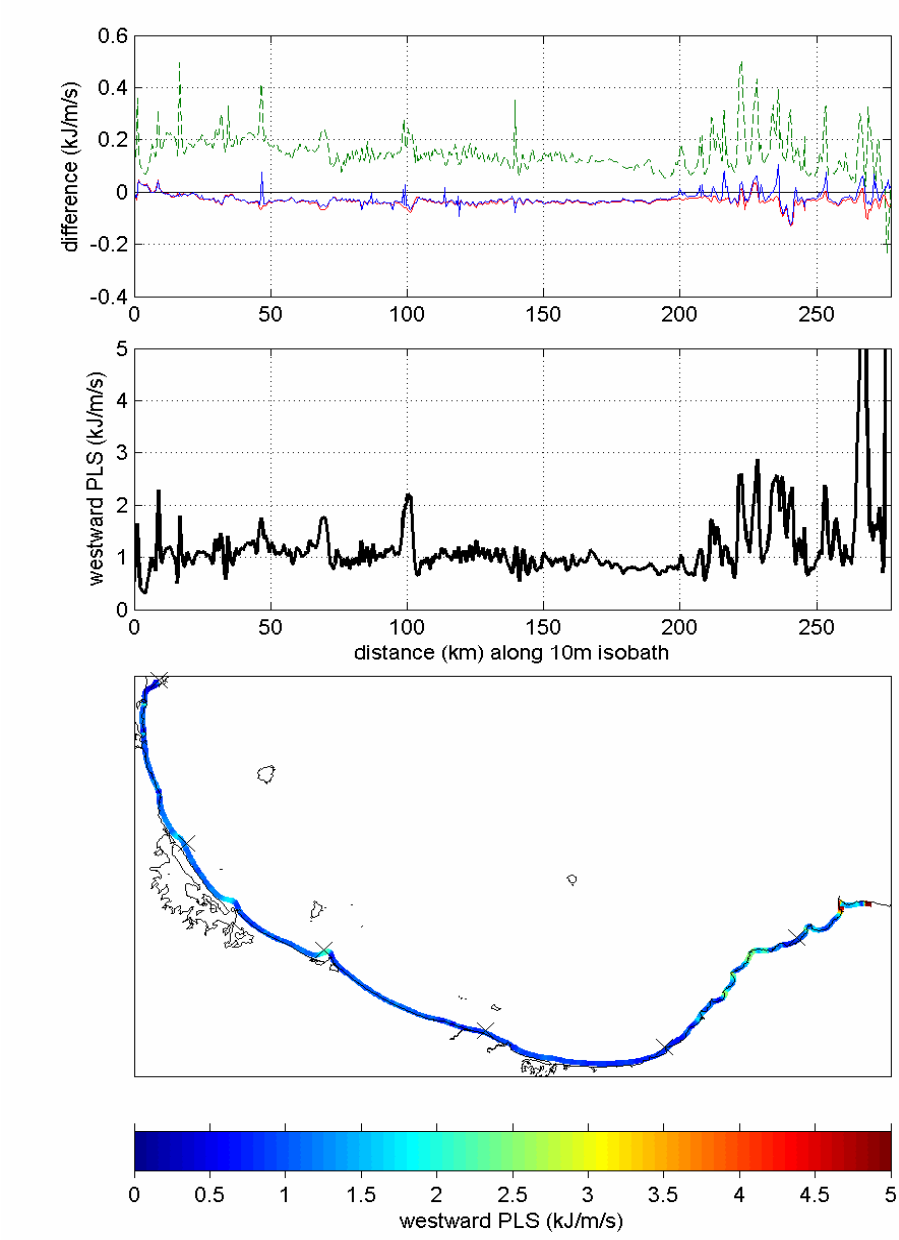

Figure 3.13: Mean westward longshore flux factor P_{ls-} for wave climate derived from hindcast data. Values for the existing climate are plotted in the lower panels in colour-scaled form, and as a function of distance along the 10 m isobath from an origin at its northwest limit. Longshore distance tick marks are marked × in the colour-scaled plot. The top panel shows changes in values relative to the present climate as predicted under the climate change scenarios: unchanged swell and 0.18 m/s added to eastward winds (red line), adjusted swell and 0.18 m/s added to eastward winds (blue line), adjusted swell and wind speed scaled up by 10% (dashed green line).

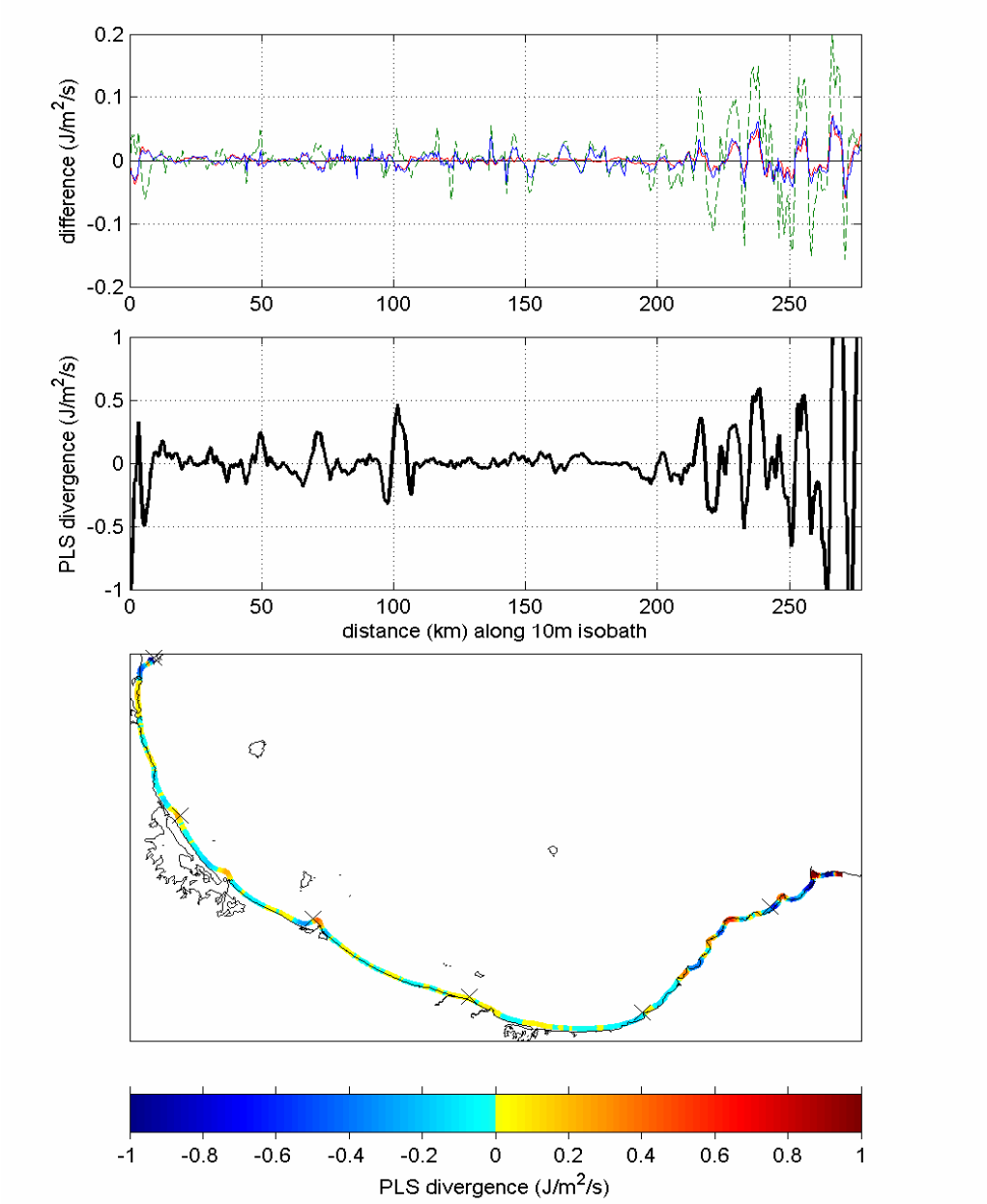

Figure 3.14: Divergence of the mean net longshore flux factor P_{ls} for wave climate derived from hindcast data. Values for the existing climate are plotted in the lower panels in colour-scaled form, and as a function of distance along the 10 m isobath from an origin at its northwest limit. Longshore distance tick marks are marked × in the colour-scaled plot. The top panel shows changes in values relative to the present climate as predicted under the climate change scenarios: unchanged swell and 0.18 m/s added to eastward winds (red line), adjusted swell and 0.18 m/s added to eastward winds (blue line), adjusted swell and wind speed scaled up by 10% (dashed green line).

3.7.2 Longshore sediment transport

Sediment transport rates have been derived by a linear scaling of P_{ls}, including an efficiency factor K, which depends on sediment characteristics. Figures 3.15 to 3.20 therefore represent sediment transport rates derived from the corresponding longshore flux factors of Figures 3.11 to 3.14 by rescaling, using a value K = 0.8. This is intended to give an estimate of the potential contribution of wave-driven longshore transport assuming the availability of sandy sediments. We see from Figure 3.15 that this would be of the order of a million m^3yr^{-1}, with small eastward values over most of the coast, with a high level of local variation associated with changes in coastal alignment.

Under present climatic conditions, the majority of the Bay of Plenty coast (Katikati (Matakana island) to Whakatane) was found to have a moderate longshore transport potential, with flux factors typically of order 1 kW/m, mostly eastward, equating to sediment transport rates of order 0.2×10^6 m^3/yr under the assumptions used. There are local variations largely associated with topographic features such as headlands.

Under the climate change scenarios considered, inreases of order 0.1 kW/m in longshore transport rates can be expected. Much of this change is associated with the predicted 10% expected change in local westerly winds, and this part of the change is expected to be quite spatially uniform across the central Bay of Plenty, and largely directed eastward. The component of the expected change associated with changing occurrence distributions of remotely-generated swell is more spatially variable. However, this reflects adjustments in a relatively small population of extreme events in the swell record, so may be strongly influenced by the particular approach direction of waves during those events. As a result, it may be statistically unreliable to attach much significance to the details of this variation.

To put this in context (refer to Section 3.7.5), under existing climatic conditions, mean interannual variability in the mean longshore flux factor is of the order of 0.5-1.0 kW/m, while the residual variability of monthly mean values is of order ±3 kW/m.

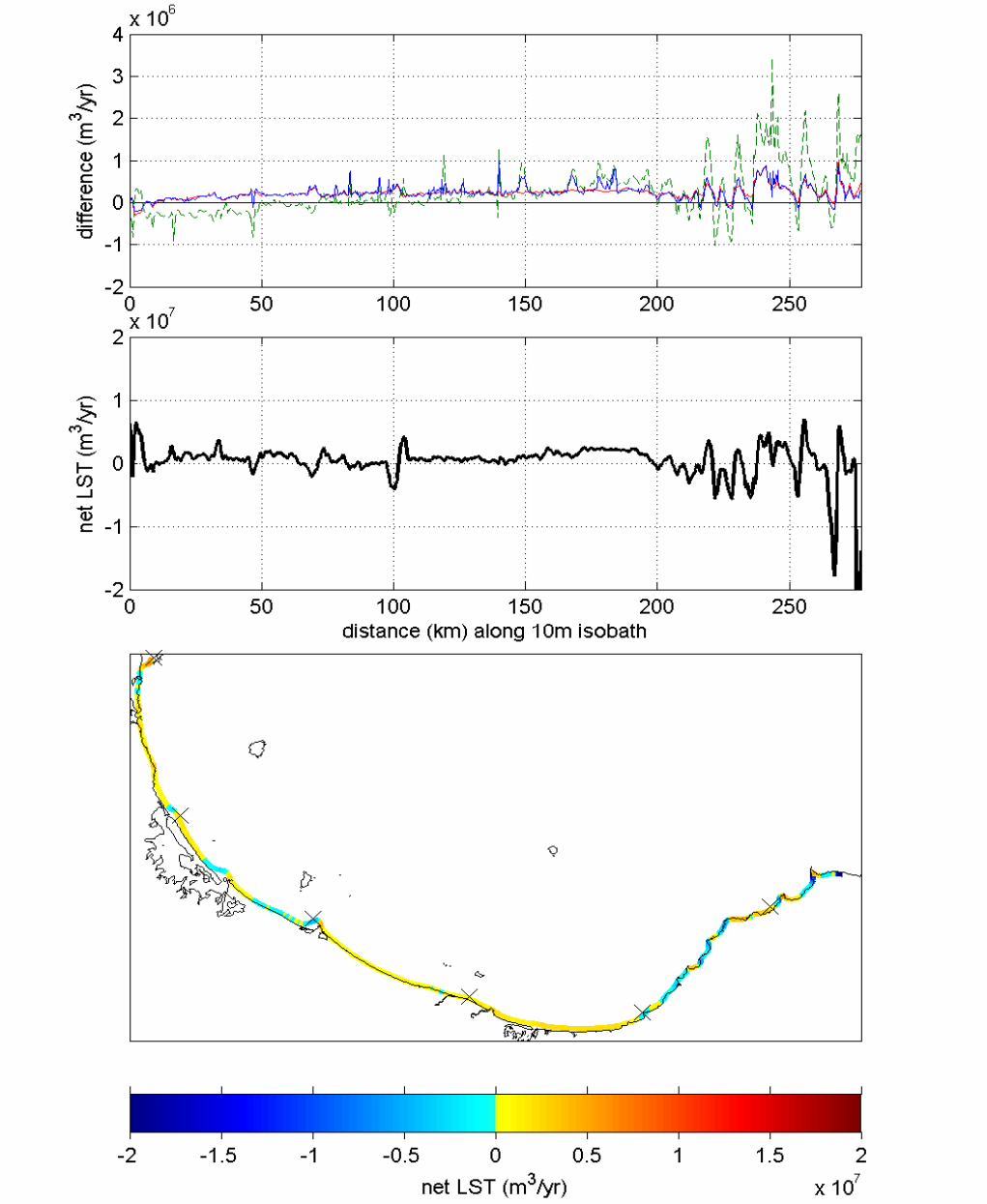

Figure 3.15: Mean net longshore sediment transport Q_{ls} for wave climate derived from hindcast data. Values for the existing climate are plotted in the lower panels in colour-scaled form, and as a function of distance along the 10 m isobath from an origin at its northwest limit. Longshore distance tick marks are marked × in the colour-scaled plot. Positive values (red) denote northward and/or westward transport. The top panel shows changes in values relative to the present climate as predicted under the climate change scenarios: unchanged swell and 0.18 m/s added to eastward winds (red line), adjusted swell and 0.18 m/s added to eastward winds (blue line), adjusted swell and wind speed scaled up by 10% (dashed green line).

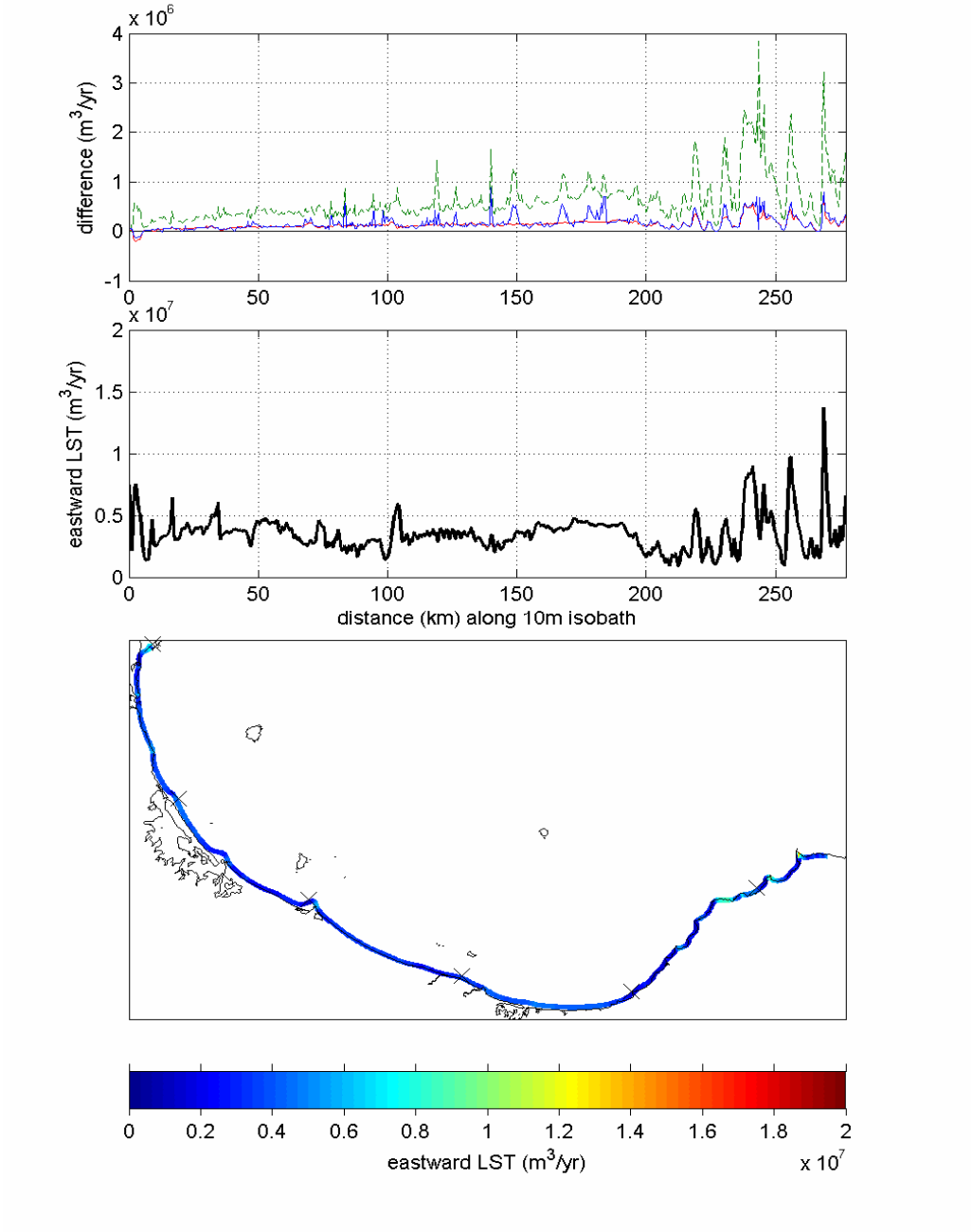

Figure 3.16: Mean north-westward longshore sediment transport Q_+ for wave climate derived from hindcast data. Values for the existing climate are plotted in the lower panels in colour-scaled form, and as a function of distance along the 10 m isobath from an origin at its northwest limit. Longshore distance tick marks are marked × in the colour-scaled plot. The top panel shows changes in values relative to the present climate as predicted under the climate change scenarios: unchanged swell and 0.18 m/s added to eastward winds (red line), adjusted swell and 0.18 m/s added to eastward winds (blue line), adjusted swell and wind speed scaled up by 10% (dashed green line).

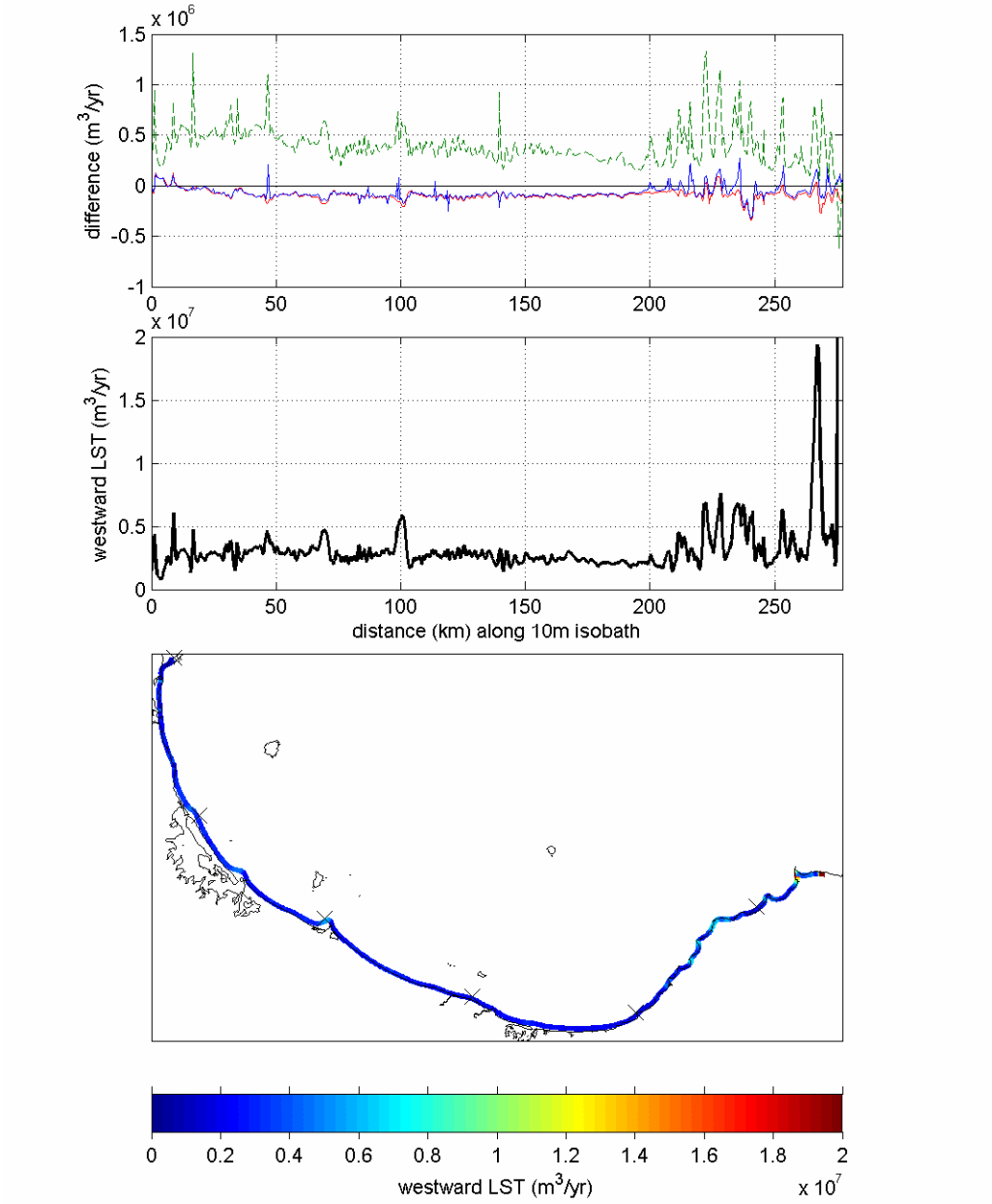

Figure 3.17: Mean south-eastward longshore sediment transport $Q_{.}$ for wave climate derived from hindcast data. Values for the existing climate are plotted in the lower panels in colour-scaled form, and as a function of distance along the 10 m isobath from an origin at its northwest limit. Longshore distance tick marks are marked × in the colour-scaled plot. The top panel shows changes in values relative to the present climate as predicted under the climate change scenarios: unchanged swell and 0.18 m/s added to eastward winds (red line), adjusted swell and 0.18 m/s added to eastward winds (blue line), adjusted swell and wind speed scaled up by 10% (dashed green line).

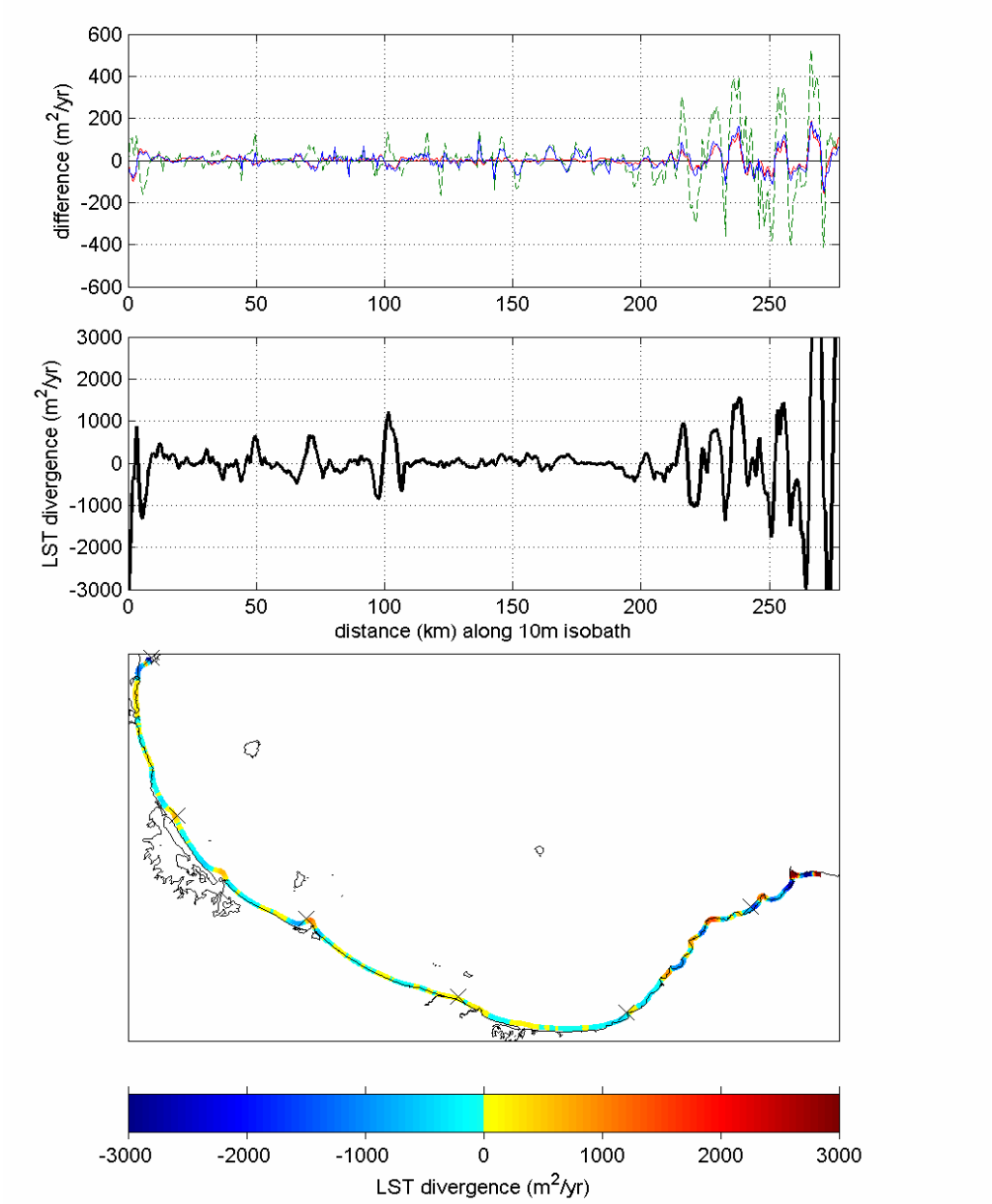

Figure 3.18: Divergence of the mean net longshore sediment transport Q_{ls} for wave climate derived from hindcast data. Values for the existing climate are plotted in the lower panels in colour-scaled form, and as a function of distance along the 10 m isobath from an origin at its northwest limit. Longshore distance tick marks are marked × in the colour-scaled plot. The top panel shows changes in values relative to the present climate as predicted under the climate change scenarios: unchanged swell and 0.18 m/s added to eastward winds (red line), adjusted swell and 0.18 m/s added to eastward winds (blue line), adjusted swell and wind speed scaled up by 10% (dashed green line). Note units are in $m^3/yr/m$, i.e. m^2/yr

3.7.3 Wave induced longshore currents

Figures 3.19 to 3.21 show the longshore currents induced by wave processes. The first of these is a result of oblique wave incidence, in which radiation stress has a longshore component that acts directly to drive currents. This component of the current is positive (eastward) of order 20-30 cm/s for much of the coastline (Figure 3.19). Increased local eastward winds will tend to enhance this current by around 10% (proportional to the assumed increase in mean eastward wind).

The second process is associated with longshore variations in breaker height, which means that even if waves have shore-normal incidence, the wave-induced setup has spatial variations which lead to currents. By its nature this is highly localised phenomenon (Figure 3.20), but can be quite large near prominent topographic features, such as headlands, which can have sheltered zones on one side. Currents flowing toward such a sheltered zone can be set up from more energetic areas of the adjacent coast. On average, this process tends to act against the effect of oblique incidence in such areas, so reducing some of the higher values of the mean net current (Figure 3.21).

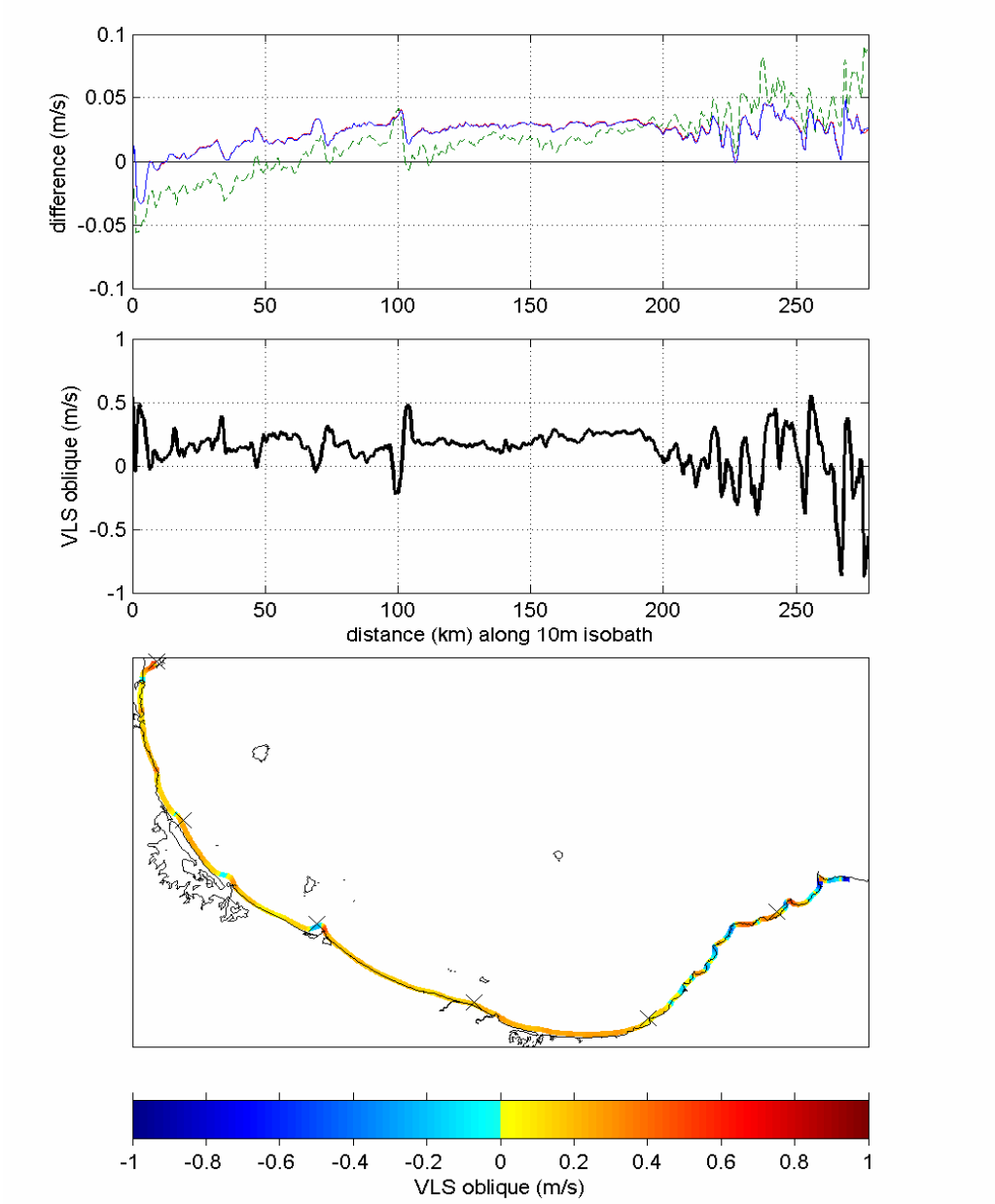

Figure 3.19: Mean longshore current at the breakpoint produced by oblique wave incidence. Values for the existing climate are plotted in the lower panels in colour-scaled form, and as a function of distance along the 10 m isobath from an origin at its northwest limit. Longshore distance tick marks are marked × in the colour-scaled plot. Positive values (red) denote northward and/or westward currents. The top panel shows changes in values relative to the present climate as predicted under the climate change scenarios: unchanged swell and 0.18 m/s added to eastward winds (red line), adjusted swell and 0.18 m/s added to eastward winds (blue line), adjusted swell and wind speed scaled up by 10% (dashed green line).

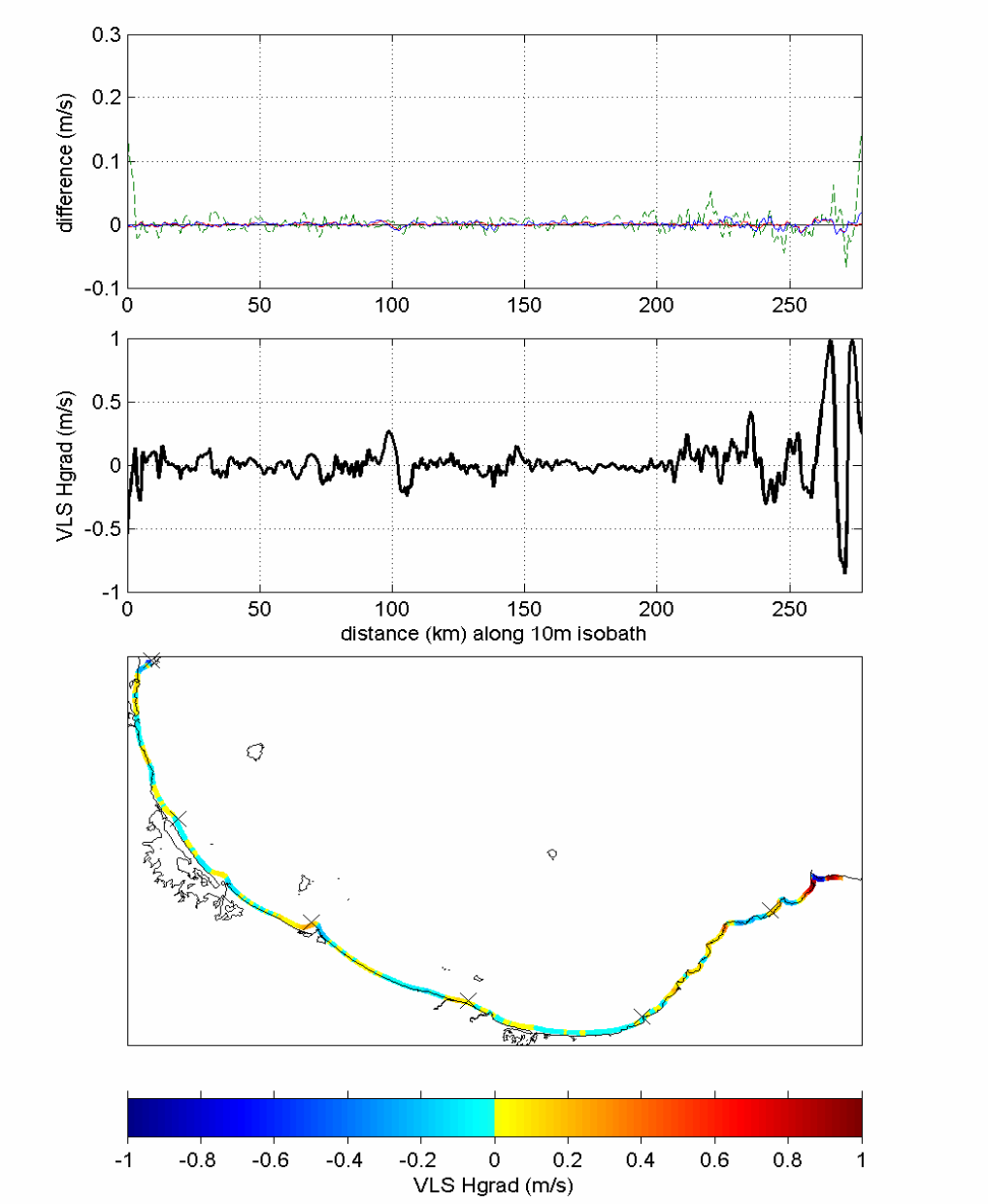

Figure 3.20: Mean longshore current at the breakpoint produced by longshore wave height gradient. Values for the existing climate are plotted in the lower panels in colour-scaled form, and as a function of distance along the 10 m isobath from an origin at its northwest limit. Longshore distance tick marks are marked × in the colour-scaled plot. Positive values (red) denote northward and/or westward currents. The top panel shows changes in values relative to the present climate as predicted under the climate change scenarios: unchanged swell and 0.18 m/s added to eastward winds (red line), adjusted swell and 0.18 m/s added to eastward winds (blue line), adjusted swell and wind speed scaled up by 10% (dashed green line).

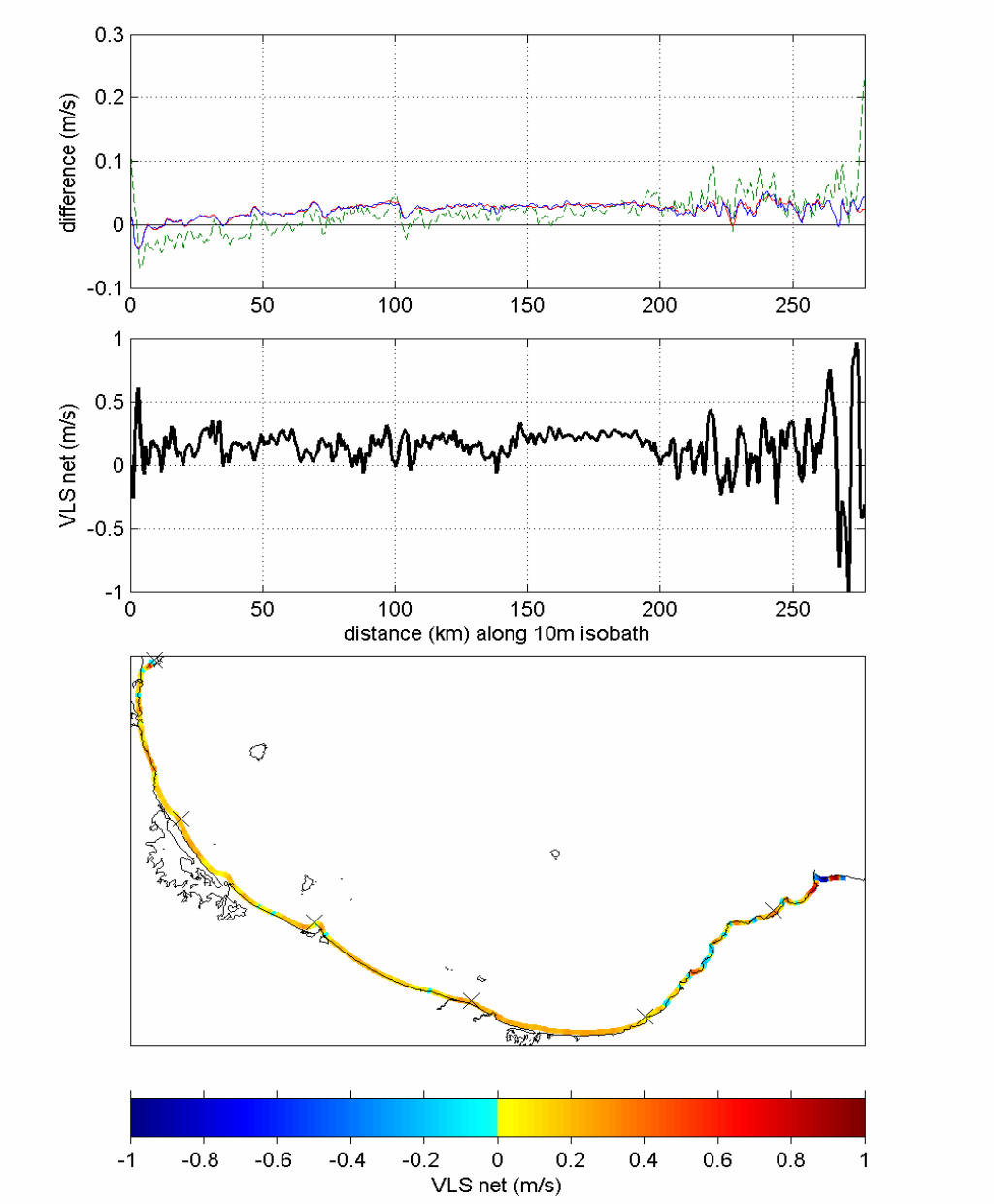

Figure 3.21: Mean net longshore current at the breakpoint produced by combined oblique wave incidence and wave height gradient. Values for the existing climate are plotted in the lower panels in colour-scaled form, and as a function of distance along the 10 m isobath from an origin at its northwest limit. Longshore distance tick marks are marked × in the colour-scaled plot. Positive values (red) denote northward and/or westward currents. The top panel shows changes in values relative to the present climate as predicted under the climate change scenarios: unchanged swell and 0.18 m/s added to eastward winds (red line), adjusted swell and 0.18 m/s added to eastward winds (blue line), adjusted swell and wind speed scaled up by 10% (dashed green line).

3.7.4 Wave induce runup and setup

Maximal values of runup and setup were estimated from portions of the coast where average beach slopes could be estimated from profile data. These are shown in Figures 3.22 and 3.23, in the form of averages (over the 20 years of the WAM hindcast), of expected annual maximum values of storm runup and setup. The runup component was estimated to mostly lie in the 1-2 m range, with highest values occurring around the central region between Katikati (Matakana Island) and Whakatane. It is appreciated that higher run-up values have been recorded at Waiotahi Beach and along the coast towards East Cape (Peter Blackwood, Pers. Comm.) but beach profile data was not available for these locations. Setup was of a similar order, resulting in combined values of order 2-4 m. These values were minimally affected in the scenario with an unchanged swell climate, with only local winds modified. When the extreme end of the swell climate was modified, expected maximum runup and setup values were significantly affected, increasing by up to approximately 0.5 m.

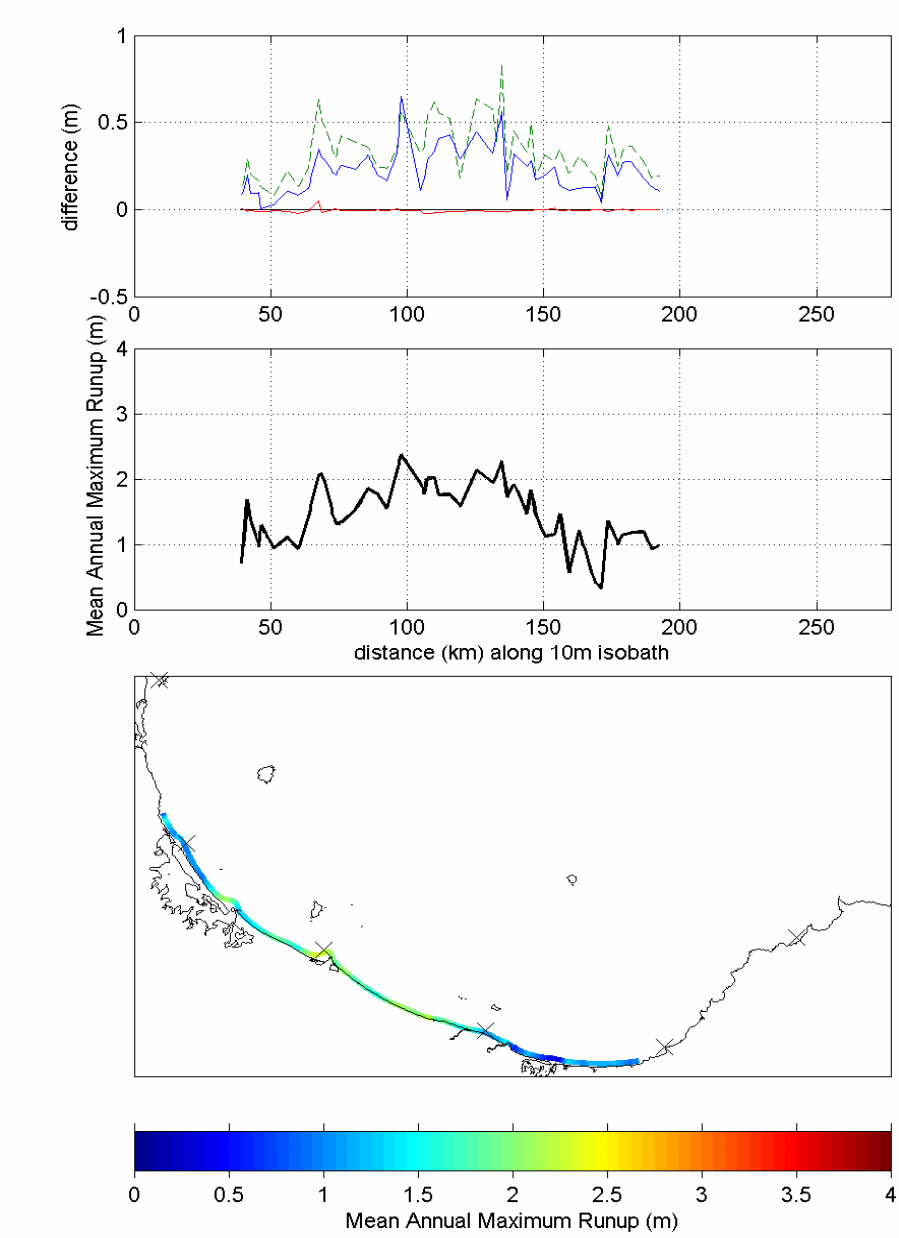

Figure 3.22: Mean values of the annual maximum swash runup. Values for the existing climate are plotted in the lower panels in colour-scaled form, and as a function of distance along the 10 m isobath from an origin at its northwest limit. Longshore distance tick marks are marked × in the colour-scaled plot. The top panel shows changes in values relative to the present climate as predicted under the climate change scenarios: unchanged swell and 0.18 m/s added to eastward winds (red line), adjusted swell and 0.18 m/s added to eastward winds (blue line), adjusted swell and wind speed scaled up by 10% (dashed green line).

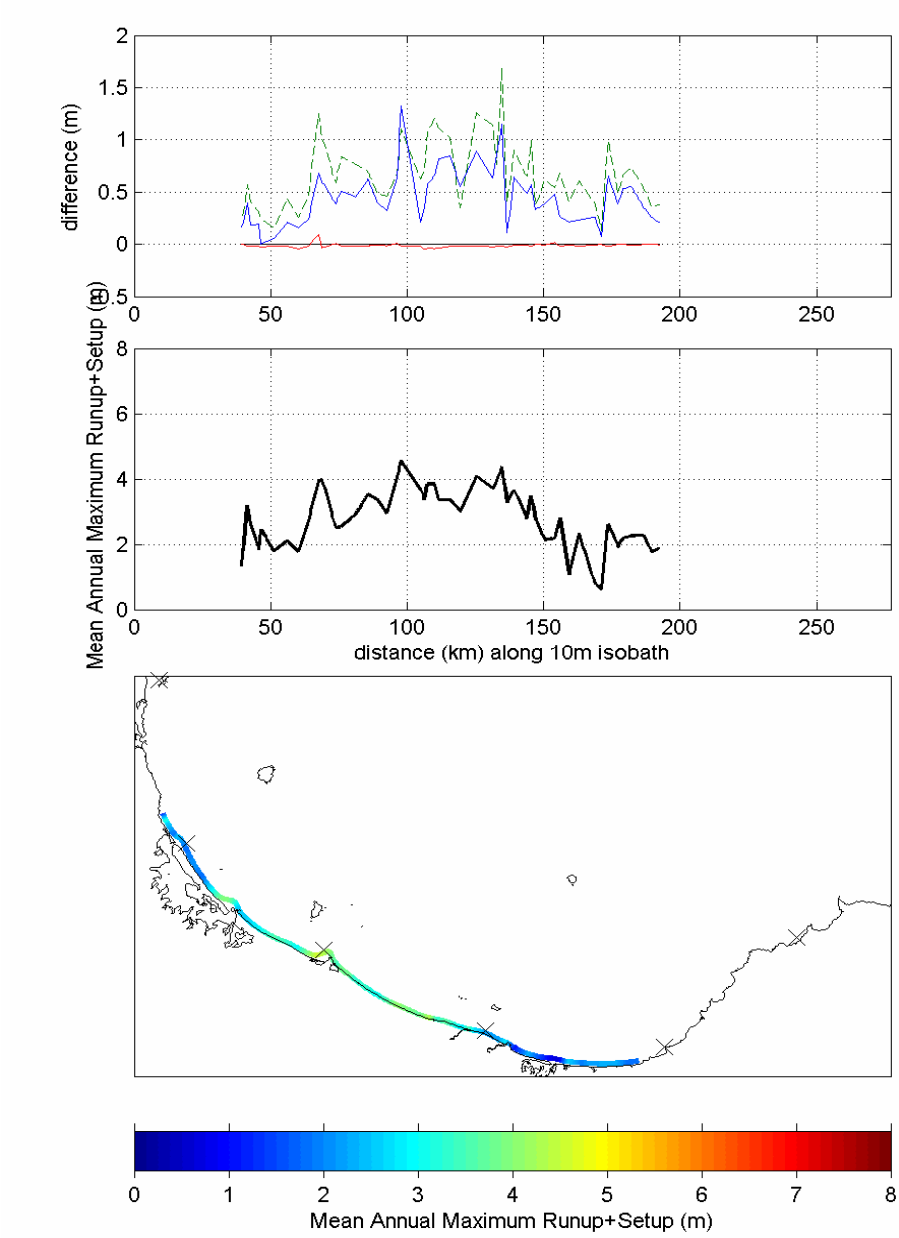

Figure 3.23: Mean values of the annual maximum of combined swash runup and wave-induced setup. Values for the existing climate are plotted in the lower panels in colour-scaled form, and as a function of distance along the 10 m isobath from an origin at its northwest limit. Longshore distance tick marks are marked × in the colour-scaled plot. The top panel shows changes in values relative to the present climate as predicted under the climate change scenarios: unchanged swell and 0.18 m/s added to eastward winds (red line), adjusted swell and 0.18 m/s added to eastward winds (blue line), adjusted swell and wind speed scaled up by 10% (dashed green line).

3.7.5 Seasonal and interannual variability

Long term climate change must also be considered in the context of "natural" variability at shorter medium scales. Beyond the synoptic-scale variability associated with individual storm systems, most weather phenomena can be expected to have seasonal variation. A 20-year record is also long enough to identify signals of some longer-period climate variations, such as the El Niño Southern Oscillation (ENSO) cycle, but insufficient to adequately reflect track interdecadal variation, such as might be associated with the Interdecadal Pacific Oscillation.

Figure 3.24 shows the variation through the 20 year hindcast period of monthly mean values of wave energy flux and longshore flux factor P_{LS} , at a representative site on the 10 m isobath in the central Bay of Plenty. The magnitude of energy flux is highly variable at a monthly scale, with values below 5 kW/m in many calmer months, but with several particularly energetic months averaging over 20 kW/m. As we saw above, typical values of the long term mean of P_{LS} are of order 1 kW/m, but we see that variations of order ±3 kW/m are typical at this scale.

Much of this variation is seasonal, and we find that long-term averages of energy flux for each calendar month (Figure 3.25) show a peak in the winter months at 10-11 kW/m, while summer averages are in the 6-7 kW/m range.

The state of the ENSO cycle can be represented by the Southern Oscillation Index (SOI), which is derived from the monthly mean pressure difference between Darwin and Tahiti (Figure 3.24). Positive values of SOI are a signal of La Niña conditions, while negative values indicate an El Niño phase.

Anomalies in the monthly mean values were calculated by subtracting the mean annual cycle, and compared with the SOI. it was found that the anomalous flux magnitude had a correlation of R = +0.18 with SOI, with a p-value of 0.006, meaning that there would be only a 0.6% probability of obtaining a correlation of this magnitude or higher if the two records were truly independent. Hence we can say that the state of the ENSO has a moderate but robust influence on the magnitude of energy fluxes reaching the Bay of Plenty coast. The positive correlation indicates that more energetic conditions than average tend to occur in La Niña years, which are associated with an increase in northeasterlies in the New Zealand region. Such winds are generally onshore for the Bay of Plenty coast. Conversely, El Niño years have a higher incidence of southwesterlies, bring reduced wave energies in the Bay of Plenty. This confirms the conclusions that beaches on the north east coast of the North Island are

more likely to experience erosion during periods of the IPO when La Niña conditions are more dominant (de Lange, 2000)

On the other hand, anomalies in P_{LS} had a correlation of R = -0.04 with SOI, at a p-value of 0.52. This indicates that SOI has negligible influence on the longshore flux factor. This suggests that most of the variation in wave flux is contained in the onshore component, with little ENSO-dependent variation in the longshore component.

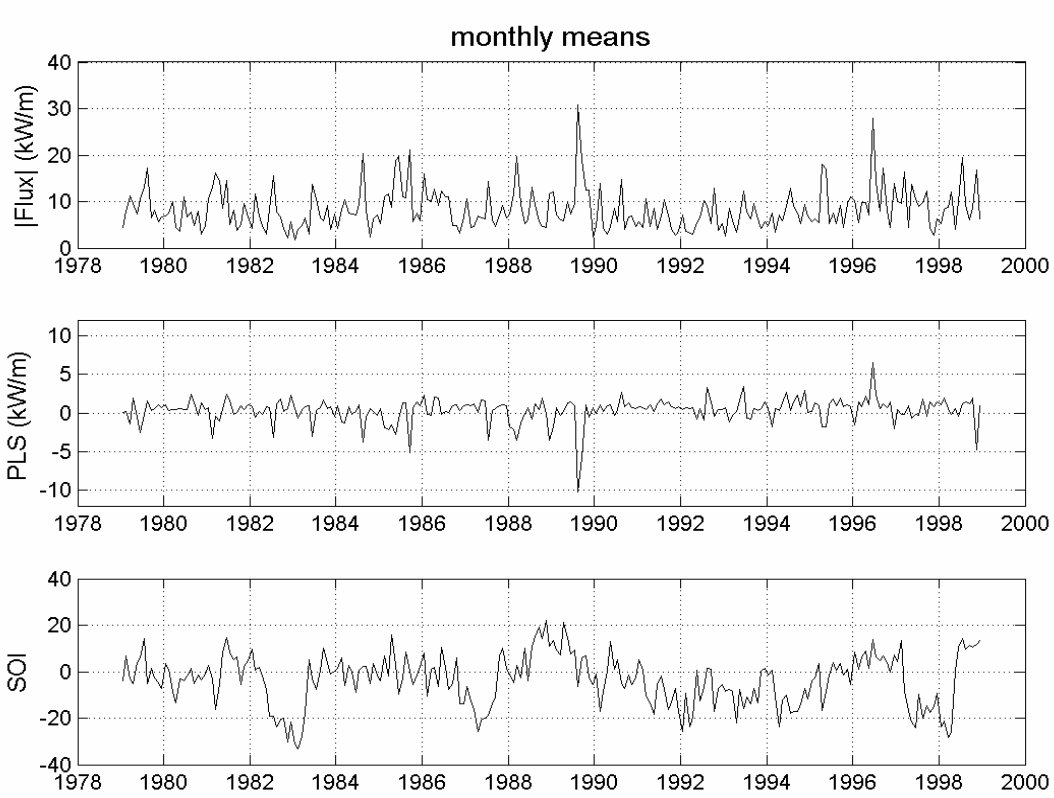

Figure 3.24: Monthly mean values of wave energy flux magnitude (top panel) and longshore flux factor P_{LS} (middle panel) at a point on the 10m isobath over the 20 year simulation based on the existing climate. These have the long-term mean value for each calendar month subtracted. The bottom panel shows variation of the Southern Oscillation Index.

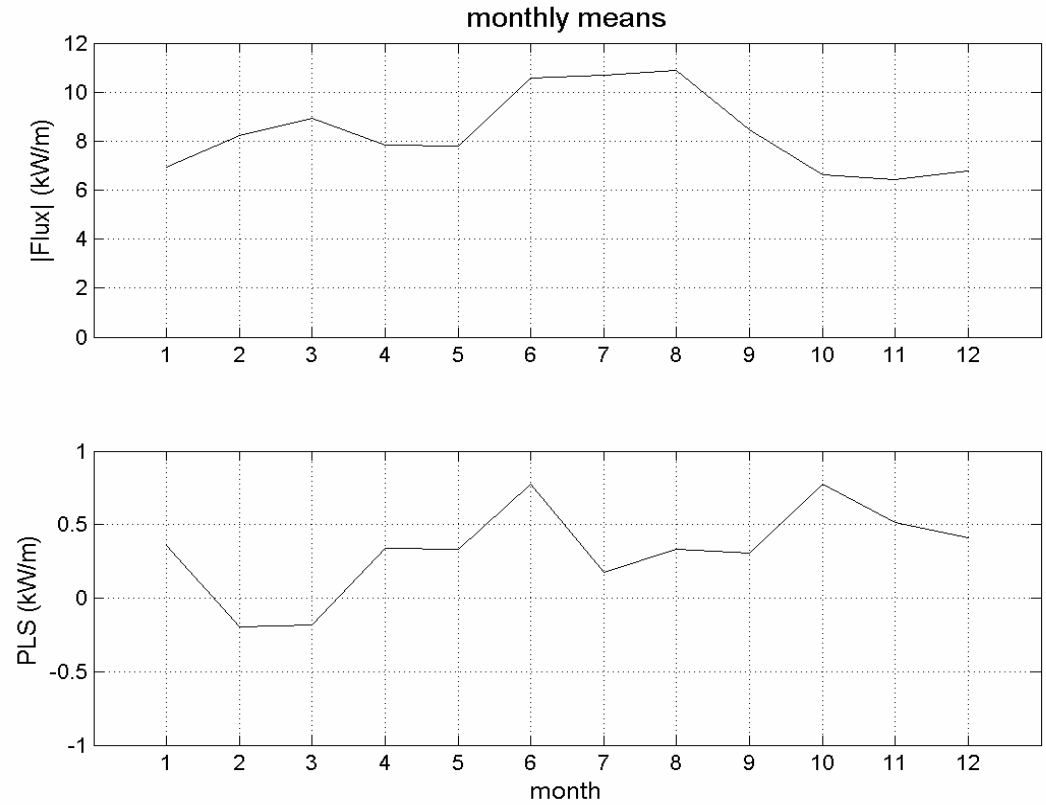

Figure 3.25: 20-year averages of wave energy flux magnitude (top panel) and longshore flux factor P_{LS} (middle panel) for each calendar month, at a point on the 10m isobath.

4. Fluvial sediment supply

4.1 Introduction

The objective of this component of the project is to assess the effects of inter-annual variability and climate change on fluvial sediment yields and supply to the Bay of Plenty coast. Of primary interest is the supply of sand and gravel, since that is the sediment that provides an input to beach systems within the region. The general approach is as follows:

- Estimate the sediment supply to the coast over recent decades
- Examine its annual variability and correlation with inter-annual climate indices such as the SOI (Southern Oscillation Index) and IPO (Interdecadal Pacific Oscillation)
- Estimate how the sediment yields might vary as a result of future climate change, including changes in the SOI or IPO patterns.

Rainfall is the main climatic driver that affects river sediment yield, since it affects both hillslope erosion rates and the transport capacity of runoff down river channels. Thus the assessment of the impacts of future climate change is keyed to estimates of future rainfall.

4.2 Methodology for assessing current sediment supplies to coast

4.2.1 General approach

River sediment loads include both suspended load and bedload. As detailed in Hicks et al. (2004), the suspended load, generally comprising finer sediment in the clay, silt, and very fine to medium sand grades, is more easily measured in rivers. Suspended sediment gaugings have been made in most of the larger rivers draining into the Bay of Plenty over recent decades (Table 4.1). These are adequate to establish 'rating' relationships between suspended sediment concentration (SSC) and water discharge (Q), which can be combined with water discharge records to estimate suspended sediment yields on annual and long-term average bases. There are also a few gaugings where the size grading of the suspended load has been measured (Table 4.1), and these can be used to estimate the percentage of sand in the suspended load. Suspended

sediment yield from ungauged catchments can be estimated using empirical relationships calibrated from gauged catchments.

The bedload comprises sand and gravel. Bedload estimates are typically made from sediment budget analyses of river bed-material. These are based on surveys of the volumes of sand or gravel bed stored in river channels, and must also allow for sand and gravel extraction. Reservoirs (e.g., Matahina Reservoir on the Rangitaiki River) are useful for this purpose since they trap all of the river bedload. Bedload is generally harder to determine than suspended load, though, and consequently there is less information available. Thus a common approximation is to estimate it as a proportion of the suspended load, where that proportion has been established from one or two rivers draining catchments of similar rock-type.

Another factor to consider is how much of the sand and gravel fractions that the rivers bring to their coastal plains from their steeper headwaters pass to the ocean and how much is trapped on the plains and/or in estuaries.

Thus the approach used here to estimate the beach-grade sediment yields is:

- estimate suspended sediment yields from gauged catchments using sediment ratings
- estimate suspended sediment yields from ungauged catchments off an empirical relation
- assume representative sand proportions of the suspended load
- assume that the bedload equates to a percentage of the suspended load
- estimate the trap efficiency of the sand and gravel load in estuaries.

4.2.2 Annual average suspended sediment yields from sediment ratings

Suspended sediment gaugings data exist for 12 rivers draining to the Bay of Plenty coast (as detailed in Table 4.1). For these, rating relationships between concurrently gauged water discharge and discharge-weighted suspended sediment concentration were fitted using NIWA's SEDRATE toolbox, and the ratings were combined with the water discharge data compressed into flow duration tables to compute mean annual suspended sediment yield over the period of discharge record (See Appendix 3 for an example output for the Whakatane River). The usual approach was to fit the rating to

the log-transformed data using LOWESS (Locally Weighted Scatterplot Smoothing), and, as appropriate, applying a log bias correction factor (e.g., Ferguson, 1986). In instances where the data showed a simple power relationship across the whole range of discharge, the Minimum Variance Unbiased Estimator (MVUE) method of Cohn et al. (1989) was used to fit the rating.

Table 4.1 Summary of suspended sediment gaugings data for rivers draining to Bay of Plenty.

Site information			Flow record			SS Data				SS Yield		
Site No	River	Site name	Catchment area (km^2)	Start	End	Data Source	Mean flow (l/s)	Number of gaugings	Max. Conc. (mg/l)	Particle size analyses	Sediment yield (kt/yr)	Suspended sediment yield ($t/km^2/yr$)
13901	Mangawhai	Omokoroa	3.0	710323	Present	NIWA	69	13	182		0.105	35.5
14614	Kaituna	Te Matai	948.0	550511	Present	EBOP	38982	18	289		51.716	54.6
15302	Tarawera	Awakaponga	493[15]	480527	Present	EBOP	31307	27	710		94.925	192.5
15412	Rangitaiki	Te Teko - pre Matahina	2893.0	480602	651231	NIWA	70920	6	5119		216.300	74.8
15412	Rangitaiki	Te Teko - post Matahina	2893.0	670101	Present	NIWA/EBOP	70920	47	181		59.700	20.6
15514	Whakatane	Whakatane	1557.0	520218	Present	NIWA	56725	39	8733		592.416	380.5
15802	Waiotahi	McNabs Road Bridge	103.0	800610	831125	NIWA	4038	27	197		11.037	107.2
15901	Waioeka	Gorge Cableway	661.1	580317	Present	NIWA	31714	55	7099	3	653.353	988.4
16006	Otara	Gault Road Br(No.2)	318.0	790711	820914	NIWA	14360	20	1550		92.574	291.1
16205	Waiaua	Edwards	92.4	810107	841012	NIWA	4959	13	1058		64.690	700.1
16501	Motu	Houpoto	1393.0	570603	Present	NIWA	91028	101	14600	4	3525.525	2530.9
17101	Raukokore	SH35 Bridge	354.3	791212	Present	NIWA	30589	33	11544	4	4705.902	13283.4
17301	Tauranga	Maruhinemaka	5.4	680910	930105	NIWA	86	19	4411		2.060	381.5

[15] Catchment area is for area contributing sediment and excludes area upstream of Lake Tarawera outlet.

4.2.3 Empirical sediment yield prediction model

Mean annual suspended sediment yields from the un-gauged catchments were estimated from an empirical model. This model was developed jointly by NIWA and Landcare Research and relates sediment yield (per unit area) to mean annual rainfall and an erosion-terrain classification defined on the basis of slope, rock-type, soils, main erosion processes, and expert knowledge. The model was calibrated with river suspended sediment gaugings from over 200 sites around New Zealand. It exists as a GIS 'grid' layer, and can be used to estimate suspended sediment delivery from within any defined catchment boundary.

4.2.4 Sand fractions of suspended load

The only Bay of Plenty rivers with particle-size analyses of their suspended sediment are the Waioeka, Motu, and Raukokore Rivers. Average size distributions and the range in sand percentages for these rivers are listed in Table 4.2. For the other rivers, we have assumed representative size distributions based on dominant catchment lithology. This follows from Hicks et al. (2004), who report that suspended sediment particle distributions in New Zealand rivers generally reflect catchment rock-type. To cover the rivers draining the pumice country, we have used particle-size data analyses from other rivers draining the pumice/rhyolite terrain of the Taupo Volcanic Zone. These are included in Table 4.2 and derive from Hicks et al. (2001). Thus we assume:

- the average size grading of the Raukokere River samples to represent the catchments draining the Tertiary mudstone terrain at East Cape
- the average size grading of the Motu and Waioeka samples to represent the catchments with dominantly greywacke-argillite basement and thinner ash cover from the Haparapara west to the eastern tributaries of the Rangitaiki
- the Rangitaiki will have had its sand fractions filtered-out in the Matahina reservoir
- the average size grading of pumice and ignimbrite sub-catchments in the Taupo Volcanic Zone represents the pumice/ignimbrite/lava terrain from the Tarawera River westwards.

Table 4.2 Average suspended sediment particle size distributions from rivers in and adjacent to the Bay of Plenty.

River	Motu & Waioeka	Raukokere	Taupo Volcanic Zone
No analyses	7	4	9
Dominant lithology	Greywacke/ argillite	Tertiary mudstones, sandstones	Ignimbrites, pumice and rhyolite
% finer than 4 μm	27.2	25.2	16.5
% finer than 16 μm	48.3	50.5	38
% finer than 32 μm	62.7	67	47.3
% finer than 63 μm	73.4	83.7	51.5
% finer than 125 μm	85.1	95	65.8
% finer than 250 μm	93	99.3	79.3
% finer than 500 μm	98	99.7	95.3
% finer than 1000 μm	99.7	100	99.5
D_{50} (μm)	18.9	16.6	52
Average % sand	26.6	16.2	48.5
Range % sand	16-39	12-24	33-90

4.2.5 Bedload

Bedload information from Bay of Plenty rivers is patchy. It derives from direct measurements, entrapment rates in reservoirs, and bed-material budgets compiled from cross-section surveys and sand/gravel extraction figures from the coastal reaches.

To our knowledge, the only Bay of Plenty river where bedload has been measured directly is the Tarawera River. There, R. Murray (NIWA, Rotorua, pers. comm.) used a Helley-Smith bedload sampler in the 1970s-1980s and found that the bedload was 50% of the total load, indicating that the bedload equated to the suspended load. At that time the Tarawera catchment was still passing the slug of ash left by the Tarawera eruption, and so is probably not representative of the pumice-ignimbrite catchments further east.

We estimate that the Rangitaiki River had a bedload that was ~ 31% of the total load before the Matahina Dam was built in 1966. This estimate was based on measurements of the Rangitaiki suspended load before and after the dam was built and surveys of sedimentation in the reservoir. These surveys showed an annual average rate of sediment deposition of 213,800 m^3/yr between 1967 and 1980 (R. Murray, NIWA Rotorua, pers. comm.). Over this period we estimate that the actual suspended load passing Te Teko, downstream of the dam, was ~ 67,000 t/yr, while we estimate (by applying the pre-dam sediment rating to the 1967-1980 flow record) that the

suspended load would have been ~ 220,000 t/yr without the dam. Assuming bulk densities of 1.0 t/m^3 for deposited suspended sediment and 1.5 t/m^3 for deposited bedload (using bulk density figures from Phillips and Nelson, 1981), we estimate a Rangitaiki bedload of 99,000 t/yr (which equates to 31% of the total load[16] or 45% of the suspended load).

We consider it reasonable to assume that the Rangitaiki's natural bedload figure equivalent of 45% suspended load should be applicable to the other rivers in the pumice/ignimbrite terrain. Of course, the presence of the Matahina Dam means that the current bedload of the Rangitaiki River will be substantially reduced from its natural level.

Environment Bay of Plenty have been collating information on river bed levels (as surveyed at cross-sections) and sand and gravel extraction from riverbeds as part of their Natural Environment Regional Monitoring Network (NERMN) River and Stream Channel Monitoring Programme (Pak, 2003; Environment Bay of Plenty, 2004) since the early 1990s. This information has permitted estimates to be made of bed material (i.e., sand and gravel) supplies to the lowland reaches from upper catchment erosion (Table 4.3).

For the greywacke-dominated catchments of the eastern Bay of Plenty, using estimated gravel supply figures from EBOP (2004) and the Matahina entrapment estimates for catchment bedload supply, and using the suspended load estimates developed for this study, we find (Table 4.3) that the bedload / suspended load ratio varies over a factor of 10, between 6.4% and 63%, and averages approximately 33%. The higher ratios tend to occur in the catchments with more ash cover (e.g., Whirinaki) and where the rivers drain directly from steep headwaters (e.g., Otara) without passing through alluvial storage reaches (e.g., Waimana). Nonetheless, there are exceptions to these rules. For example, the Waioeka has a relatively low bedload, but this may simply be a reflection of its high suspended load. Indeed, its specific bedload yield (82 t/km^2/yr) is much the same as the average specific yield from all sites in Table 4.3.

[16] While Callandar and Duder (1979) performed a similar calculation and derived a Rangitaiki bedload equating to 14% of the total load, this was based on their assumption that the bedload deposits in Lake Matahina had a bulk density of 1 t/m^3. We believe this unlikely, given the data provided by Phillips and Nelson (1981) and the significant greywacke component of the Rangitaiki's bed material.

Table 4.3 Bedload (BL) and suspended sediment load (SS) estimates, eastern Bay of Plenty rivers. Bulk density of bedload assumed to be 1.8 t/m^3 for greywacke-catchment rivers to east of Rangitaiki.

River	Catchment area (km^2)	Main lithology	BL (m^3/yr)	BL (t/yr)	BL (t/km^2/yr)	SS (t/yr)	SS (t/km^2/yr)	BL / SS (%)	BL reference
Rangitaiki pre-Matahina	2893	Ash & greywacke		99000	34	220000	76	45.0%	This study
Whirinaki	534	Ash & greywacke	24000	43200	81	68900	129	62.7%	EBOP 2004
Waimana	440	Greywacke	20000	36000	82	564000	1282	6.4%	EBOP 2004
Whakatane u/s Waimana	1117	Greywacke	40000	72000	64	240000	215	30.0%	EBOP 2004
Waioeka	661	Greywacke	30000	54000	82	727000	1100	7.4%	EBOP 2004
Otara	318	Greywacke	24000	43200	136	92600	291	46.7%	EBOP 2004
Average					**80**			**33%**	

Thus in this study, we have assumed that gravel-rich bedload supplies to the coastal plains from the dominantly greywacke catchments east of the Rangitaiki equate to the average value of 33% suspended load, but note that the actual yield may vary from river to river by a factor of two at least. For the rivers west of the Rangitaiki, we have assumed a bedload equivalent to 45% of the suspended load based on the results from Matahina Dam.

We stress also that these are estimates of bedload supply to the coastal plain. How much is delivered to the coast depends on what deposition occurs naturally on the coastal plain (e.g., Environment Bay of Plenty 2004 note that the Otara River is aggrading), what bedload is deposited or scoured from the coastal reach due to river engineering works, and rates of sand and gravel extraction. In rivers such as the Whakatane, Waimana, and Waioeka, Environment Bay of Plenty (2004) report that bed levels have been stable in recent decades, but there, gravel extraction has consumed much of the supply, thus the exports to the coast are likely to have been small. The present Environment Bay of Plenty policy is to carefully regulate the locations and rates of gravel extraction, directing extraction to sites of aggradation with the aim of maintaining stable bed levels. It is not clear how far this policy extends to maintaining continuity of the coastal sediment supply.

In the Kaituna River, bed-material delivery to the coast has been affected by the Lower Kaituna River Scheme, which was undertaken for flood control. The Kaituna bed along the coastal plain upstream of Te Matai has been degrading in recent years in response to the historical channel-straightening and dredging (mainly since 1957)

further downstream. These works have steepened the river profile, initiating a headward erosion response that has added a surcharge to the bed material sourced from the Kaituna tributaries. However, the delivery to the coast has been muted because of sediment deposition in the dredged reach between Te Matai and the coast. Based on information in Pak (2003), we estimate that the Kaituna's net average bed material delivery to the coast over recent decades (~ 17,000 t/yr) is only ~ 1/3 of the average supply from its tributaries (~ 50,000 t/yr).

For this study, with the exception of the Kaituna and Rangitaiki Rivers, we have assumed continuity of bedload transfer across the coastal plains.

4.2.6 Estuary entrapment

We have assumed that the larger estuaries (Tauranga, Waihi, and Ohiwa) will be complete traps for bedload and suspended sand supplied by their tributary rivers and streams. We have assumed that the Kaituna's sand and gravel load will bypass the Maketu estuary.

4.3 Current annual average sediment supplies to coast

4.3.1 Suspended sediment yields by catchment

The estimated annual average suspended sediment yields for the Bay of Plenty catchments are listed in Table 4.4. Figure 4.1 maps the catchments, with the catchment identifiers ranked in order of decreasing sediment yield. The East Cape catchments deliver the largest yields, with 85% of the total Bay of Plenty yield (13.7 Mt/yr) supplied by the Motu and the rivers east of it.

4.3.2 Stationarity of sediment ratings

The Whakatane at Whakatane suspended sediment rating was examined for change with time. As shown in Figure 4.2, this rating includes 39 depth-integrated gaugings over the period 16 July 1963 to 13 October 1998. Seventeen of these were collected by Ministry of Works (MWD) or NIWA up to 10 August 1992; the remaining 22 were collected by EBOP from 19 February 1997 (the EBOP sampling site at Valley Road is adjacent to the NIWA recorder site). The approach was to fit a sediment rating curve through the total dataset using LOWESS (as explained in section 4.2.2), then to examine the residuals for a time signal. Log values were used to ensure that the residuals were homoschedastic (i.e., the scatter stays uniform with discharge and time) and normally distributed. Figure 4.3 does not show any clear trend with time. A Students T-test showed that the slope of the linear regression fit to the data in Figure

4.3 was not significantly different from zero at the 5% level, while a two-sample t-test (with unequal-variance) showed no significant difference in the mean residuals for the 1963-92 and 1997-98 data groups. On this basis we conclude no significant change in the sediment rating with time at Whakatane. We have assumed that the same applies to the other rivers with the exception of the Rangitaiki.

Similar statistical tests confirm that the sediment rating of the Rangitaiki at Te Teko has changed significantly since the Matahina Dam was commissioned in 1966 (Figure 4.4). Overall, SSC in the Rangitaiki at Te Teko has decreased by about a factor of 4.

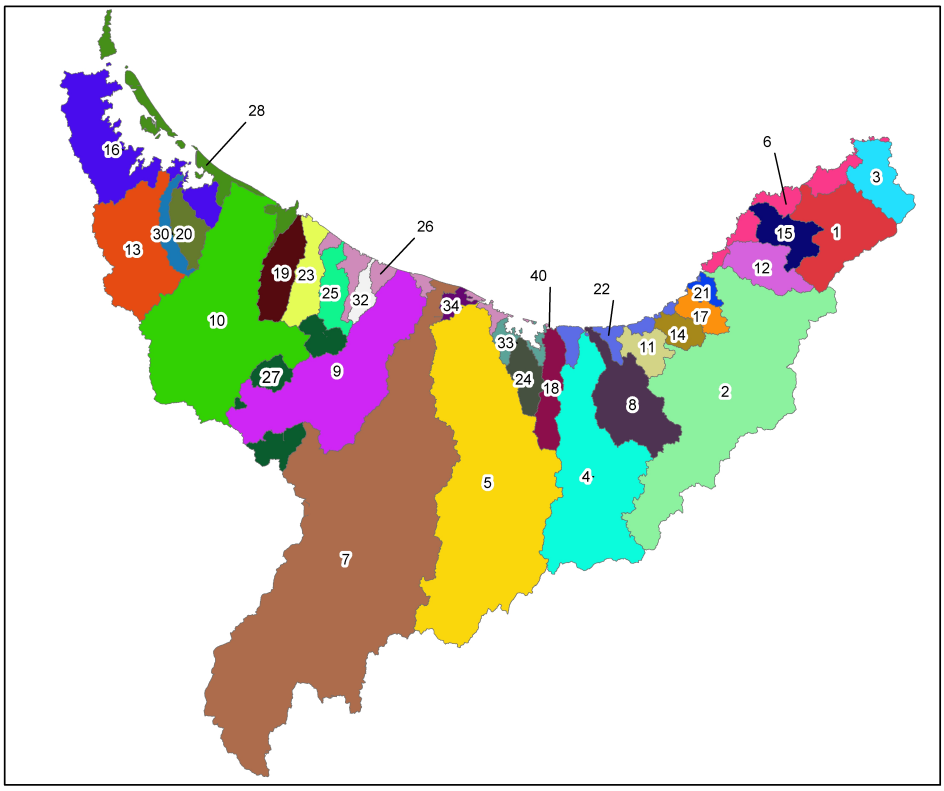

Figure 4.1 Bay of Plenty catchments, ranked in order of suspended sediment delivery to coastal waters.

Table 4.4 Yields of suspended sediment and bedload to the coastal plain, and yields of sand and gravel to the Bay of Plenty coast.

Catchment	Yield rank	Area (km^2)	Main lithology	Susp. sedt. yield (t/yr)	Sand % of susp. sedt.	Bedload as % susp. sedt.	Sand & gravel yield to coastal plain (t/yr)	Delivery % across floodplain	Delivery % to open coast	Current delivery to coast (t/yr)
Whangaparoa	3	179	Mudstone	2990000	16.2%	15.0%	932880	100%	100%	933000
Raukokere	1	354	Mudstone	4710000	16.2%	15.0%	1469520	100%	100%	1470000
Small coastal catchments east of Motu	6	172	Mudstone	321000	16.2%	15.0%	100152	100%	100%	100000
Kereu	15	141	Greywacke-argillite	23100	26.6%	33.0%	13768	100%	100%	14000
Haparapara	12	168	Greywacke-argillite	41400	26.6%	33.0%	24674	100%	100%	25000
Motu	2	1382	Greywacke-argillite	3510000	26.6%	33.0%	2091960	100%	100%	2090000
Waiaopoahu	21	37	Greywacke-argillite	9960	26.6%	33.0%	5936	100%	100%	5900
Hawai	17	73	Greywacke-argillite	22200	26.6%	33.0%	13231	100%	100%	13000
Torere	14	75	Greywacke-argillite	29400	26.6%	33.0%	17522	100%	100%	18000
Waiaua	11	98	Greywacke-argillite	64900	26.6%	33.0%	38680	100%	100%	39000
Small coastal catchments between Motu and Ohiwa	22	102	Greywacke-argillite	9530	26.6%	33.0%	5680	100%	100%	5700
Otara	8	330	Greywacke-argillite	93900	26.6%	33.0%	55964	100%	100%	56000
Waioeka	4	839	Greywacke-argillite	727000	26.6%	33.0%	433292	100%	100%	430000
Waiotahi	18	143	Greywacke-argillite	13900	26.6%	33.0%	8284	100%	100%	8300
Small catchments draining to Ohiwa harbour	33	57	Greywacke-argillite	3520	26.6%	33.0%	2098	100%	0%	0
Waingara	24	103	Greywacke-argillite	9310	26.6%	33.0%	5549	100%	0%	0
Whakatane	5	1733	Greywacke-argillite	804000	26.6%	33.0%	479184	100%	100%	480000
Orini/Kopeopeo/Te Rahu	34	35	Greywacke-argillite	1880	26.6%	33.0%	1120	100%	100%	1100
Rangitaiki	7	2979	Ignimbrite & pumice	59700	37.3%	45.0%	5700	100%	100%	6000
Tarawera	9	821	Ignimbrite & pumice	87600	48.5%	45.0%	81906	100%	100%	82000
Small coastal catchments between Ohiwa and Maketu	26	149	Ignimbrite & pumice	7960	48.5%	45.0%	7443	100%	100%	7000
Herepuru	32	51	Ignimbrite & pumice	3830	48.5%	45.0%	3581	100%	100%	4000
Waitahanui	25	118	Ignimbrite & pumice	8820	48.5%	45.0%	8247	100%	100%	8000
Pongakawa	23	153	Ignimbrite & pumice	9450	48.5%	45.0%	8836	100%	0%	0
Kaikokopu	19	175	Ignimbrite & pumice	11900	48.5%	45.0%	11127	100%	0%	0
Kaituna	10	1199	Ignimbrite & pumice	68200	48.5%	45.0%	63767	30%	100%	19000
Small catchments draining to coast and Tauranga Harbour	28	167	Ignimbrite & pumice	5470	48.5%	45.0%	5114	100%	50%	3000
Waiorohi	20	107	Ignimbrite & pumice	10200	48.5%	45.0%	9537	100%	0%	0
Kopurererua	30	73	Ignimbrite & pumice	5420	48.5%	45.0%	5068	100%	0%	0
Wairoa	13	454	Ignimbrite & pumice	35900	48.5%	45.0%	33567	100%	0%	0
Small catchments draining to Tauranga Harbour	16	465	Ignimbrite & pumice	22700	48.5%	45.0%	21225	100%	0%	0

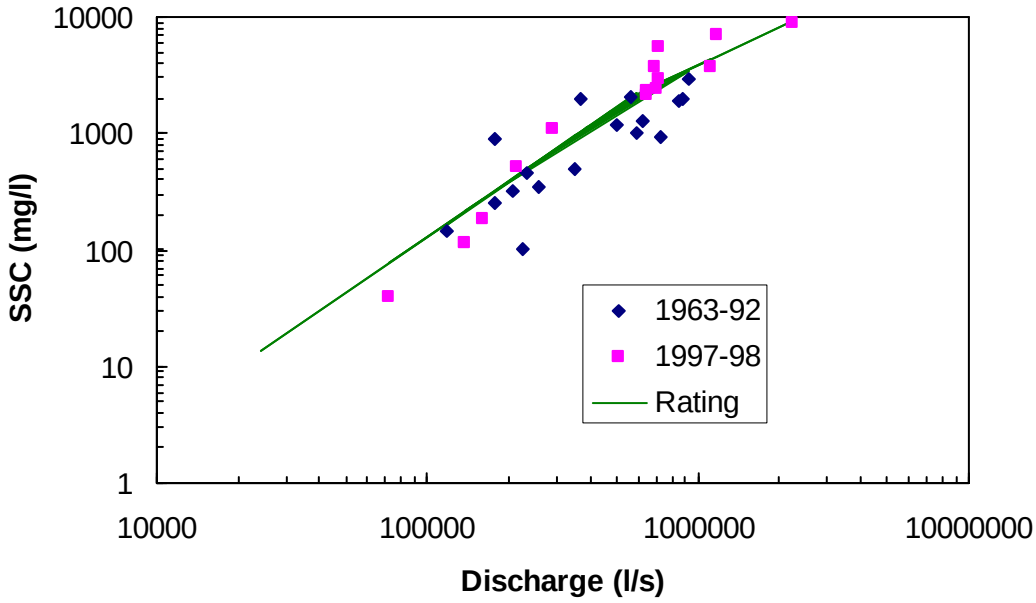

Figure 4.2 Whakatane at Whakatane suspended sediment gaugings. The green curve plots the LOWESS-fitted rating.

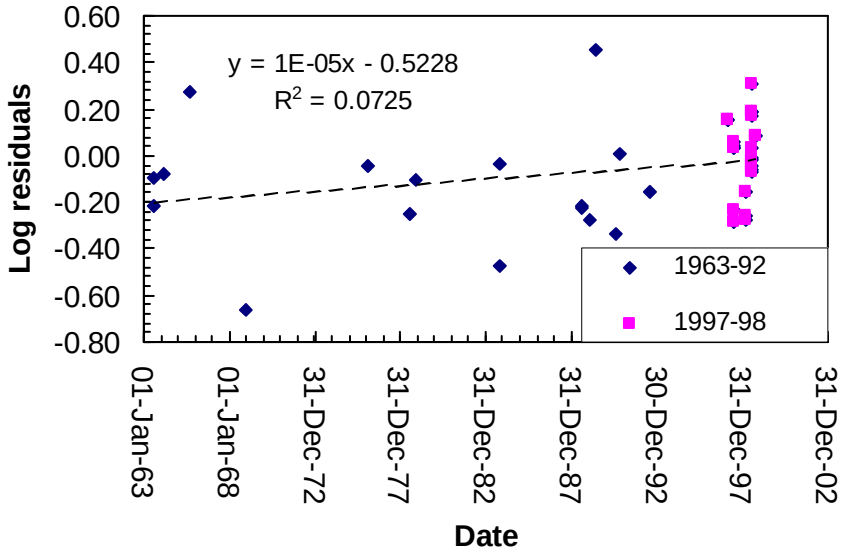

Figure 4.3 Time-series plot of residuals from the Whakatane suspended sediment rating plotted in Figure 4.2.

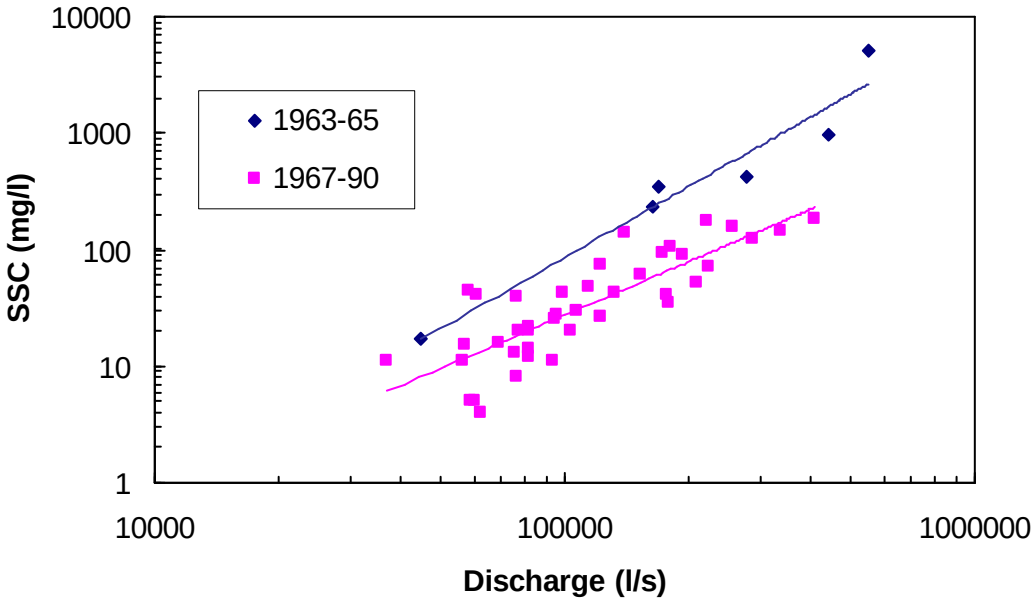

Figure 4.4 Rangitaiki at Te Teko suspended sediment rating before and after Matahina Dam commissioning in 1966.

4.3.3 Sand and gravel supplies to coast

The estimated annual average sand and gravel supplies to the Bay of Plenty coast over recent decades are listed in Table 4.4 and mapped in Figure 4.5. As detailed in Section 4.2, these combine the sand proportion of the suspended load with the bedload, generally assume that bedload delivered to the coastal plain is conveyed to the coast, and contain a simple assessment of estuarine entrapment. Exceptions are that the Rangitaiki load to the coast has been adjusted for sand and gravel trapped in Matahina Reservoir, while the Kaituna sand and gravel yield has been adjusted for storage changes in the lower channel arising from the Lower Kaituna River Scheme.

The bay-wide sand and gravel delivery totals 5.8 Mt/yr. Of this, 80% derives from the Motu and the rivers further to the east. The Motu River is the largest contributor, supplying some 2 Mt/yr (36% of the total).

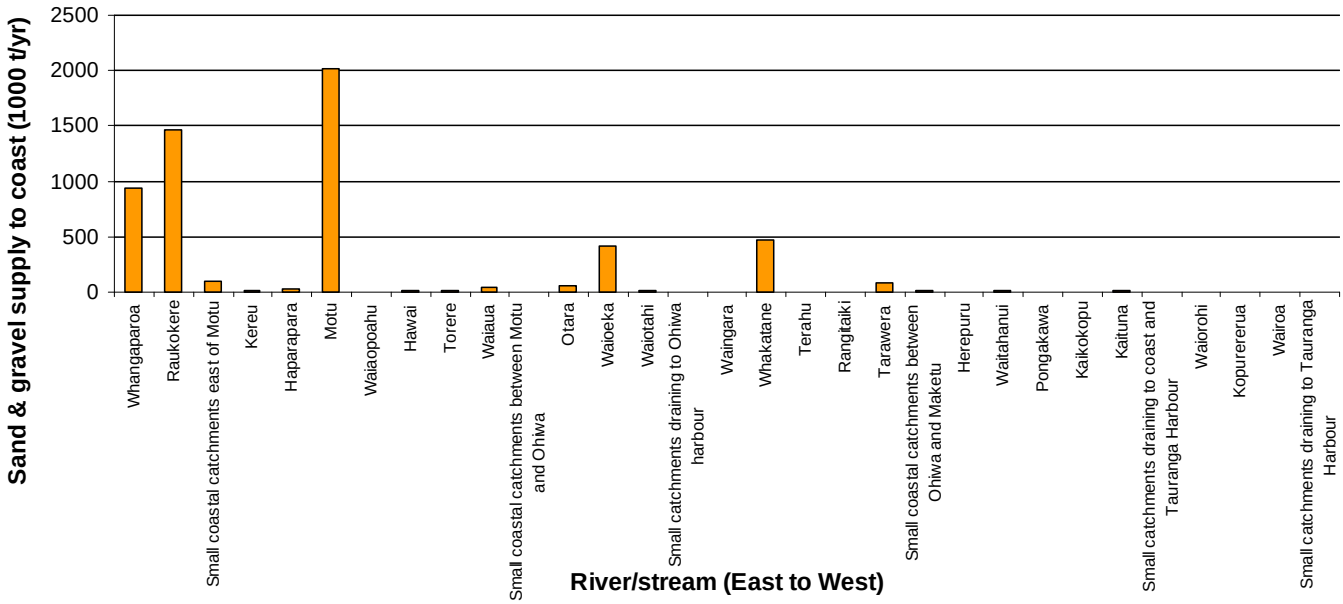

Figure 4.5 Estimated annual average supplies of river sand and gravel to the Bay of Plenty coast over recent decades.

4.4 Methodology for assessing annual variability

4.4.1 Annual sediment yields

Annual variability in sediment yield is indexed off four of the larger rivers that have relatively long flow records (at least from 1959 to the present) and suspended sediment ratings (Tarawera, Whakatane, Waioeka, and Motu). For each of these, annual suspended sediment yields were generated from the flow records and sediment ratings.

A key assumption with this approach is that the sediment ratings do not vary from year to year, perhaps due to the impact of a major storm or to a long-term trend in sediment supply associated with a catchment landuse change. The longest period of sediment gaugings was available from the Whakatane River (1963 through 1998). These gaugings were examined to check the stationarity assumption.

4.4.2 Climate variability indices

Time series of the Southern Oscillation Index (SOI) and Interdecadal Pacific Oscillation (IPO) are available since 1876 and 1871, respectively.

The SOI is the normalised difference of the atmospheric pressure at Darwin (Australia) and Tahiti, and it indexes the El Nino – Southern Oscillation (ENSO). When the SOI is in its positive (La Nina) phase, the pressure gradient drives a strong E-W trade wind airflow in the tropics (with associated patterns in sea surface temperature and sea level), New Zealand tends to experience weaker westerly winds generally, and the Bay of Plenty region tends to experience more storms associated with depressions of tropical origin. During the negative (El Nino) phase, the tropical flow is damped and the mid-latitude westerly airflow tends to be stronger and more persistent, thus the Bay of Plenty might be expected to experience less stormy weather. We have used annual average values of the SOI.

The IPO is the Pacific-wide manifestation of the Pacific Decadal Oscillation described by Mantua et al. (1997). It is based on a multi-decadal sea surface temperature (SST) pattern similar to that associated with ENSO, but differing in several ways. Power et al. (1999) showed that the IPO modulates ENSO climate teleconnections. When the IPO is in its negative phase, La Nina events are more common and the Bay of Plenty typically experiences greater rainfall and storminess. When the IPO swings positive, El Nino conditions tend to prevail and the Bay of Plenty weather becomes more benign. We note, however, that these are tendencies, with many exceptions occurring. The annual series of IPO we have used is derived from a series of seasonal values that has been smoothed over an approximately 11 year time scale (Folland, 2004).

Cross-correlation techniques (Box and Jenkins, 1976) on annual data from 1959 to 2004 were used to search for correlations among sediment loads, the SOI, and the IPO. With this, the cross-correlation coefficient $r_{xy}(k)$, representing the correlation between two series X and Y, where X is lagged by k observations, is found from

$$r_{xy}(k) = c_{xy}(k) / s_x s_y \text{ for } k = 0, \pm 1, \pm 2, \ldots \quad (1)$$

where $c_{xy}(k)$ is the cross covariance at lag k and s_x and s_y are the standard deviations of series X and Y.

4.5 Annual variability in sediment yields

Annual suspended sediment yields for the Tarawera, Whakatane, Waioeka, and Motu Rivers for the period 1959 to 2004 are compared in Figure 4.6, while the average and range of annual yields are listed in Table 4.5.

Table 4.5 Statistics of annual suspended sediment yields (kt) for Tarawera, Whakatane, Waioeka, and Motu Rivers for period 1959 to 2004.

	Mean	Minimum	Maximum	Standard Deviation
Tarawera	90	38	329	52
Whakatane	804	60	4210	891
Waioeka	727	20	4340	741
Motu	3682	840	10110	2054

All show large inter-annual variability. The standard deviations of annual yields are similar to the means, while the ranges cover at least a factor-of-10 and the Waioeka yields range over a factor of 217. The Tarawera yields show least variability and this likely reflects the damping effect of the pumice and lakes in the catchment.

Generally, the largest sediment yields from the Whakatane, Waioeka and Motu occurred in 1970, 1998, and 2004 but the annual pattern is not particularly consistent from one river to the next.

4.6 Correlation analysis

A correlation analysis of annual values showed generally significant un-lagged correlations between the four rivers (Table 4.6). As expected, the IPO and SOI are inversely correlated, but the only significant correlation between the climate indices and sediment yield was from the Tarawera River. This showed a tendency for greater sediment yields during (positive SOI) La Nina years. The Waioeka begins to correlate significantly with the IPO if the IPO is lagged by several years (Table 4.7). The mechanistic significance of this is not clear.

When the annual sediment yields were ranked for each river, there was no indication that higher annual yields tended to be associated with one phase or other of the SOI or IPO.

We conclude that while there is substantial variability in annual sediment yield in the Bay of Plenty Rivers, as a general rule there do not appear to be reliable correlations between annual sediment yield and the IPO or SOI.

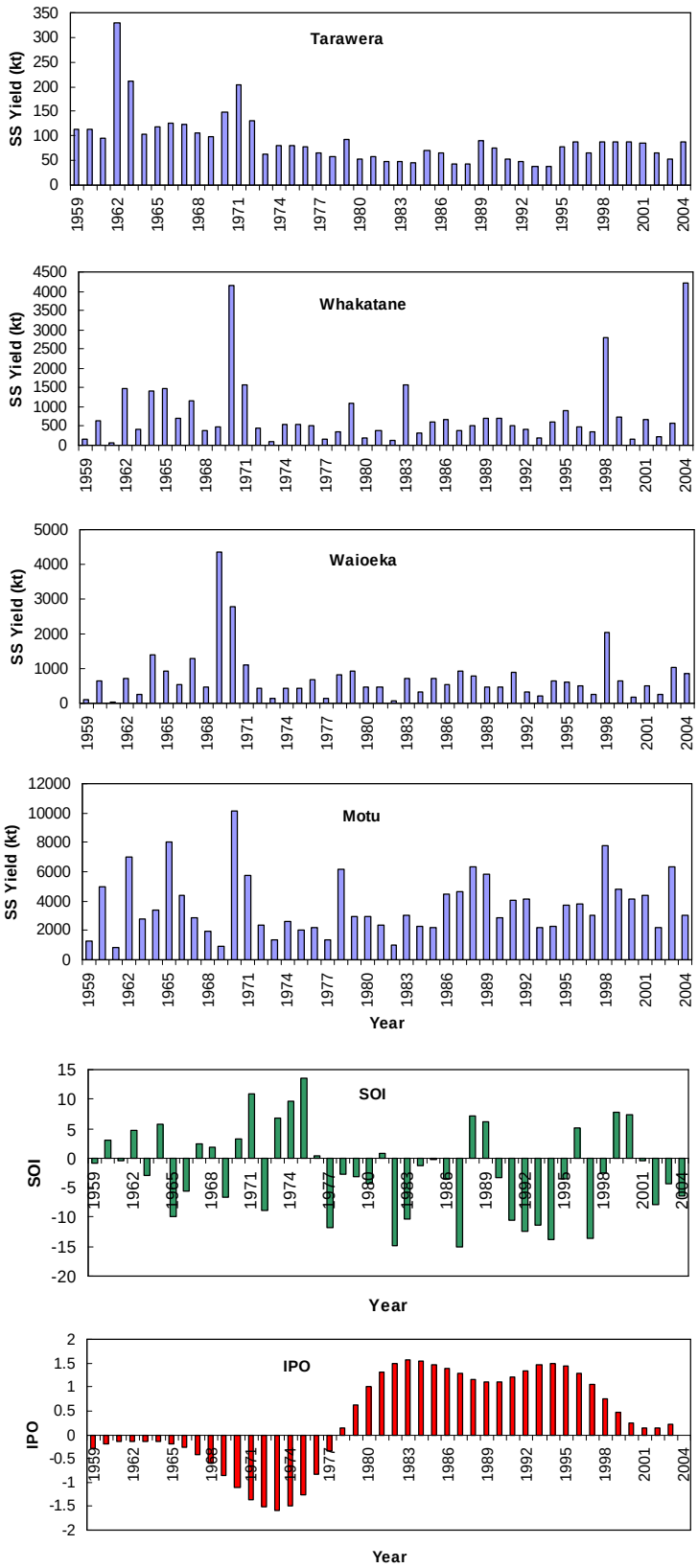

Figure 4.6 Annual suspended sediment yields for the Tarawera, Whakatane, Waioeka, and Motu Rivers and annual average values of the SOI and IPO for the period 1959 to 2004.

Table 4.6 Un-lagged correlation coefficients between annual suspended sediment yields for Tarawera, Whakatane, Waioeka, and Motu Rivers and annual average IPO and SOI for period 1959 to 2004. Bold figures indicate results that are significant at the 5% level.

	Tarawera	**Whakatane**	**Waioeka**	**Motu**	**IPO**	**SOI**
Tarawera	1					
Whakatane	**0.37**	1				
Waioeka	0.16	**0.57**	1			
Motu	**0.32**	**0.71**	**0.33**	1		
IPO	**-0.47**	-0.16	-0.22	0.00	1	
SOI	**0.35**	0.18	0.04	0.18	**-0.45**	1

Table 4.7 Lagged correlation coefficients between annual suspended sediment yields for Tarawera, Whakatane, Waioeka, and Motu Rivers and annual average IPO and SOI for period 1959 to 2004. Bold figures indicate results that are significant at 5% level.

	Lagged correlations with IPO					Lagged correlations with SOI			
Lag (years)	**Tarawera**	**Whakatane**	**Waioeka**	**Motu**	**SOI**	**Tarawera**	**Whakatane**	**Waioeka**	**Motu**
-12	0.09	0.07	0.07	0.14	-0.03	-0.02	-0.14	-0.03	-0.07
-11	0.05	0.01	0.01	0.13	-0.05	0.07	-0.21	-0.12	-0.11
-10	0.03	0.01	0.01	0.20	-0.04	0.07	0.04	0.14	0.05
-9	0.00	0.01	0.01	0.24	-0.04	0.02	0.10	0.11	-0.17
-8	-0.03	0.00	0.00	0.27	-0.05	0.04	0.21	0.10	-0.02
-7	-0.07	0.01	0.01	0.27	-0.06	-0.01	-0.22	0.07	-0.07
-6	-0.10	0.00	0.00	0.24	-0.07	0.00	-0.03	-0.03	-0.29
-5	-0.14	0.00	0.00	0.23	-0.14	0.03	0.01	0.07	-0.21
-4	-0.21	0.00	0.00	0.21	-0.19	0.07	0.00	-0.20	-0.07
-3	**-0.31**	-0.02	-0.02	0.14	-0.27	0.07	0.08	0.06	0.19
-2	**-0.36**	-0.04	-0.04	0.12	**-0.34**	0.09	-0.03	0.09	-0.01
-1	**-0.42**	-0.08	-0.08	0.05	**-0.41**	0.29	-0.19	-0.13	-0.21
0	**-0.48**	-0.13	-0.13	0.00	**-0.46**	**0.35**	0.10	0.03	0.19
1	**-0.52**	-0.20	-0.20	-0.06	**-0.46**	0.16	0.17	0.20	0.11
2	**-0.56**	-0.25	**-0.25**	-0.10	**-0.42**	0.19	0.04	0.21	0.02
3	**-0.58**	-0.28	**-0.28**	-0.13	**-0.35**	0.13	0.11	-0.03	0.00
4	**-0.58**	-0.30	**-0.30**	-0.15	-0.27	0.28	0.17	0.28	0.01
5	**-0.58**	-0.29	**-0.29**	-0.15	-0.18	0.24	0.27	**0.34**	0.06
6	**-0.56**	-0.26	**-0.26**	-0.15	-0.10	0.05	0.10	0.25	-0.10
7	**-0.54**	-0.22	-0.22	-0.15	-0.04	0.05	-0.11	-0.04	-0.17
8	**-0.53**	-0.17	-0.17	-0.15	0.00	0.22	-0.03	-0.14	0.16
9	**-0.51**	-0.11	-0.11	-0.16	0.01	0.30	0.12	0.09	0.17
10	**-0.47**	-0.06	-0.06	-0.17	0.00	0.13	0.09	0.06	0.26
11	**-0.42**	-0.02	-0.02	-0.16	-0.02	0.21	0.06	0.05	0.22
12	**-0.36**	0.03	0.03	-0.13	-0.03	0.19	-0.21	-0.12	-0.14

Note that a positive lag period means that the river sediment yield signal lags behind the IPO or SOI.

4.7 Impacts of climate change

The main and most direct effect of future climate change on fluvial sediment supply to the Bay of Plenty coast is expected to be through changes in rainfall. An increase in rainfall, with increased rainfall intensities, would intensify rain-driven slope erosion processes (including landslips) and also increase runoff and river sediment transport capacity. Thus increases in both bedload and suspended load would occur. The reverse is expected for a rainfall decrease.

4.7.1 Future Bay of Plenty rainfall scenarios

Projected changes in mean annual rainfall across the Bay of Plenty were reported by Griffiths et al. (2003) and have since been revised in NIWA (2004).

Figure 4.7, from Griffiths et al. (2003), maps projected changes in mean annual rainfall across the central North Island for the 2030s and the 2080s relative to the 1970-1999 rainfall normals. These are based on averaged predictions form several different climate models, each assuming 1% compounding CO_2 emissions to the atmosphere without any further scaling to IPCC scenarios (B Mullan, NIWA, pers. comm.). This suggests an overall pattern for the Bay of Plenty region of rainfall reducing by about 2% by the 2030s, with the situation tending back towards no net change by the 2080s.

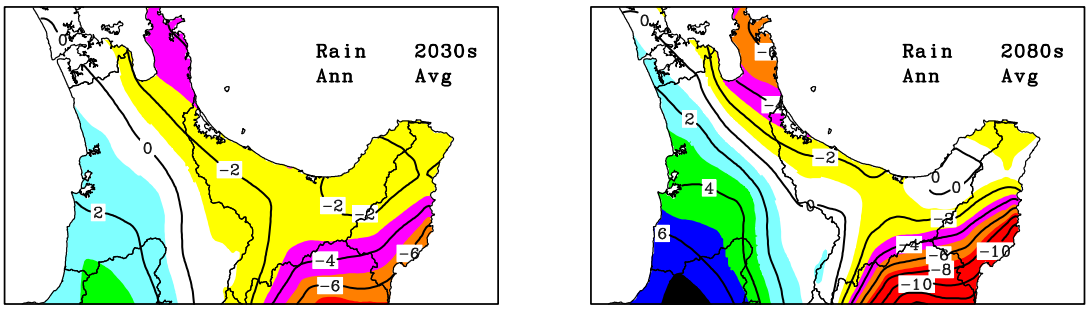

Figure 5.7 Percentage changes in mean annual rainfall over central North Island by 2030s and 2080s (Figure 36 from Griffiths et al., 2003).

In contrast, NIWA's (2004) projections for the Tauranga and Taupo areas, summarising predictions from a range of climate models, range from up to a 15% reduction in rainfall to a 2% increase in rainfall at Tauranga by the 2080s (Table 4.8).

The broad ranges represent the extremes from six climate models and reflect uncertainty in two key areas: first, future greenhouse gas concentration in the atmosphere; second, differences between the climate models (B. Mullen, NIWA, pers. comm.).

Table 4.8 Projected changes for Bay of Plenty seasonal and annual precipitation (in %) for the 2030s and 2080s (from Tables 2.4 and 2.5 of the Guidance Note).

Period	Location	Summer	Autumn	Winter	Spring	Annual
2030s	Tauranga	-10 to +4	-16 to +4	-5 to +7	-20 to +8	-9 to +2
	Taupo	-8 to +3	-9 to +4	-3 to +16	-14 to +2	-5 to +3
2080s	Tauranga	-7 to +19	-18 to +15	-2 to +9	-41 to -3	-15 to +2
	Taupo	-6 to +31	-12 to +7	-10 to +32	-25 to +4	-6 to +10

Pragmatic scenarios

Given this wide uncertainty, the approach followed in this study is simply to investigate possible scenarios covering the range in predictions and the mid range, and assume that these might apply uniformly over the Bay of Plenty region. Thus we investigate the sensitivity of sediment yields to the 2080s extremes of a 15% decrease in rainfall and a 2% increase, and also a mid-range decrease of 8%.

4.7.2 Sensitivity of coastal sediment yield to changes in rainfall

The approach used to assess sediment yield sensitivity to future rainfall change was based on the empirical model for predicting suspended sediment yield from un-gauged catchments. This takes the form $S = aR^{1.7}$, where S is mean annual suspended sediment yield per unit area of uniform erosion terrain, R is the locally-averaged mean annual rainfall for the unit area, and a is a 'sediment supply' coefficient specific to a given erosion terrain. The exponent 1.7 was determined by relating S to R for gauged catchments of uniform erosion terrain, and has been found to be independent of erosion terrain. Differentiating this relation yields $dS/dR = 1.7aR^{0.7}$, thus $dS/S = 1.7\ dR/R$. In other words, for every 1% change in mean annual rainfall the sediment yield will change by 1.7%.

We have assumed that a temporal change in mean annual rainfall will follow this relation, which has been calibrated off spatial variations in rainfall. Table 4.9 lists the expected percentage increases in sediment yield associated with the extreme and midrange rainfall change scenarios discussed above. The change in sediment yield

ranges from a 25% reduction to a 3% increase. We assume here that bedload yields would change in the same proportion.

Table 4.9 Rainfall scenarios to 2080s (as a % change from 1970-99 normals), and equivalent changes in sediment yield

Scenario	Change in mean annual rainfall (%)	Change in mean annual suspended sediment yield (%)
Minimum	-15%	-25.5%
Mid-range	-8%	-13.6%
Maximum	+2%	+3.4%

4.8 Impacts of climate change on sediment yields

As discussed above, the expectation is that river sediment supplies to the coast should change by 1.7% for every 1% change in mean annual rainfall. On this basis, the broad range of projected future rainfalls could lead to changes in sediment yields ranging from a reduction of 25% to an increase of 3%, with a mid-range estimate of a 13% reduction (Table 4.9). These changes are small compared with the factor-of-ten to factor-of-100 variability shown on an inter-annual basis.

The lack of a good existing correlation between annual sediment yields and climate indices suggests that even if the climate modellers could confidently predict a future shift in the balance of El Nino and La Nina events, it would not be clear how this might impact on sediment yields.

Furthermore, we suspect that changes in future rainfall might impact inversely on sediment availability by affecting vegetation growth. For example, a higher rainfall may encourage more intense vegetation growth, protecting the ground from erosion, whereas the reverse may ensue from a reduction in rainfall. These effects on erosion resistance could offset those due to changes in rainfall erosion potential and runoff.

4.9 Recommendations for planning

Given the above results and uncertainties in future climate predictions and effects, our recommendation would be to base estimates of future supplies of river sediment to the coast on the estimates from recent decades.

The existing estimates of sediment fluxes to the open coast could best be improved by

- improving estimates of bedload delivered to the coastal reaches
- continuing to monitor changes in bed-material storage across the coastal reaches
- improving the information base on suspended sediment particle size.

5. Overview of climate change impacts on present day coastal hazard drivers

The primary focus of the study was to assess climate variability and changes in the "drivers" of coastal physical processes and hazards, and assess the potential impacts these changes or trends may have on the coastal margin of the Bay of Plenty region. In particular it looks to summarise our present knowledge, in the context of the Bay of Plenty region, of the impacts of potential climate change on:

- Tides, storm surges and sea levels within the Bay of Plenty.
- Wave conditions along the Bay of Plenty coastline.
- Sediment supply from rivers in the Bay of Plenty to the coastline.
- The potential movements of beach sediment and hence impact on the patterns of coastal erosion or accretion along the Bay of Plenty coastline.

5.1 Tides, storm surges and sea levels

The analysis of sea levels was conducted using data from 8 recorders in the western and central-eastern areas of the Bay of Plenty. The quality of the data varied considerably with some sites having many data dropouts, gaps and spikes, with only the gauge at Moturiki Island having more than 20 years of "continuous" digital record. The importance of long-term records from this gauge network cannot be overstated and it is suggested Environment Bay of Plenty play a coordinating role in encouraging the various gauge owners to be more proactive in maintaining the gauges and apply regular QA procedures to the data.

Based on analysis of sea level data, (of varying length and data quality) from eight tide gauges with the Bay of Plenty region, the characteristics of tides, storm surge and sea levels within the region are summarised as:

- Tides are semi-diurnal, with monthly perigean/apogean effects predominating over fortnightly spring/neap effects.
- Storm surge has the following properties:
    - Storm surge at Moturiki Island leads atmospheric pressure on average by 3 hours. At 48 hour timescales there is a direct equivalence between

storm surge and the inverted barometer sea-level response, while at longer timescales and overall there is an attenuation of the sea-level response to between 60 and 70% of inverted barometer.

- Storm surge is generally persistent (i.e., present conditions indicate future conditions in following hours to days), except for the central-eastern Bay of Plenty sites (Whakatane and Ohiwa). At these latter two sites storm surge overall is larger than at Moturiki Island confirmed by observations during larger cyclone events by Blackwood (1997). At Whakatane this difference can sometime be explained by river flows (but not always the case), but this is not a factor at Ohiwa. Detailed analysis of the processes causing such an increase is beyond the scope of this study, requiring a hydrodynamic model but at present caution is required in applying Ohiwa storm-surge heights directly to the open coast of the eastern region. Over time, the recently installed open coast sea-level gauge at Kohi Point by EBOP will assist with assessing open coast storm-surge levels along this section of coast in comparison to the longer Whakatane and Ohiwa gauge records. In Tauranga Harbour storm tide levels tend to be lower than that recorded at Moturiki, confirming the conclusions of Tonkin and Taylor (1999).

- There has been no apparent change in the number of storm surge events from 1975 to 2005 in the Moturiki record. This conclusion differs from the conclusions of de Lange & Gibb (2000), possibly because their storm surge analysis was different (i.e., it included long period (> 1 month) effects and was based on high tide measurements). It is also perhaps too early into the negative phase of the Interdecadal Pacific Oscillation (IPO) to make any definitive conclusions.

And for sea levels:

- Comparison of the mean annual sea levels between Moturiki and the longer Port of Auckland gauge records showed a close relationship between the two sites. This means that the much longer Port of Auckland (Waitemata Harbour) record (since 1899) can be used as a surrogate for the historic sea-level rise at Mt. Maunganui. Based on this longer-term sea level record from the Port of Auckland gauge, it is suggested that the average rate of mean sea-level rise at Mt. Maunganui over the last century and up until 2005 is around 1.4 mm/yr.

- Long-term vertical land movements at geological timescales appear to vary considerably along the coastline from Waihi Beach to Lottin Point (near Cape Runaway). Between Waihi and Papamoa, land movements appear to be relatively stable. Where the Taupo Volcanic zone intersects the coast (roughly between Maketu and the Whakatane River, average subsidence rates may have been up to 1-2 mm/yr at the coast over geological timescales, whereas form Whakatane to East Cape uplift of between 0.1-2.5 mm/yr has been occurring over geological timescales. However, these rates are generally not continuous and tend to occur in incremental steps during seismic events.

- Present day vertical land movements are now being recorded by a network of Continuous Global Position Systems operated by GEONET. However, in the Bay of Plenty, data for the Tauranga area is only available since around 2003, with meaningful rates of vertical movement only possible after around 10 years of GPS monitoring.

- Given the current lack of information on present-day vertical land movements and the similarity of the rate of sea level rise over the last century in the Bay of Plenty with global averages, it is suggested that current global rate of rise projections (IPCC, 2001) are reasonable at this stage for planning and design purposes. It is recommended that the values of sea-level rise of 0.2 m and 0.5 m (relative to 1990 sea level) be used respectively for 2050 and 2100 planning horizons, in keeping with current MfE (2004b) guidance. This translates to a mean level of the sea of 0.26 m MVD-53 and 0.56 m MVD-53 by 2050 and 2100 respectively.

- At present there is no clear indication whether there will be an increase or decrease in storm surge magnitude and hence how storm tide levels will change. At present it is assumed that storm-tide elevations will rise at the same level as the mean level of the sea.

5.2 Nearshore waves and longshore transport patterns

Wave action is the dominant forcing process causing changes in erosion and accretion patterns along the Bay of Plenty coastline. It also contributes to coastal inundation through locally raising water levels (set-up) and wave run-up on to the land. Assessing the potential effects of climate change on wave conditions experienced at the coastline of the Bay of Plenty is complex, depending on the interaction between both changes in

local conditions around New Zealand and in the wider South Pacific region (e.g., changes in local and regional winds, storm and cyclone tracks and intensity).

Wave modelling was used to assess the variability of nearshore wave conditions and the resulting effect on longshore sediment transport processes, and how these processes may be altered by long-term climate change, along the Bay of Plenty coastline:

- Root mean-square breaking wave heights are generally between 1 m to 1.3 m along the majority of the Bay of Plenty coast and generally decrease from west to east along the coast from Waihi to Opotiki before increasing again towards East Cape, largely reflecting variation in exposure. Under the climate change scenarios considered, increases in root mean-square breaking wave height are estimated to be less than 0.05 m between Waihi and Whakatane and up to 0.1 m further east, towards East Cape over the next 50 years.

- The El-Niño Southern Oscillation (ENSO) cycle has a moderate influence on the magnitude of wave energy experienced within the Bay of Plenty. More energetic conditions than average occur during La Niña years, which are associated with an increase in northeasterlies in the New Zealand region. During El Niño years, where a higher occurrence of southwesterlies occurs, wave energies in the Bay of Plenty are reduced. However, there is little correlation between ENSO state and longshore transport potential.

- Maximum values of wave run-up were estimated for the sections of coast where beach profile data was available to estimate average beach slope. Combined annual maximum values of wave set-up and wave run-up vary between 2 to 4 m, with the highest values occurring in the region between Katikati and Whakatane. It is appreciated that higher values have previously been recorded during extra-tropical cyclones at Waiotahi Beach and along beach areas towards East Cape which was not included in the analysis (P. Blackwood, pers. comm.). Based on the climate change scenarios used, annual maximum combined set-up and run-up values may be increased by up to 0.5 m over the next 50 years.

- Longshore transport is an important process along much of the Bay of Plenty coastline, particularly between Waihi and Opape. Potential net longshore transport flux is generally eastwards but with local variations around headland areas, and between Maketu and Papamoa potentially due to the effects on

Motiti Island on nearshore wave directions. The climate scenarios in general suggested that any changes in longshore transport pattern will be spatially uniform over the Bay of Plenty region, although this is dependent on the impacts that climate change will have on remotely-generated swell conditions.

- Potential longshore transport flux is typically of the order of 1 kW/m equating to potential net sediment transport of 200,000 m^3/yr under the general assumptions used. Under the climate change scenarios simulated, increases in longshore transport flux of the order of around 10% are expected, associated with the predicted 10% change in local westerly winds. By way of comparison, under existing climatic conditions, mean interannual variability in the mean longshore flux factor is of the order of 0.5-1.0 kW/m, while the residual variability of monthly mean values is of the order of ±3 kW/m.

5.3 Fluvial sediment supply

Rainfall is the main climatic driver that affects river sediment yield, since it affects both hillslope erosion rates and the transport capacity of runoff down river channels. Thus the assessment of the impacts of future climate change is keyed to estimates of future rainfall. Our primary interest is the supply of sand and gravel, since that is the sediment that provides an input to beach systems within the region. The assessment covered the effects of inter-annual variability and climate change on fluvial sediment yields and supply to the Bay of Plenty coast. The key findings include:

- Suspended sediment delivery to the coast from rivers and streams in the Bay of Plenty region averages approximately 13.7 Mt/yr. 85% of this derives from the Motu River and the catchments east of the Motu. The largest suspended sediment source to the central Bay of Plenty is the Whakatane River (0.8 Mt/yr). The yield of the Rangitaiki River has been reduced by a factor of four by the Matahina Dam.

- No significant shifts in the relationship between water discharge and suspended sediment concentration occurred in the Whakatane River over the period 1963-1998, which is the duration of the sediment gauging record. On this basis we assume that sediment ratings have remained stationary at the other Bay of Plenty rivers.

- The sand content of the river suspended loads varies with catchment lithology. We estimate that it averages 16% for the mudstone terrain at East Cape, 27%

for the largely greywacke terrain of the eastern Bay of Plenty, and 48% for the pumice and ignimbrite terrain of the central Bay of Plenty.

- The eastern, greywacke catchment rivers have a gravely bedload that equates to approximately 33% of the suspended load on average but this proportion can vary from river to river by at least a factor of two. The central-western rivers draining the pumice and ignimbrite terrain have mainly sandy bedloads equating to 45% of the suspended load on average. Bedload from the mudstone catchments may equate to approximately 15% of the suspend load.

- Bedload delivery efficiency across the coastal floodplains to the coast varies from river to river, depending on the geomorphic setting, sand and gravel extraction, and river control schemes that may shorten channels and create bed-material traps.

- We assume that the larger estuaries (Tauranga, Ohiwa, Waihi) will trap all sand and gravel input from rivers and streams in their upper reaches so that none will be delivered to the open coast.

- Assuming equilibrium bedload delivery to the coast at most rivers, and considering the size grading of the suspended load and estuarine sediment entrapment, the total fluvial supply of beach-grade sediment (i.e., sand and gravel) to the Bay of Plenty open coast averages approximately 5.8 Mt/yr. 80% of this derives from the Motu River and the rivers and streams to the east of the Motu.

- The Bay of Plenty rivers show large inter-annual variability in sediment yields, with annual yields ranging over at least a factor-of-ten.

- In general, there does not appear to be a significant correlation between annual sediment yield and annual average values of the Southern Oscillation Index or the Interdecadal Pacific Oscillation index. The exception is the Tarawera River, which tends to have higher yields during La Niña phases (when the SOI is positive).

- It is expected that annual average river sediment yield should change by 1.7% for every 1% change in mean annual catchment rainfall. Projections of future annual average rainfall in the region vary widely, ranging from a 15% decrease to a 2% increase by the 2080s. This translates to anywhere from a

25% reduction in average annual sediment yields to a 3% increase. Since the range of these projected future changes is small compared to the existing inter-annual variability, it is recommended that planning be based on the existing climate, and research efforts be directed at improving estimates of bedload delivery to the coast and the sand component of the suspended load.

Taking this, and the likelihood that changes to the general longshore movement of beach material is also likely to have a relatively small effect at a regionwide scale, suggests that the patterns of erosion experienced along the open coast of the Bay of Plenty region are unlikely to change substantially relative to that occurring at present and over the last few decades. The most susceptible areas to coastal changes will still occur at locations such as estuary and river mouths, adjacent to promontories and along spit features. However, areas that have traditionally been relatively stable, such as to the south of Papamoa, in the lee of Motiti Island, may begin to show a greater tendency to erode.

6. Acknowledgements

The Authors would like to thank EBOP staff for supplying data, technical documents and photos to assist in composing the section on sea levels. Sea-level data from EBOP, Tauranga City Council, Port of Tauranga Ltd. and Ports of Auckland Ltd are acknowledged.

7. References

Berryman, K., and Hull, A.G. (2003). Tectonic controls on Late Quaternary shorelines: A review and prospects for future research. *In*: "The New Zealand Coast-Te Tai o Aotearoa", Goff, J.R., Nichol, S.L., Rouse, H.L. (*Eds.*), Dunmore Press, with Whitireia Publishing and Daphne Brasell Associates Ltd., p. 25–58.

Blackwood, P.L. (1997). Cyclone Fergus and Drena storm surge: Report on the magnitude of storm surges recorded and implications for design maximum sea levels. Environment BoP Operations Report 97/1, Whakatane. 11 p. + appendices.

Blick, G.H., and Flaherty, M.P. (1989). Regional vertical deformation associated with the 1987 Edgecumbe earthquake, New Zealand. *NZ Journal of Geology & Geophysics 32(1)*: 99–108.

Brandefelt, J., and Källén, E. (2004). The response of the Southern Hemisphere atmospheric circulation to an enhanced greenhouse gas forcing. *Journal of Climate 17*: 4425–4442.

Box, G.E.P., and Jenkins, G.M. (1976). *Time series analysis: forecasting and control*. Holden-Day, San Francisco.

Callander, R.A., and Duder, J.N. (1979). Reservoir sedimentation in the Rangitaiki River. *New Zealand Engineering 34(9)*: 208–215.

CERC, (1984). *Shore protection manual*. Coastal Engineering Research Center, US Army Corps of Engineers, Vicksburg, Mississippi, USA.

Cohn, T.A., DeLong, L.L., Gilroy, E.J., Hirsch, R.M., and Wells, D.K. (1989). Estimating constituent loads. *Water Resources Research 25*: 937–942.

de Lange, W.P., & Gibb, J.G. (2000) Seasonal, interannual, and decadal variability of storm surges at Tauranga, New Zealand. *NZ Journal of Marine & Freshwater Research 34*: 419–434.

de Lange, W. (2000). Interdecadal Pacific Oscillation (IPO): A mechanism for forcing decadal scale coastal change on the northeast coast of New Zealand. *Journal of Coastal Research. ICS 2000 Proceedings*. 657-664.

Environment Bay of Plenty (2004). Bay Trends 2004 –State of the Bay of Plenty environment. Environment Bay of Plenty, Whakatane August 2004.

Ferguson, R.I. (1986). River sediment loads underestimated by rating curves. *Water Resources Research 22*: 74–76.

Folland, C.K. (2004). Interdecadal Pacific Oscillation time series. Unpublished document. Hadley Centre, Met Office, Exeter, UK. Held by Brett Mullan, NIWA.

Geng, Q., and Sugi, M. (2003). Possible change of extratropical cyclone activity due to enhanced greenhouse gases and sulfate aerosols-study with a high-resolution AGCM. *Journal of Climate 16 (13)*: 2262–2274.

Goring, D.G. (1995). Short-term variations in sea level (2 – 15 days) in the New Zealand region. *NZ Journal of Marine & Freshwater Research 29*: 69–82.

Goring, D.G. (2006). Storm surge in the Bay of Plenty. Mulgor Consulting Ltd. Client Report 2006/01, prepared for NIWA, January 2006.

Goring, D.G., and Bell, R.G. (1996). Distilling information from patchy tide gauge records: the New Zealand experience. *Marine Geodesy 19*: 63–76.

Goring, D.G., Pearson, C.P., and Kingsland, S. (1997). Extreme sea levels on the Mt Maunganui shoreline (Moturiki Island). NIWA Client Report No. 97/32, Christchurch. Prepared for Environment Bay of Plenty, July 1997. 21 p.

Gorman, R.M., and Laing, A.K. (2001). Bringing wave hindcasts to the New Zealand coast. *Journal of Coastal Research Special Issue 34 (ICS 2000 New Zealand)*: 30–37.

Griffiths, G., Mullan, B., Thompson, C., Burgess, S., and Tait, A. (2003). The climate of the Bay of Plenty: past and future? NIWA Client Report AKL2003-44, prepared for Environment Bay of Plenty, June 2003. 100 p.

Hannah, J. (2004). An updated analysis of long-term sea level change in New Zealand. *Geophysical Research Letters 31(L03307)*: 1–4.

Hicks, D.M., Webby, M.G., Duncan, M.J., and Harding, S. (2001). Waikato River sediment budget and processes. NIWA Client Report CHC01, NIWA, Christchurch, June 2001. 105 p.

Hicks, M., Quinn, J., and Trustrum, N. (2004). Stream sediment load and organic matter. Chapter 12 *In*: "Freshwaters of New Zealand", J. Harding, P. Mosley, C. Pearson, B Sorrell (*Eds.*), NZ Hydrological Society & NZ Limnological Society, Christchurch.

Hubbard, B.B. (1996). The world according to wavelets: the story of a mathematical technique in the making. A. K. Peters. 264p.

IPCC, (2001). Climate change 2001: The scientific basis. Contribution of Working Group I to the Third Assessment Report of the Intergovernmental Panel on Climate Change. Houghton, J.T., Ding, Y., Griggs, D.J., Noguer, M., van der Linden, P.J., Dai, X., Maskell, K., and Johnson, C.A. (*Eds.*). Cambridge University Press, Cambridge, United Kingdom and New York, NY, USA. 881 p.

Komen, G.J., Cavaleri, L., Donelan, M., Hasselmann, K., Hasselmann, S., and Janssen, P.A.E.M. (1994). *Dynamics and modelling of ocean waves*, Cambridge University Press, Cambridge.

Mantua, N.J., Hare, S.R., Zhang, Y., Wallace, J.M., & Francis, R.C. (1997). A Pacific interdecadal climate oscillation with impacts on salmon production. *Bulletin of American Meteorological Society 78*: 1069–1079.

Ministry for the Environment (2004a). Climate Change Effects and Impacts Assessment: A Guidance Manual for Local Government in New Zealand. Prepared by David Wratt, Brett Mullan and Jim Salinger (NIWA), Sylvia Allen and Tania Morgan (MWH New Zealand Ltd), and Gavin Kenny (Earthwise Consulting). Ministry for the Environment Report ME 513, Wellington, 153 p. Available from: http://www.climatechange.govt.nz/resources/local-govt/effects-impacts-may04/index.html

Ministry for the Environment (2004b). Coastal Hazards and Climate Change: A Guidance Manual for Local Government in New Zealand. Prepared by Rob Bell, Terry Hume, Darren King and David Ray (NIWA), Don Lyon, Steven Taylor, David Papps, Amelia Linzey and Neil Beattie (Beca Consultants), Derek Todd

(DTec Consultants), and Sally Marx (Tonkin and Taylor). Ministry for the Environment Report ME 512, Wellington, 156 p. Available from: http://www.climatechange.govt.nz/resources/local-govt/coastal-hazards-may04/index.html

Mullan, B., Bowen, M., Chiswell, S. (2001). The crystal ball: model predictions of future climate. *Water and Atmosphere 9*: 10–11.

Nairn, I.A., and Beanland, S. (1989). Geological setting of the 1987 Edgecumbe earthquake, New Zealand. *NZ Journal of Geology & Geophysics 32(1)*: 1–13.

Pak, I. (2003). Natural Environment Regional Monitoring Network River and Stream Channel Monitoring Programme 2000/2001 and 2001/2002. Environment Bay of Plenty Environmental Publication 2003/16.

Pawlowicz, R., Beardsley, B., and Lentz, S. (2002). Classical tidal harmonic analysis including error estimates in MATLAB using T_TIDE. *Computers and Geosciences 28*: 929–937.

Phillips, C.J., and Nelson, C.S. (1981). Sedimentation in an artificial lake – Lake Matahina, Bay of Plenty. *New Zealand Journal of Marine & Freshwater Research 15*: 459–473.

Pillans, B. (1986). A Late Quaternary uplift map for North Island, New Zealand. *Royal Society of New Zealand Bulletin 24*: 409–417.

Pillans, B. (1990). Pleistocene marine terraces in, New Zealand: A review. *NZ Journal of Geology & Geophysics 33(2)*: 219–231.

Power, S., Casey, T., Folland, C.K., Colman, A, and Mehta, V. (1999). Inter-decadal modulation of the impact of ENSO on Australia. *Climate Dynamics 15*: 319–323.

Sinclair, M.R., and Watterson, I.G. (1999). Objective assessment of extratropical weather systems in simulated climates. *Journal of Climate 12(12)*: 3467–3485.

Tawn, J.A., and Vassie, J.M. (1991). Recent improvements in the joint probability method for estimating extreme sea levels. *In:* "Tidal Hydrodynamics", Parker B.B. (*Ed.*), John Wiley & Sons: 813–828.

Tolman, H.L. (1999). User manual and system documentation of WAVEWATCH-III Version 1.18, NOAA / NWS / NCEP / OMB. 110 p.

Tolman, H.L., Balasubramaniyan, M., Burroughs, L.D., Chalikov, D.V., Chao, Y.Y., Chen, H.S., and Gerald, V.M. (2002). Development and implementation of wind-generated ocean surface wave models at NCEP. *Weather and Forecasting 17(2)*: 311–333.

Tonkin & Taylor Ltd. (1999). Storm surge inundation study for Tauranga Harbour. Report prepared for Tauranga District Council, Ref No. 16161. 45 p. + appendices.

Walters, R.A., Goring, D.G., and Bell, R.G. (2001). Ocean tide around New Zealand. *NZ Journal of Marine & Freshwater Research 35(4)*: 567–579.

WAMDIG - The WAM Development and Implementation Group: Hasselmann, S., Hasselmann, K., Bauer, E., Bertotti, L., Cardone, C.V., Ewing, J.A., Greenwood, J.A., Guillaume, A., Janssen, P.A.E.M., Komen, G.J., Lionello, P., Reistad, M., and Zambresky. L. (1988). The WAM Model—a third generation ocean wave prediction model. *Journal of Physical Oceanography 18(12)*: 1775–1810.

8. Appendix 1: Summary of tide gauge data analysis methodologies

The methods used in the analysis of the data in this study were standard, but a brief description of them is provided here for readers who are not familiar with them.

8.1 Fourier spectra

An important tool used in the analysis of data such as sea levels is the Fourier spectrum. The Fourier spectrum of a signal is calculated by convolving the signal with a series of sine and cosine waves. It is difficult to discern anything from oscillatory data such as the sea-level record shown in Figure 7.1(A), but when they are transformed into their Fourier spectra (Figure 7.2(B)), patterns in the data become clear. Spectra have frequency (inverse of time) as their abscissa (x-axis) and power spectral density (PSD) which is a measure of energy as their ordinate (y-axis). The area under a spectrum is the variance (2nd statistical moment, or square of the standard deviation). Spectra are usually presented as log-log plots.

Portions of the spectrum where the slope is uniform and negative (such as the storm surge portion in Figure 7.1(B) indicate scaling or fractal properties. In this region the spectrum $S(f)$ can be described by:

$$S(f) \propto f^{-\beta} \tag{1}$$

where f is the frequency and β is the slope which is related to an important fractal number called the Hurst parameter, H, as follows:

$$\beta = 2H + 1 \tag{2}$$

The Hurst parameter takes values between zero and unity and is an indication of "persistence". If a signal is persistent, then the data up to the present can be used to forecast future values, but if a signal is non-persistent, then there is insufficient pattern to the data and forecasting is impossible. The closer H is to unity, the more persistent is the signal, but if H is less than 0.5, the signal is non-persistent.

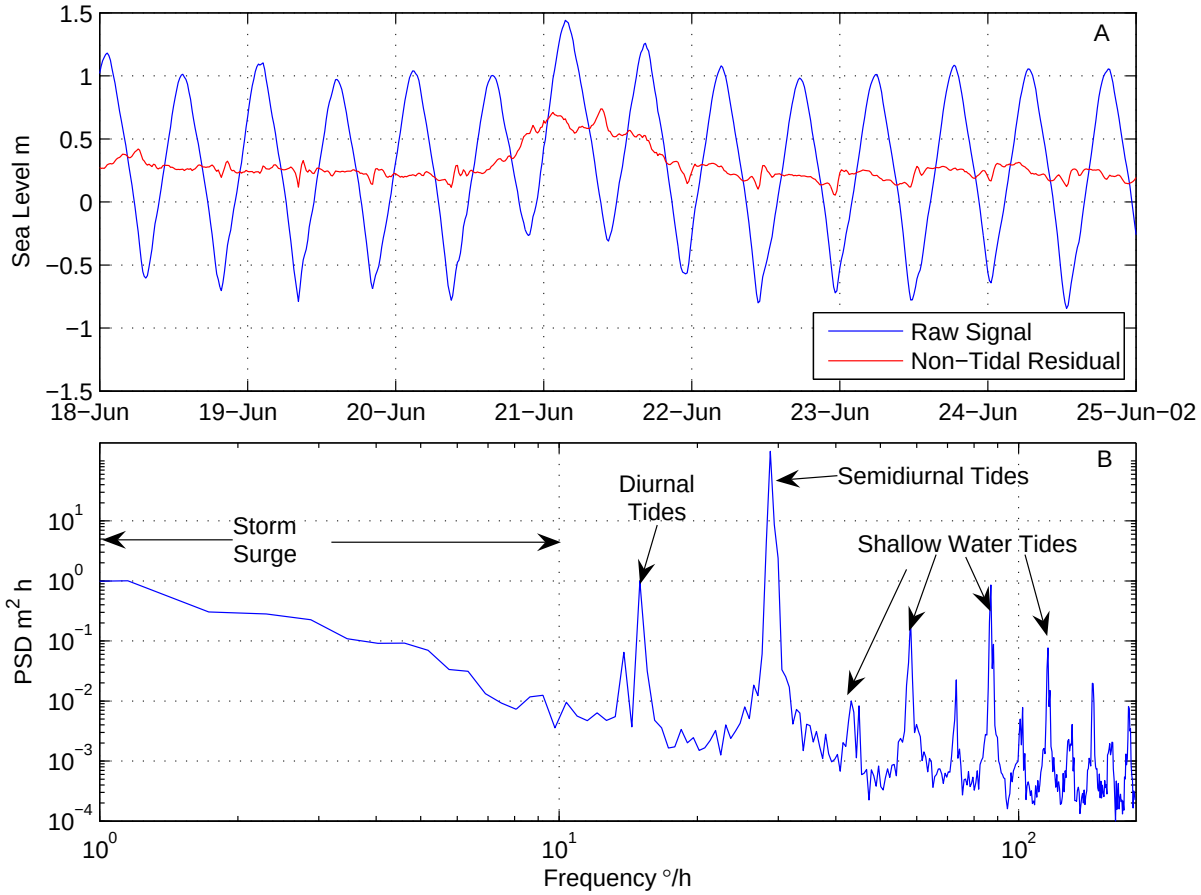

Figure 7.1: Data from Hairini Bridge showing a typical week during which a storm surge occurred (A), and the Fourier spectrum of a year of data (B).

8.2 Tidal analysis

The tide consists of numerous constituents, each related to a particular astronomical phenomenon. Each of these constituents can be identified from a record like that shown in Figure 7.1(A), providing the record is long enough. Ideally, this would be 18.6 years (a tidal epoch), but in practice such long records are rarely available. However, for New Zealand, all the important constituents can be identified from a record of just 206 days in length. In this study, the standard tidal analysis routines of Pawlowicz[17] were used, as described in Pawlowicz et al (2002). A signal-to-noise ratio of 10 was used as the threshold in determining if a particular constituent was significant.

[17] See: http://www2.ocgy.ubc.ca/~rich/#T_Tide.

8.3 Extracting storm surge

Extracting the storm surge from a record like that shown in Figure 2A involves the following steps:

1. Forecast the tide from its constituents and subtract it from the record to form the "non-tidal residual" (see Figure 7.1A);

2. Interpolate across any gaps in the non-tidal residual, keeping a record of the position of the gaps;

3. Band-pass filter the degapped non-tidal residual between 1 and 10º/h (corresponding to 360 to 36 h timescales);

4. Re-introduce the gaps.

There are several options for band-pass filtering including the tapered boxcar method described in Goring & Bell (1996) in which the degapped non-tidal residual is Fourier transformed to the frequency domain, the energy outside of the frequency band is eliminated, and the signal is inverse-Fourier transformed back into the time domain. This method has been used widely in the past, but it has a rather subtle disadvantage in that Fourier transforms assume stationarity[18] of the signal, which is clearly not so for the non-tidal residual shown in Figure 7.2(A). The reason this is a problem is that the sine and cosine basis functions used in the Fourier transform are global functions – they extend from minus infinity to infinity. An alternative is to use wavelet analysis in which the basis functions are localised (mathematically, they have compact support) as shown in Figure 7.2.

In wavelet analysis the mother wavelet (Figure 7.2) is fitted to the signal to produce a set of coefficients, then the mother wavelet is dilated and fitted again to the remainder, and so on. The result is a set of wavelet details plus a remainder called the approximation. Each of the details has a characteristic timescale, with the first one being $3\Delta t$, where Δt is the interval between the data, and thereafter the timescale doubles for each level of decomposition. The original signal can be reconstituted by adding together all the details and the approximation. To band-pass filter, the appropriate details are combined. For hourly data, the timescales are: 3, 6, 12, 24, 48, 96, 192, 384, 768,…, so to obtain storm surge between 36 and 360 h timescales, we must combine details 5 to 8.

[18] Stationarity in this context means that the variance of any window of the data is the same.

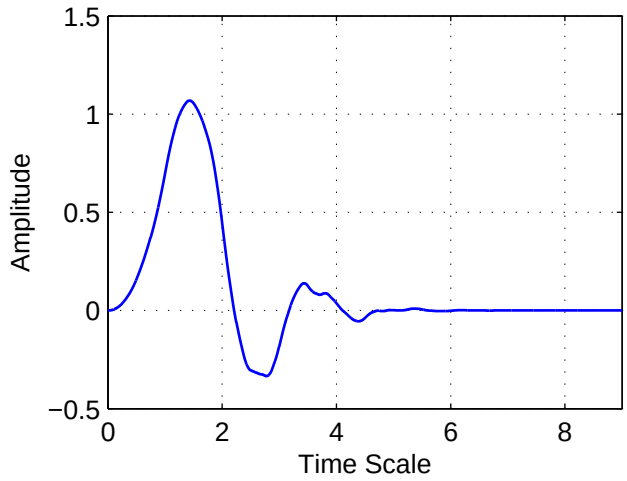

Figure 7.2: Daubechies No 5 mother wavelet.

Wavelet decomposition can have serious end effects, so to reduce these the signal needs to be pre-processed as follows:

1. Generate a linear ramp between the ends of the signal and subtract. This makes both end points zero.

2. Pad out the each end of the signal with *n*/4 zeros, where *n* is the number of data.

After decomposition, the padding is removed. For low-pass filtering, the linear ramp needs to be added back in again, but for band-pass and high-pass filtering this is not necessary. Figure 7.3 shows the wavelet details for the non-tidal residual shown in Figure 7.1(A) and the resulting storm surge.

8.4 Extracting MLOS

Extracting MLOS from a record follows in a straightforward manner from the procedure for extracting storm surge. It is simply the remainder after decomposing to Level 8. In other words, everything in the record with timescales longer than 384 h is assumed to be MLOS. It is usually expressed in monthly means.

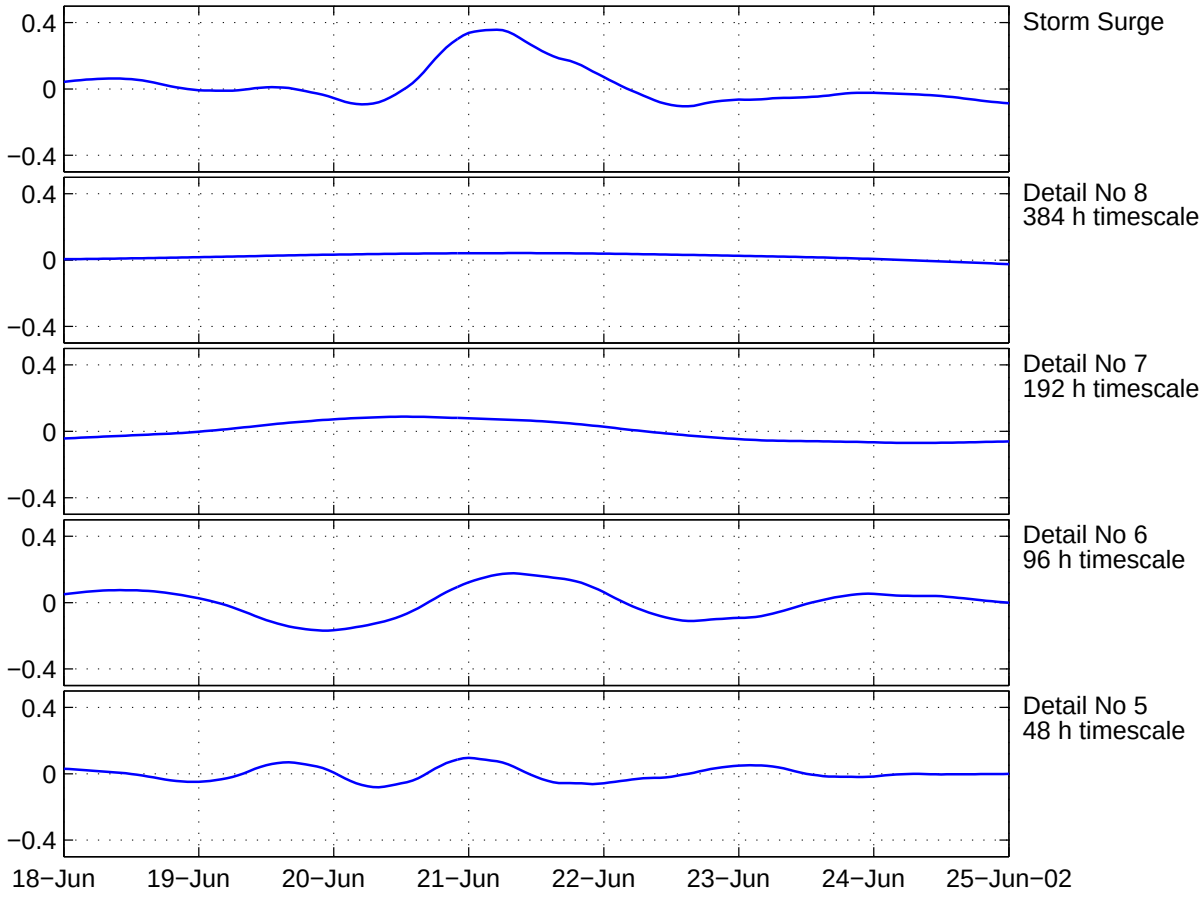

Figure 7.3: Wavelet details for the storm surge event at Hairini Bridge shown in Figure 7.1, with the top panel being the sum of wavelet details 5 to 8.

8.5 Statistical Moments

The statistical moments of a signal provide information on how the data are distributed, having no regard to their sequence. In the context of storm surge, the statistical moments have the following meanings:

- 1st Order Moment (mean) will always be zero for band-pass filtered data like storm surge.
- 2nd Order Moment (variance) is an indication of the energy in the signal.
- 3rd Order Moment (skewness) if it is negative implies more troughs than peaks and vice versa.

- 4th Order Moment (kurtosis) if it is large and positive implies there are a few significant spikes in the record. If skewness is negative these spikes will be mainly troughs, whereas if skewness is positive they will be mainly peaks, and if skewness is zero, they will be evenly distributed between peaks and troughs.

8.6 Regression analysis

Regression analysis attempts to explain the variation of one variable by the variations in one or more other variables. In the present case, we wish to find the relationship between atmospheric pressure and storm surge at Moturiki Island, and between storm surge at Moturiki Island and storm surge at the other sites. There are many ways of doing this. Goring (1995) used regression in both the time domain and the frequency domain. They gave essentially the same results, but regression in the frequency domain provided additional information on the time shift between the signals.

In this study, wavelet decomposition is used to produce a set of wavelet coefficients for each level of decomposition, then regression is applied to those coefficients. This is equivalent to a partial transform into the frequency domain because the wavelet coefficients vary with time, whereas in a full decomposition, time is eliminated as a variable. Hubbard (1996) explains this process very nicely by reference to the Heisenberg Uncertainty Principle and Heisenberg boxes. Cross correlation between the variables at various lags is used to determine the time shift. The normalised cross correlation function between two discrete functions x_i and y_i is defined as:

$$R_j = \frac{\left\langle x_i y_{i-j} \right\rangle_i}{\sigma_x \sigma_y} \tag{3}$$

where j is the lag (which takes positive and negative values), $\left\langle ..... \right\rangle_i$ denotes the mean over i and σ denotes standard deviation.

8.7 Event analysis

Both statistical moments and regression analysis produce parameters that apply to the entire record, but for ~90% of the time, storm surge will be between ± 0.1 m and therefore insignificant. The main interest in storm surge is for the ~5% of the time when it exceeds 0.1 m. This is event analysis.

The threshold of 0.1 m is entirely arbitrary, but it is the level used by de Lange & Gibb (2000), so it will be used here also.

8.8 Storm tide analysis

Storm surge has timescales of 48 h and longer, as shown in Figure A3. This means that in a single 24 hour period there will be at most one trough and one peak. Tides in the Bay of Plenty are primarily semidiurnal. This means that in a 24-hour period there will be two peaks (i.e., high tides) and two troughs (i.e., low tides). Now, consider the case of an average tide (0.7 m at high tide) and a large storm surge of 0.4 m. If high tide coincides with peak storm surge, the storm tide will be 0.7 + 0.4 = 1.1 m, but if low tide coincides with peak storm surge, the storm tide peak will occur 6 h earlier or later when the storm surge height is ~ 0.2 m, producing a storm tide of 0.7 + 0.2 = 0.9 m. Thus, when a storm surge combines with the tide to form a storm tide, the actual height of the storm tide depends on exactly when the waves from the two phenomena occur, but it will always occur at a high tide. Tawn & Vassie (1991) addressed this issue for storm tides around the UK and developed the "revised joint probability method" (RJPM) to calculate the return period for various levels to be exceeded. Their procedure was adapted for New Zealand conditions by NIWA, and a program EXTLEV[19] was developed. This program will be used with Moturiki Island data to generate storm tide statistics. The RJPM procedure separates the sea level signal into tides and storm surge, including the long period oscillations (MLOS) as part of the storm surge. This is not appropriate for New Zealand conditions, so for this study the data used for EXTLEV were generated by adding forecast tide and calculated storm surge. Thus, the statistics are for storm tide to which MLOS (incorporating seasonal, annual, ENSO, IPO, and long-term effects) must be added.

[19] http://www.niwascience.co.nz/ncwr/tools/extlev/

8.9 References

de Lange, W.P., Gibb, J.G. (2000) Seasonal, interannual, and decadal variability of storm surges at Tauranga, New Zealand. NZ Journal of Marine and Freshwater Research, 34: 419-434.

Goring, D.G. (1995) Short-term variations in sea level (2 – 15 days) in the New Zealand region. NZ Journal of Marine and Freshwater Research, 29: 69-82.

Goring, D.G., & Bell, R.G. (1996) Distilling information from patchy tide gauge records: the New Zealand experience. Marine Geodesy, 19: 63-76.

Hubbard, B.B. (1996) The World According to Wavelets: the story of a mathematical technique in the making. A. K. Peters, 264pp.

Pawlowicz, R., Beardsley, B., & Lentz, S. (2002) Classical tidal harmonic analysis including error estimates in MATLAB using T_TIDE, Computers and Geosciences 28: 929-937.

Tawn, J.A., & Vassie, J.M. (1991) Recent improvements in the joint probability method for estimating extreme sea levels. In Tidal Hydrodynamics, B.B. Parker (ed.), John Wiley & Sons: 813-828.

9. Appendix 2: Description of the nearshore wave model, verification and application

9.1 The SWAN wave model

The SWAN model (Booij et al., 1999; Ris et al., 1999) is also a spectral wave model like WAM and Wavewatch III, but is particularly intended for shallow water applications in coastal and estuarine environments. It computes the evolution of the wave energy spectrum in position (x, y) and time (t), explicitly taking into account the various physical processes acting on waves in shallow water. These include the effects of refraction by currents and bottom variation, and the processes of wind generation, white-capping, bottom friction, quadruplet wave-wave interactions, triad wave-wave interactions and depth-induced breaking. The model can incorporate boundary conditions representing waves arriving from outside the model domain.

9.2 Wave climate applications

The SWAN model can be used for a direct simulation of wave conditions in a given coastal region, provided that adequate input data are available to represent wind fields and incident deep-water wave conditions during the period of interest. However, computing limitations mean that such a fine-resolution simulation covering a large area is only feasible for relatively short time periods, typically up to several weeks. Less direct methods are required to simulate the multi-year time scales needed to provide information on seasonal and interannual variations in wave climate, and also allow the sensitivity of the wave climate to changes in wind climate to be readily investigated.

We describe here a method based on first running the model under a full range of nominal forcings, then applying the resulting transfer functions to long term records of observed or hindcast forcing parameters, to derive nearshore wave conditions.

Offshore wave conditions can be parameterised by (a) significant height H_{s0}, (b) peak direction θ_{p0}, and (c) peak period T_{p0}, as obtained from the deep-water model hindcast. Wind conditions can be parameterised by (d) wind speed U_{ref} and (e) wind direction ϕ_{ref} at a suitably representative meteorological station. Wave and wind data can be analysed to select a finite number of discrete values of each of the forcing parameters to adequately cover their range of observed values.

A SWAN simulation is run with each combination of the discrete forcing parameters, i.e. simulation *n* uses wave parameters $\left(H_{s0}^{(n)}, \theta_{p0}^{(n)}, T_{p0}^{(n)}\right)$ applied at the offshore boundaries, and wind fields $\left(U_{ref}^{(n)}, \phi_{ref}^{(n)}\right)$ applied uniformly over the grid. The output from each simulation will give a set of wave parameters $F\left(x, y : H_{s0}^{(n)}, \theta_{p0}^{(n)}, T_{p0}^{(n)}, U_{ref}^{(n)}, \phi_{ref}^{(n)}\right)$ at all positions (*x, y*) on the model domain ("*F*" includes H_s , θ_p , T_p , wave energy flux, among others). This forms the basis of a "lookup table" describing wave conditions inshore for a finite set of forcing conditions.

Given a climate record that includes values of the wind and deep-water wave parameters $\left(H_{s0}, \theta_{p0}, T_{p0}, U_{ref}, \phi_{ref}\right)$ at each time *t* of the record, multilinear (five dimensional) interpolation is used to provide weights $w_n(t)$ into the set of discrete forcing parameters used in the simulations. The weights are derived from products of linear weights for each forcing parameter, e.g. if H_{s0} lies halfway between $H_{s0}^{(1)}$ and $H_{s0}^{(2)}$, all simulations with those offshore wave heights will pick up a 0.5 "wave height" weighting, and all other simulations will have zero weight. Similar weightings are picked up from the other forcing parameters. These weights are then used to enter the "lookup table", and compute values for each wave parameter at each output location in the grid:

$$F(x, y, t) = \sum_n w_n(t) F\left(x, y : H_{s0}^{(n)}, \theta_{p0}^{(n)}, T_{p0}^{(n)}, U_{ref}^{(n)}, \phi_{ref}^{(n)}\right) \quad (1)$$

Note that vector interpolation is needed for directional wave parameters, i.e. the energy flux vector is interpolated, rather than θ_p .

This method uses stationary SWAN simulations to take waves from the offshore boundary in to the coast. That is, an equilibrium sea state is computed for the given boundary wave conditions and wind field as if they had been present for an indefinite time. This does not take into account the history of these forcings, which may, for example, result in the sea state being not fully developed in a strengthening wind, or remnant seas being left in a weakening wind. This is a relatively small limitation over short spatial scales. At typical wave speeds of 8 ms^{-1} (for 10 s period waves in deep-water), a 200 km domain is crossed in around 6 hours. So only variations in the forcing at shorter time scales than this will be subject to these "hysteresis" errors. In any case, such variations will largely be averaged out in taking long-term climatic means.

9.3 SWAN model application to the Bay of Plenty coast

A model grid was established covering the Bay of Plenty. The wave model was run at 1000 m resolution on a grid of 196 cells in the east-west direction by 112 cells in the north-south direction. The grid origin (cell (1,1)) was at NZMG (2765000.0E, 6346000.0N). The spectral grid had 25 discrete frequencies logarithmically placed between 0.0418 Hz and 0.802 Hz, and 32 direction bins at 11.25° increments. This is a finer directional resolution (by a factor 2) than was used in the WAM hindcast, as coarsely discretised wave directions can cause greater errors in nearshore simulations than in the open ocean, for example in resolving the edge of a "wave shadow" behind an island or headland. All other model settings were SWAN defaults as described in the manual (Holthuijsen et al., 2000).

A spatially uniform boundary condition was applied, using a JONSWAP spectral form (Hasselmann et al., 1973) of specified significant height, peak period and peak direction. A peak enhancement factor $\gamma = 3.3$ and 20° directional spread were specified.

9.3.1 Scenario simulations

Discrete values of the offshore wave parameters used in the simulations were significant height H_{s0} = 1, 2, 4 and 6 m, peak period T_{p0} = 2.5, 5, 10, 15 and 20 s, peak direction (from) θ_{p0} = 270° through 360° = 0° to 180° in 22.5° increments (directions relative to True North). Wind speed took values U_{ref} = 5, 10, 15 and 25 ms^{-1}, from the sixteen directions ϕ_{ref} = 0° through 315° in 22.5° increments. These were selected to span values of each parameter observed in the data, without necessitating a prohibitive number of SWAN simulations. This is a necessary consideration, as all combinations of these forcing parameters were used, as well as zero wind runs for each wave combination and zero incident wave runs for each wind combination.

The simulations were used to establish a "lookup table", from which inshore wave conditions could be interpolated for any given set of forcing parameters $\left(H_{s0}, \theta_{p0}, T_{p0}, U_{ref}, \phi_{ref}\right)$. We first simulated the existing nearshore wave climate by using forcing parameters from a historic period, then simulated the possible effects of climate change by rerunning the simulations with forcing parameters adjusted consistent with climate change scenarios as outlined below.

To provide environmental forcing parameters for the present study, wave parameters were extracted from two deep-water hindcasts, along with the wind fields used as their inputs. The first was the NIWA WAM wave hindcast covering the period January 1979 to December 1998. These were taken from the nearest cell (37.125°S, 177.75°E) of the 1.125°×1.125° hindcast grid. The second was the NOAA/NCEP Wavewatch III wave hindcast covering the period February 1997 to May 2005. These were taken from the nearest cell (37°S, 177.5°E) of the 1.25°×1.00° hindcast grid. These time series were used directly in the baseline simulations representing present day climate. In order to simulate nearshore wave conditions under climate change scenarios, modifications can be made to the forcing parameter time series.

9.3.2 Comparison with measurements

Comparisons were made between wave buoy data and predictions of both the direct simulation and the scenario-based climate simulation (both forced by the Wavewatch deep-water hindcast) over the period 26/2/2004 – 8/3/2004 for which the direct simulation was run (Figure 8.1). This included one of the more energetic events in the wave buoy record, in which significant wave heights over 7 m were recorded. Both the direct and climate simulation tracked the general evolution of the significant wave height reasonably well, although the shorter-term variation which produced separate storm peaks on successive days was not reproduced. In this, the SWAN model results simply reflected similar behaviour in the offshore forcing from the Wavewatch III model. During this period, wave directions were from the NNE, so small variations in the simulations of nearshore processes and local winds would have relatively little influence.

The peak period was also reasonably well represented by all the model simulations through the main storm event, except that the rapid switch to a longer swell period at the height of the storm, and its subsequent decay, was not picked up by Wavewatch, and hence not by the nearshore simulations. Also, the data shows dominance by long period swell several days before and after the storm event. The models did not quite pick this up, but a flipping back and forth in the model peak periods between windsea and swell values before the storm suggests that the full spectra simulated by Wavewatch III included both swell and wind sea components, but possibly with a slightly incorrect balance in their relative energies. This illustrates that there may be improvements to be gained in using full directional spectra as boundary inputs. Where these are available, this is certainly feasible for direct simulations. Spectral boundaries would, however, be difficult to incorporate in the scenario-based approach.

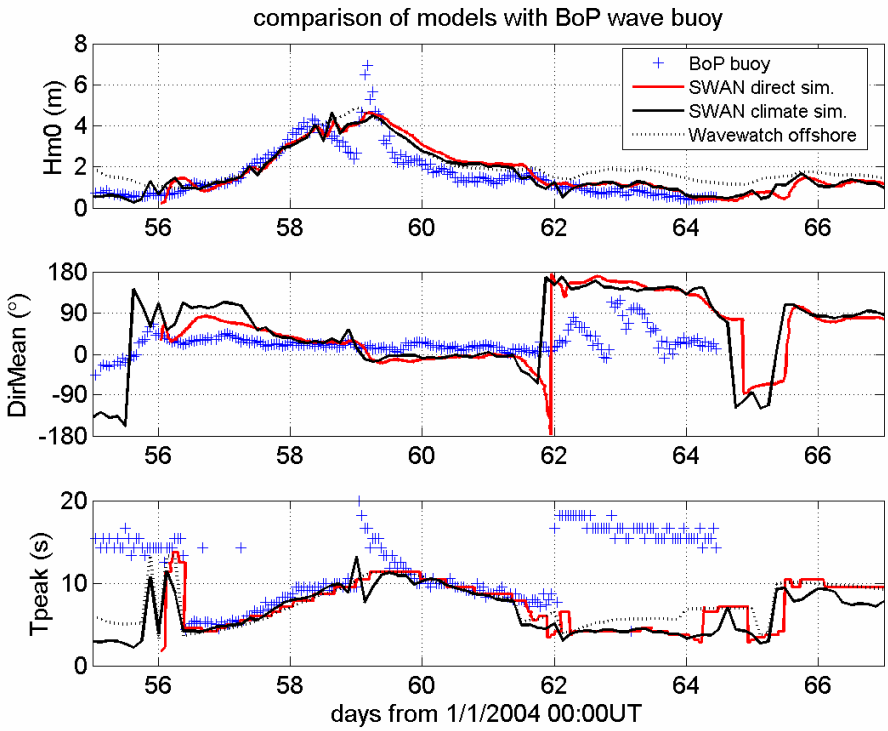

Figure 8.1: Comparison of time series data from the Bay of Plenty wave buoy with output from a direct SWAN simulation (red line) and a scenario-based climate simulation (black line) at the same location. Wave parameters shown are (top) significant wave height, (middle) mean wave direction, and (bottom) peak wave period.

Unlike the direct simulation, the climate simulation covered the full period of the buoy record. Comparing measured and simulated significant wave heights (Figure 8.2), we find that the simulation somewhat overestimates heights in mean conditions ($H_{m0} \approx$ 1 m), while there is closer agreement on average in more energetic conditions, albeit with considerable scatter. This is reflected in the comparison of wave height occurrences (Figure 8.3), which show some differences at low wave heights, but converge in the tail of the distributions. This is a satisfactory result for climate studies focussed on the statistics of extreme events rather than reproducing wave conditions in individual storms.

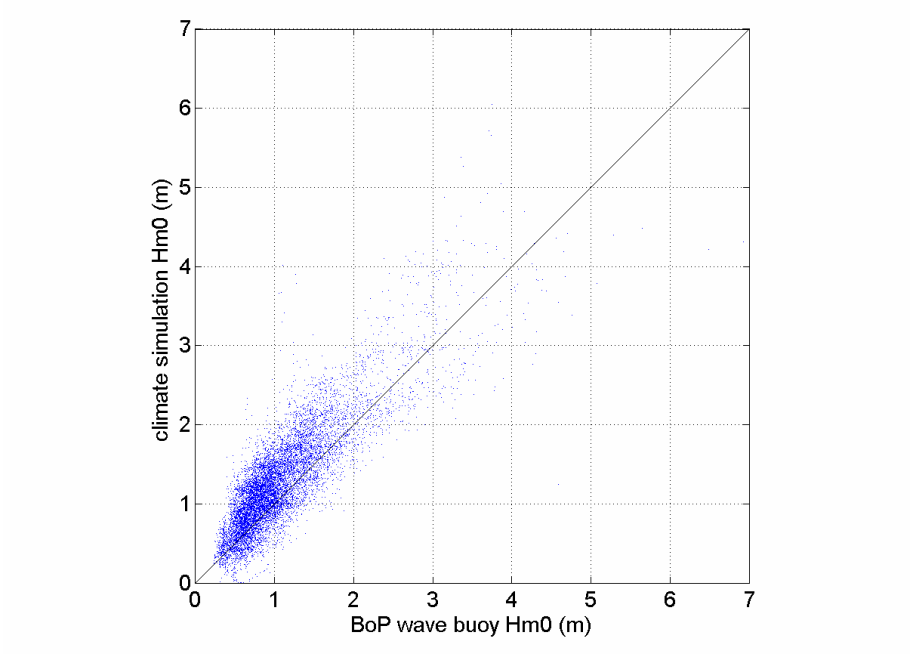

Figure 8.2: Comparison of significant wave height data from the Bay of Plenty wave buoy with output from a scenario-based climate simulation (based on the Wavewatch deep-water hindcast) at the same location.

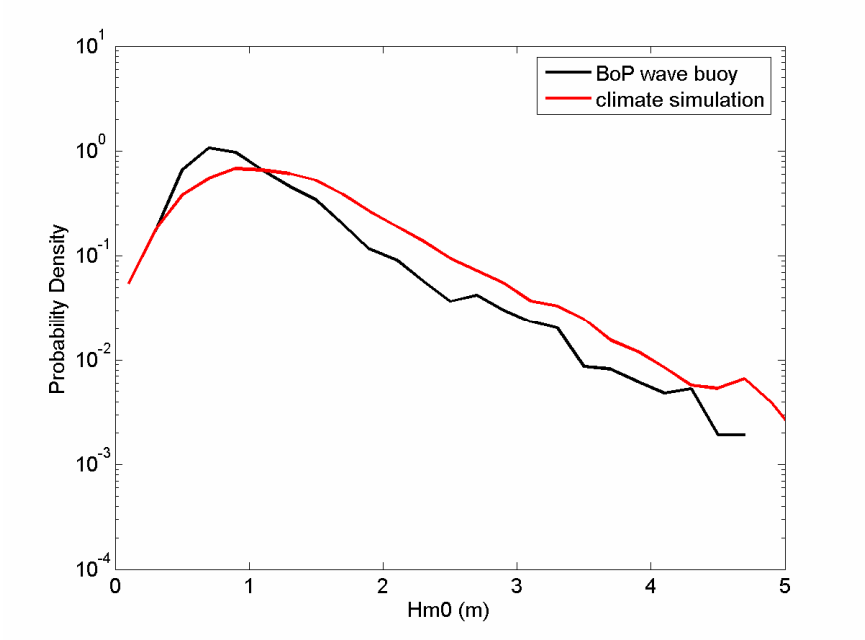

Figure 8.3: Comparison of occurrence distributions of significant wave height data from the Bay of Plenty wave buoy and from output from a scenario-based climate simulation (based on the Wavewatch deep-water hindcast) at the same location, using the same output times as the data.

Next, the two climate-based simulations were compared over the overlap period May 1997 – December 1998, again using outputs at the wave buoy site. Time series of all wave statistics (Figure 8.4) show close agreement between the two hindcasts for almost the entire comparison period. A scatter plot (Figure 8.5) of nearshore significant wave heights derived from the two hindcasts shows some scatter about the equivalence line, with little relative bias in low- and medium-energy conditions, but some tendency for Wavewatch to prooduce larger wave heights than WAM in the higher-energy range.

The most important result of the validation exercise is that the scenario-based method can produce comparable results to the direct simulation, so that the accuracy of the forcing data becomes the main determinant of the quality of the results.

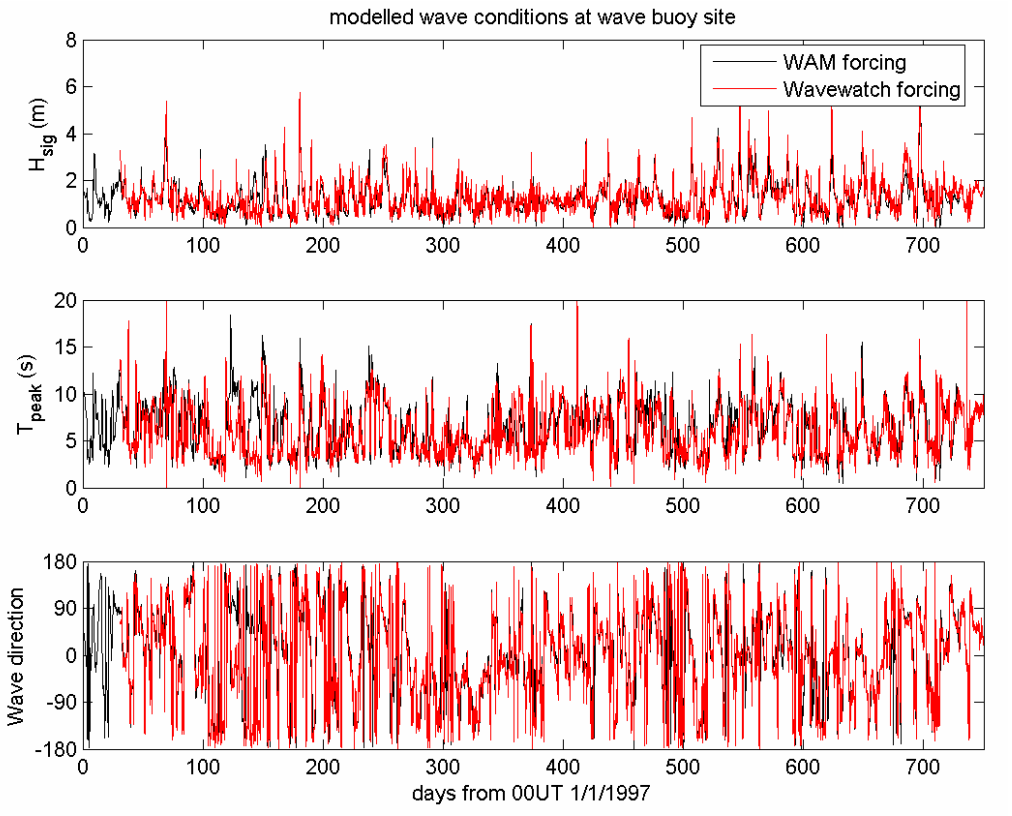

Figure 8.4: Comparison of wave statistics (significant wave height, peak period, wave direction) at the Bay of Plenty wave buoy site from scenario-based climate simulations based on the Wavewatch and WAM deep-water hindcasts.

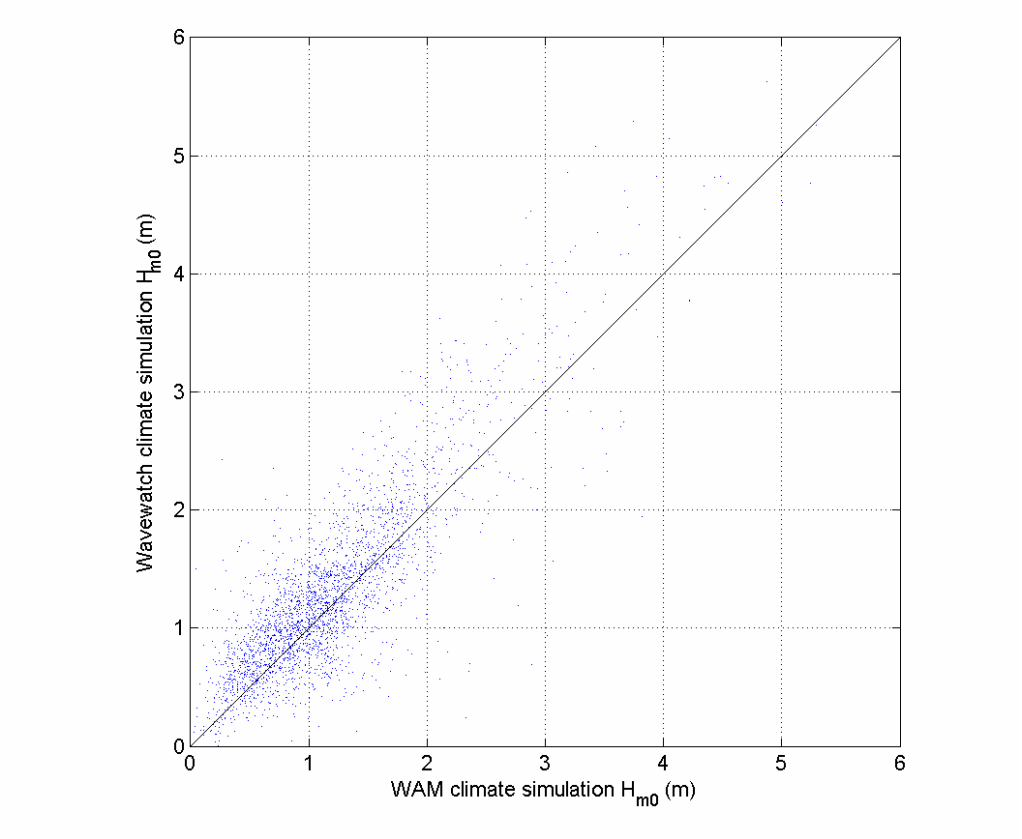

Figure 8.5: Scatter plot of significant wave height at the Bay of Plenty wave buoy site from scenario-based climate simulations based on the Wavewatch and WAM deep-water hindcasts.

9.4 References

Booij, N., Ris, R.C. & Holthuijsen, L.H. (1999). A third-generation wave model for coastal regions 1. Model description and validation, *Journal of Geophysical Research, 104* (C4), 7649-7666.

Holthuijsen, L.H., Booij, N., Ris, R.C., Haagsma, I.G., Kieftenburg, A.T.M.M, & Kriezi, E.E. (2000). SWAN Cycle 3 version 40.11 user manual, Delft University of Technology, Delft.

Hasselmann, K., Barnett, T.P., Bouws, E., Carlson, H., Cartwright, D.E., Enke, K., Ewing, J.A., Gienapp, H., Hasselmann, D.E., Kruseman, P., Meerburg, A., Müller, P., Olbers, D.J., Richter, K., Sell, W., & Walden, H. (1973). Measurements of wind-wave growth and swell decay during the Joint North Sea Wave Project (JONSWAP), *Deutsche Hydrographische Zeitschrift. Supplement, A8* (12), 1-95.

Hasselmann, S., Hasselmann, K., Bauer, E., Bertotti, L., Cardone, C.V., Ewing, J.A., Greenwood, J.A., Guillaume, A., Janssen, P.A.E.M., Komen, G.J., Lionello, P., Reistad, M., and Zambresky, L. (1988). The WAM Model - a third generation ocean wave prediction model, *Journal of Physical Oceanography, 18* (12), 1775-1810.

Ris, R.C., Holthuijsen, L.H., & Booij, N. (1999). A third-generation wave model for coastal regions 2. Verification, *Journal of Geophysical Research, 104* (C4), 7667-7681.

10. Appendix 3: Surf zone wave and sediment transport properties

For a single-component sinusoidal wave of height H travelling with group velocity C_g, the energy transport (i.e. the energy crossing unit length of wave front per unit time) is a vector quantity directed normal to the wave crest, with magnitude

$$F = \frac{1}{8}\rho g C_g H^2 \tag{1}$$

where $\rho \approx 1025$ kg.m^{-3} is the density of seawater and g = 9.81 m.s^{-2} is the gravitational acceleration. For shallow water of depth h, the group velocity has magnitude

$$C_g \approx \sqrt{gh} \tag{2}$$

and the wave height on breaking is proportional to the depth, i.e.

$$H_b \approx \gamma h_b, \tag{3}$$

with a constant of proportionality $\gamma \approx 0.5$. Hence the (conserved) magnitude of the energy transport at both the 10 m isobath and at the breakpoint is

$$F_b = F \approx \frac{\rho g^{1.5}}{8\gamma^{0.5}} H_b^{2.5}. \tag{4}$$

The SWAN modelling procedure provides an estimate of wave parameters on the 10 m isobath, but does not have sufficient resolution to directly compute wave transformation to the breaker zone. However, an estimate of wave height and direction at the breakpoint can be made by assuming that the seabed has simple topography shoreward of the 10 m isobath, with shore-parallel depth contours. Then conservation of energy flux F can be used to find H_b and h_b through Equations (3) and (4), while conservation of the longshore component of wavenumber gives

$$\frac{\sin\alpha_b}{\sin\alpha} = \frac{k}{k_b} \approx \sqrt{\frac{h_b}{h}} \tag{5}$$

where α and α_b are the angles between the wave propagation direction and the shore-normal direction at the 10 m isobath and at the breakpoint, respectively, and h = 10 m and h_b are the corresponding depths. Equivalently, the wave crests are at an angle α_b to the beach.

The energy transport at the breakpoint has longshore and onshore components $F \sin\alpha_b$ and $F \cos\alpha_b$ respectively. The flux of *longshore directed* wave energy across a *shore-parallel* line is then given by the longshore flux factor

$$P_{ls} = F \cos\alpha_b \sin\alpha_b = \tfrac{1}{2} F \sin 2\alpha_b \approx \frac{\rho g^{1.5}}{16\gamma^{0.5}} H_b^{2.5} \sin 2\alpha_b \qquad (6)$$

while the flux of *onshore-directed* wave energy across a *shore-parallel* line is

$$P_{os} = F \cos^2 \alpha_b \approx \frac{\rho g^{1.5}}{8\gamma^{0.5}} H_b^{2.5} \cos^2 \alpha_b . \qquad (7)$$

The longshore sediment flux can be approximated by an empirical relationship

$$Q = fKP_{ls} \qquad (8)$$

where f = 3308 $m^2.s^3.kg^{-1}.year^{-1}$ = 1.05×10^{-4} $m^2.s^2.kg^{-1}$ is a unit-conversion constant, while K is a dimensionless efficiency factor dependent on sediment properties. A value of K = 0.8 has been found to be appropriate for sandy beaches on the new Zealand east Coast (Hicks, 1993), although much lower values may be required where coarser material is present. For the present study we have not attempted to incorporate information on the varying beach sediment properties across the Bay of Plenty region. Rather, we maintain the value K = 0.8 throughout the study region, with the caveat that the transport rates so obtained should be considered as potential values, applying only if the relevant sediment type is available.

For the Bay of Plenty coast study, transport along the coast in the north-westward direction was deemed to be positive.

The longshore flux factor (Eqn. 6) and sediment transport rates (Eqn. 8) for each shore station were computed as time series, and then averaged, e.g.

$$Q_{net} = \frac{1}{N}\sum_{n=1}^{N} Q(t_n) \tag{9}$$

Also of interest are the averages of solely positive (north-westward) and negative (south-eastward) components, i.e.

$$Q_{+} = \frac{1}{N}\sum_{Q>0} Q(t_n) \tag{10}$$

and

$$Q_{-} = \left| \frac{1}{N}\sum_{Q<0} Q(t_n) \right| \tag{11}$$

From these we derive a net/gross drift ratio

$$N/G = \frac{Q_{net}}{Q_{+} + Q_{-}} \tag{12}$$

The drift/swash ratio is defined as the ratio of the mean magnitude of the longshore flux factor to the mean onshore energy transport:

$$D/S = \frac{\sum_{n=1}^{N} \left| P_{ls}(t_n) \right|}{\sum_{n=1}^{N} P_{os}(t_n)} \tag{13}$$

Also of interest are the divergences (in the longshore direction) $\partial P_{ls}/\partial y$ and $\partial Q/\partial y$, of the longshore flux factor and the longshore sediment transport, respectively. These represent an imbalance between transport into one end of a section of coast and transport out of the other end. Positive and negative values of these divergences respectively indicate zones of erosion or deposition.

he maximum swash runup expected during a given storm can be estimated by he method described by Resio (1987) as:

$$A = \xi H_{m08} \left[1.253 - 1.053 \left(\ln \left(\frac{N_s}{N_s - 1} \right) \right)^{0.19} \right] \quad (14)$$

where H_{m08} is the significant wave height in 8m water depth, N_s is the expected number of waves during the storm, and ξ is the surf similarity parameter

$$\xi = \frac{\tan \theta}{\sqrt{H_{m08} / L_p}} \quad (15)$$

for a beach of slope angle θ, and waves of wavelength L_p in 8m water depth at the spectral peak. For the present study, storms were identified from the time series of nearshore significant wave height using the Peaks Over Threshold method, with a threshold (i.e. minimum separation between storm peaks) of 3 days. The storm duration, and hence N_s, was derived from the interval between storms identified in this way. Annual maxima of runup A were then computed as described above, and averaged over the 20-year hindcast. Similar mean annual maxima were also computed from the combined runup plus wave setup, which was estimated using the conservative relationship of Holman (1986):

$$\overline{\eta} = \xi H_{m0} \quad (16)$$

10.1 References

CERC (1984). *Shore protection manual*, Coastal Engineering Research Center, US Army Corps of Engineers, Vicksburg, Mississippi.

Hicks, D.M. (1993). *Modelling long-term change of the Pegasus Bay shoreline*, NIWA, Christchurch.

Holman, R.A. (1986). Extreme value statistics for wave runup on a natural beach. *Coastal Engineering 9(6)*: 527–544.

Resio, D.T. (1987). *Extreme runup statistics on natural beaches*. Miscellaneous Paper CERC-87-11, U.S. Army Corps of Engineers Coastal Engineering Research, Vicksburg, Mississippi.